OT REPORT 73-10

MOLECULAR ATTENUATION AND PHASE DISPERSION BETWEEN 40 AND 140-GHz FOR PATH MODELS FROM DIFFERENT ALTITUDES

OT

U.S. DEPARTMENT OF COMMERCE/Office of Telecommunications

FORM OT-29
(3-73)

U.S. DEPARTMENT OF COMMERCE
OFFICE OF TELECOMMUNICATIONS

BIBLIOGRAPHIC DATA SHEET

	1. PUBLICATION OR REPORT NO.	2. Gov't Accession No.	3. Recipient's Accession No.
	OTR 73-10		

4. TITLE AND SUBTITLE
Molecular Attenuation and Phase Dispersion Between 40 and 140 GHz for Path Models from Different Altitudes

5. Publication Date
May 1973

6. Performing Organization Code
ITS

7. AUTHOR(S)
Hans J. Liebe and W. M. Welch

9. Project/Task/Work Unit No.
9103221

8. PERFORMING ORGANIZATION NAME AND ADDRESS
U. S. Department of Commerce
OT/ITS
325 South Broadway
Boulder, Colorado 80302

10. Contract/Grant No.

11. Sponsoring Organization Name and Address
U. S. Department of Commerce
Office of Telecommunications
1325 G. Street N. W.
Washington, D. C. 20005

12. Type of Report and Period Covered
OT Report

13.

14. SUPPLEMENTARY NOTES

15. ABSTRACT *(A 200-word or less factual summary of most significant information. If document includes a significant bibliography or literature survey, mention it here.)*

Radio wave propagation in the 40 to 140 GHz band through the first hundred kilometers of the atmosphere is strongly influenced by the microwave spectrum of oxygen (O_2-MS). A unified treatment of molecular attenuation and phase dispersion is formulated. Results of molecular physics are translated into frequency temperature, pressure, and magnetic field dependencies of a complex refractive index. The intensity distribution of the O_2-MS undergoes several changes with increasing altitude: when $h < 10$ km, all lines, but one at 119 GHz, are merged to a continuum spectrum under the influence of pressure-broadening; when $h > 30$ km, a line spectrum with isolated Lorentzians is displayed; when $h > 40$ km, Zeeman-splitting of each line occurs due to the influence of the earth's magnetic field; for $h > 60$ km, a Voigt profile governs the transition to a Gaussian line shape and

(continued on next page)

16. Key works *(Alphabetical order, separated by semicolons)*

Atmospheric transmissivity; atmospheric millimeter wave propagation; complex refractive index of air; oxygen microwave spectrum.

17. AVAILABILITY STATEMENT

☒ UNLIMITED.

☐ FOR OFFICIAL DISTRIBUTION.

18. Security Class *(This report)*
Unclassified

20. Number of pages
112

19. Security Class *(This page)*
Unclassified

21. Price:

USCOMM-DC 29716-P73

(continued)

eventually the Doppler-broadened line spectrum vanishes. The influence of water vapor is discussed separately.

Attenuation and dispersion rates for path models are evaluated by computer routines. Examples of computer plots are given as a function of altitude for homogeneous, zenith, and tangential path geometries. Molecular resonances of minor atmospheric gases are discussed briefly, as is the noise which originates from the O_2-MS.

☆ U.S. GOVERNMENT PRINTING OFFICE: 1972-783 461/171 REGION NO. 8

MOLECULAR ATTENUATION AND PHASE DISPERSION BETWEEN 40- AND 140-GHz FOR PATH MODELS FROM DIFFERENT ALTITUDES

H. J. LIEBE

W. M. WELCH

U.S. DEPARTMENT OF COMMERCE
Frederick B. Dent, Secretary

OFFICE OF TELECOMMUNICATIONS
John M. Richardson, Acting Director

MAY 1973

UNITED STATES DEPARTMENT OF COMMERCE

OFFICE OF TELECOMMUNICATIONS

STATEMENT OF MISSION

The mission of the Office of Telecommunications in the Department of Commerce is to assist the Department in forstering, serving, and promoting the Nation's economic development and technological advancement by improving man's comprehension of telecommunication science and by assuring effective use and growth of the Nation's telecommunications resources. In carrying out this mission, the Office:

Performs analysis, engineering, and related administrative functions responsive to the needs of the Director of the Office of Telecommunications Policy in the performance of his responsibilities for the management of the radio spectrum;

Conducts research needed in the evaluation and development of telecommunications policy as required by the Office of Telecommunications Policy, Executive Office of the President, pursuant to Executive Order 11556;

Conducts research needed in the evaluation and development of other policy as required by the Department of Commerce;

Assists other government agencies in the use of telecommunications;

Conducts research, engineering, and anlaysis in the general field of telecommunication sciences to meet government concerns;

Acquires, analyzes, snythesizes, and disseminates information for the efficient use of telecommunications resources.

Preface

The work described in this report was done at the Institute for Telecommunication Sciences as part of a research program on quantitative millimeter wave spectroscopy of atmospheric oxygen. The project was partially supported by the following agencies:

(a) NASA Langley Research Center under Order No. AAFE, L58, 506, dated January 8, 1971, and monitored by Mr. R. E. Davis.

(b) NOAA - National Environmental Satellite Service under Order No. E-579-71, dated February 16, 1971, and monitored by Mr. J. Alishouse.

The authors are with the Applied E. M. Sciences Division of I. T. S. at Boulder, Colorado. Inquiries should be addressed to them at the Institute for Telecommunication Sciences, U. S., Department of Commerce, Boulder, Colorado 80302.

CONTENTS

		Page
	ABSTRACT	1
1.	INTRODUCTION	3
2.	THEORY	7
	2.1 Atmospheric Transfer Function	7
	2.2 Frequency-Independent Phase Delay	9
	2.3 Microwave Spectrum of Oxygen (O_2-MS)	11
	2.3.1 Line Center Frequencies	11
	2.3.2 Line Strengths	13
	2.3.3 Zeeman Splitting of O_2-MS Lines	15
	2.4 Line Shapes of the Atmospheric O_2 Microwave Spectr.	23
	2.4.1 Pressure-Broadening	24
	2.4.2 Nonresonant O_2-Spectrum	28
	2.4.3 Transition to Doppler Broadening (Voigt Profile)	29
	2.5 Attenuation and Dispersion Due to Water Vapor	30
3.	COMPUTER ANALYSIS OF ATMOSPHERIC PATH MODELS	43
	3.1 Homogeneous Path Transmissivity at Various Altitudes	43
	3.1.1 Analysis of Attenuation and Dispersion (48 and 72 GHz)	48
	3.1.2 Phase Dispersion Between 10 and 140 GHz	58
	3.2 Slant Path Transmissivity	67
	3.2.1 Calculation Procedure and Critical Comments	67
	3.2.2 Zenith and Tangential Paths From Various Altitudes (48 to 72 GHz)	69
	3.2.3 Ozone and Other Minor Atmospheric Gases	72
	3.2.4 Atmospheric Noise Due to Molecular Absorption	73
4.	CONCLUSIONS	96
	Acknowledgement	96
5.	REFERENCES	97

LIST OF FIGURES

Figure		Page
1.	Millimeter wave attenuation in the 49 to 72 GHz band due to atmospheric oxygen for zenith paths from different initial heights.	6
2.	Line strength parameter for the O_2-MS at 200°K and 300°K.	19
3.	Temperature dependence of the O_2-MS line strengths.	21
4.	Normalized Lorentzian shape of an isolated line for dispersion and extinction.	33
5.	Reported line width parameters for the self-broadened O_2-MS.	35
6-8.	Computer plots of the pressure-broadened O_2-MS at 300°K, for p = 10, 50, 150, 250, 500, and 760 torr.	37
9.	Attenuation of oxygen between 54 and 66 GHz at four different pressures.	38
10.	Normalized Voigt profiles for dispersion and extinction.	40
11.	Frequency loci of the maximum dispersion and line half-width for a Voigt profile.	41
12.	Pure water vapor attenuation at 61.2 and 30.6 GHz.	42
13.	Linewidth versus altitude and pressure from the CMR-model.	51
14-17.	Horizontal transmissivity at altitudes h = 0, 10, 20, 30 km.	52-55
18.	Effect of Zeeman-splitting upon the 9^+O_2 line at h = 50 km.	56
19.	Effect of Zeeman-splitting upon the 27^-O_2 line at h = 50 km.	57
20.	Phase dispersion in dry air between 10 and 140 GHz.	64
21.	Total dispersion of the O_2-MS between 0 and 80 GHz at 760 torr.	65
22.	Phase dispersion, differential dispersion, and attenuation in dry air at sea level for the two frequency pairs, 55/66- and 51.0/71.4-GHz.	66
23.	Model profiles of relative concentrations for atmospheric constituents versus altitude.	74
24.	Algorithm used for the calculation of the differential slant path length.	75

Figure		Page
25 to 37. (odd nos.)	Total attenuation and phase dispersion for a Zenith path (h_1 = 0, 5, 10, 15, 20, 25, and 30 km).	79, 81, 83, 85, 87, 89, 91
26 to 38 (even nos.), and 39.	Total attenuation and phase dispersion for a Tangential path (h_0 = 5, 10, 15, 20, 25, 50, and 75 km).	80, 82, 84, 86, 88, 90, 92, 93

LIST OF TABLES

1.	Relative concentration of dry air constituents and the refractivity measured for air components at 61 GHz.	10
2.	Observed and calculated line center frequencies of the O_2 Microwave Spectrum.	17
3.	Line strengths at 300°K and strength correction for the O_2-MS.	18
4.	Temperature dependence of the line strength of the O_2-MS.	20
5.	Frequency shift and intensity functions of Zeeman components for lines of O_2-MS.	22
6.	Reported width parameters and their temperature dependence for self-pressure-broadened lines of the O_2-MS.	34
7.	Spectroscopic parameters for 44 lines of the O_2-MS.	36
8.	Shape functions for an isolated spectral line.	39
9.	Extreme values of zenith phase dispersion and electrical path length change (CMR-Model).	63
10.	Zenith oxygen attenuation from sea level.	76
11.	Example of computer print-out on tangential attenuation and phase dispersion.	77
12.	Stronger spectral lines of minor atmospheric gases in the 40 to 140 GHz band.	94

MOLECULAR ATTENUATION AND PHASE DISPERSION BETWEEN 40 AND 140 GHz FOR PATH MODELS FROM DIFFERENT ALTITUDES

Hans J. Liebe and W. M. Welch*

ABSTRACT

Radio wave propagation in the 40 to 140 GHz band through the first hundred kilometers of the atmosphere is strongly influenced by the microwave spectrum of oxygen (O_2-MS). A unified treatment of molecular attenuation and phase dispersion is formulated. Results of molecular physics are translated into frequency, temperature, pressure, and magnetic field dependencies of a complex refractive index. The intensity distribution of the O_2-MS undergoes several changes with increasing altitude: when $h < 10$ km, all lines, but one at 119 GHz, are merged to a continuum spectrum under the influence of pressure-broadening; when $h > 30$ km, a line spectrum with isolated Lorentzians is displayed; when $h > 40$ km, Zeeman-splitting of each line occurs due to the influence of the earth's magnetic field; for $h > 60$ km, a Voigt profile governs the transition to a Gaussian line shape and eventually the Doppler-broadened line spectrum vanishes. The influence of water vapor is discussed separately.

Attenuation and dispersion rates for path models are evaluated by computer routines. Examples of computer plots are given as a function of altitude for homogeneous, zenith, and tangential path geometries. Molecular resonances of minor atmospheric gases are discussed briefly, as in the noise which originates from the O_2-MS.

Key words: Atmospheric transmissivity; atmospheric millimeter wave propagation; complex refractive index of air; oxygen microwave spectrum.

*The authors are with the Institute for Telecommunication Sciences, Office of Telecommunications, U. S. Department of Commerce, Boulder, Colorado 80302.

1. INTRODUCTION

Much of the future growth of telecommunications will occur by extending the radio spectrum into the millimeter wavelength range (30 to 300 GHz). As shown in a recent review by Thompson et al. (1972), the successful exploitation of this largely unused portion of the spectrum hinges on the accurate and complete account of all propagation effects. The greatest obstacles to the use of such high frequencies are attenuation and phase dispersion caused permanently by the clear air and intermittently by rain and clouds. This report addresses the use of the frequency spectrum 40 to 140 GHz for radio propagation through the clear atmosphere and discusses in detail ultimate limitations due to air molecules of which oxygen is a major species. The microwave spectrum of oxygen, abbreviated O_2-MS, dominates the transfer properties of air throughout the specified frequency range, while molecular effects of water vapor influence them to a lesser extent. Roughly forty lines of the O_2-MS contribute to the atmospheric spectrum. Each line has individual pressure and temperature dependencies, and the overlapping of lines below 30 kilometers changes the structure of the spectrum drastically with altitude.

Of prime concern to system engineers are signal degradations (amplitude and phase distortions; interferences) and the minimum transmitted pulse length supported by the propagation medium. These concerns lead in Section 2 to the formulation of a complex transfer function $\tau(\alpha, \phi)$ for a well-mixed, homogeneous atmosphere. Spectroscopic knowledge of the O_2-MS is translated into engineering terms of attenuation α, phase-delay ϕ_o, and dispersion $\Delta\phi$ rates for atmospheric conditions up to altitudes of 100 kilometers. In Section 3 these results are applied to calculate transfer properties of path models through the U. S. Standard Atmosphere (1962). Cumulative attenuation A and phase

dispersion ΔT along slanted ray paths through the total (inhomogeneous) atmosphere are evaluated by computer calculations. An example is shown in Figure 1 for one-way zenith path attenuation between 49 and 72 GHz from different initial altitudes. A graphical presentation is the best introduction to atmospheric transmission and shielding properties due to the O_2-MS.

As part of spectrum management, a first step was taken to allocate bands for specific applications through an international agreement (ITU, 1971). For the first time several bands have been reserved exclusively for passive systems. A clear understanding of the O_2-MS is required to promote the most efficient use of the millimeter wave spectrum which, just as its lower frequency counterpart, is a saturable resource. Reliable knowledge of the transfer function τ provides the basis for designing systems which take advantage of unique molecular transmission and emission properties associated with the relatively stable dry part of the atmosphere. The O_2-MS affords interference resistance and transmission security for broadband radio communications. Optimum system performances can be assured by tradeoff studies between environmental degradations and component limitations.

The following key phrases give examples of telecommunication applications which incorporate O_2-MS properties:

(a) Shielding of broadband satellite-to-satellite links from ground interferences (e.g., Crane, 1971).

(b) Secure high-altitude communication in the valleys of the O_2-MS with special channel characteristics (balance between transmission and shielding, phase-dispersive pass-band, phase keying, etc.).

(c) Restricted range, variable range, and local distribution broadband communication systems (e.g., Murray, 1971).

(d) Aircraft collision avoidance by means of ≈60 GHz beacons and "threshold" receivers (M. L. Meeks, private communication, 1969).

(e) Restrictions of radar range (Blake, 1972).

(f) Occultation experiments between orbiting satellites for studies of atmospheric structures.

(g) Absolute differential phase measurements between frequency pairs on either side of the O_2-MS over line-of-sight paths for correction of radio distance (MITRE, 1965; Thompson, 1968; see Section 3.1.1).

More applications will almost certainly follow if the basics are better known.

Active systems may eliminate desirable molecular properties (e.g., shielding) when operating at extremely high power densities. A very rough estimate indicates that, for the onset of saturation at an isolated line center, the power density has to exceed $10 \cdot p^2 [W/(cmtorr)^2]$. The nonlinear power saturation effects, however, are not treated any further in this report.

The following applications are based on frequency-selective emission originating from the O_2-MS:

(a) Remote sensing of atmospheric temperature structures (Meeks and Lilley, 1963; Lenoir, 1968; Wilheit, 1969; Waters, 1970; Westwater, 1970). Ground-based stratospheric temperature soundings (Waters, 1973) and the NIMBUS-5 (launched Dec. 1972) satellite (Sabatini, 1972), both operate radiometers within the O_2-MS band. The conversion from measured radio noise to meteorological quantities requires accurate knowledge of oxygen absorption. This application in particular has fostered theoretical and experimental work on the O_2-MS (see Sect. 3.2.4).

(b) Stratospheric navigation aids such as velocity and altitude indicators (Mardon, 1969).

(c) Horizon sensor for satellite navigation (Guidice, 1971; Grauling, 1972).

(d) Radiometric detection of strong temperature gradients in the atmosphere for the identification of clear air turbulences (Haroules and Brown, 1969).

(e) Earth magnetic field strength measurements from satellites by means of the normal Zeeman effect (Sect. 2.3.3 and 3.1.1).

(f) Line emission (e.g. 119 GHz) used as a tracer in biological research, for example, to study oxygen exchange rates.

Radio astronomy efforts which are searching for millimeter wavelength emissions from exterrestrial sources are interested in accurately defining the boundaries of the atmospheric O_2-MS, which masks their useful frequency bands.

This report shall provide baseline data on unique atmospheric transfer properties for a largely unused portion of the spectrum.

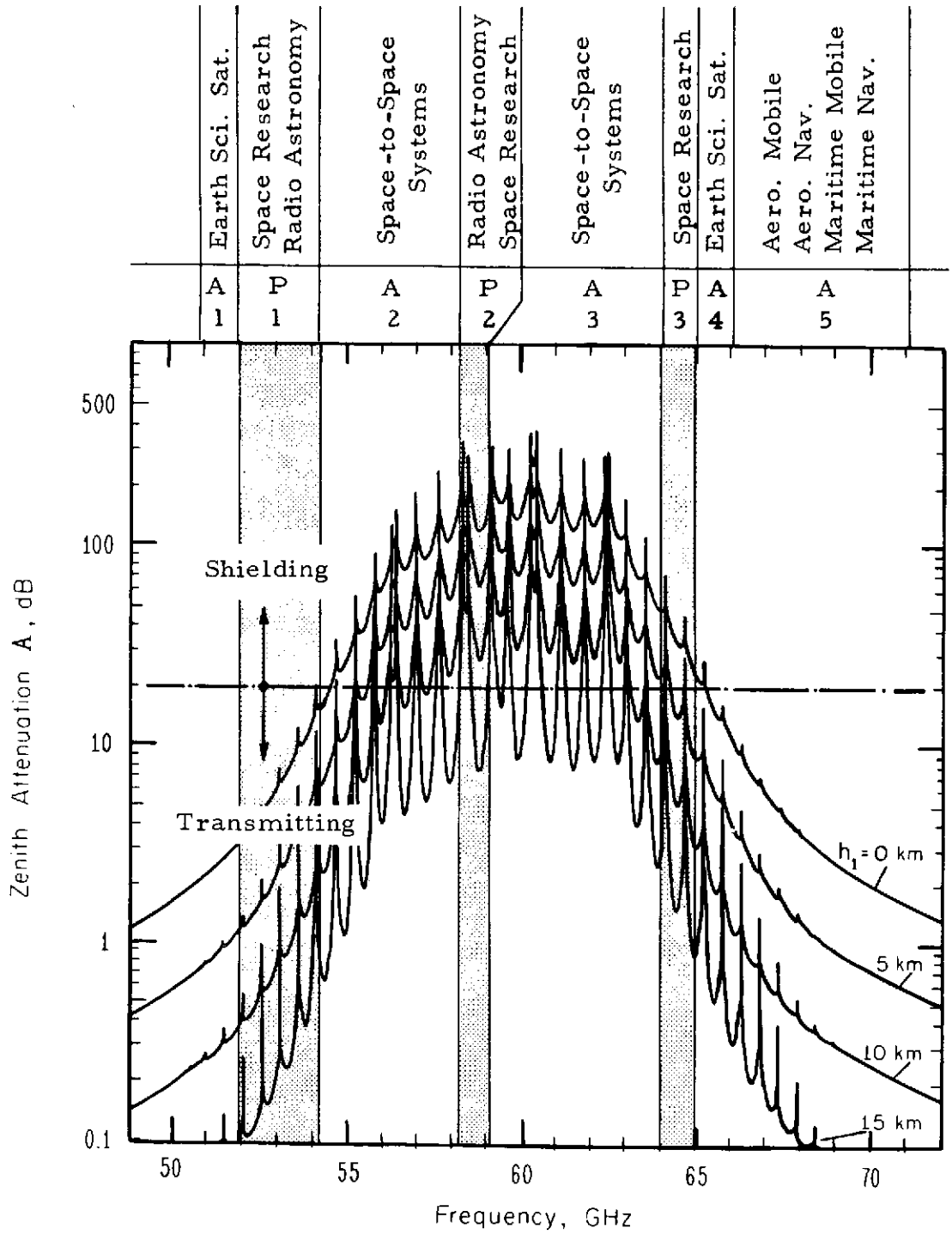

Figure 1. Millimeter-wave attenuation in the 49 to 72 GHz band due to atmospheric oxygen resonances for zenith paths through the U. S. Standard Atmosphere 1962 from different initial heights h_1 to outer space (see also Section 3.2). Allocated band utilizations are: A(1-5)-active telecommunications; P(1-3) - passive systems only (I. T. U., 1971; Klass, 1971).

2. THEORY

2.1 Atmospheric Transfer Function

Signal analysis of millimeter waves propagating through a well mixed atmosphere is facilitated by treating the medium as a linear system and applying the transfer function concept, (Morgan and Ekdahl, 1966). The central topic is the development of a microwave transfer function for moist air as reliably as can be at the present state of knowledge. To accomplish this, one has to track down macroscopic properties of the propagation medium to their molecular origin and be confronted with a combination of classical and quantum mechanical theories which describe the interaction between radiation and gas molecules. A rigorous test of these theories is still wanting since it can not be provided by the small amount of inaccurate and sometimes conflicting experimental data. The complex transfer function is defined by

$$\underline{\tau} \equiv \underline{E}/E_o = \exp\left[-\left(\frac{\alpha}{20 \log e} + j\phi\right)L\right] = \exp\left[j\, 2\pi\nu\, \underline{L}n/c\right] \qquad (1)$$

where E_o is the initial amplitude and $\underline{E}$ is the amplitude and phase received after the geometric path length L for free space propagation; $j = \sqrt{-1}$. Power attenuation rate α and phase-delay rate ϕ are the well known propagation parameters

$$\begin{aligned} \alpha &= (10 \log e)\,(4\pi\nu/c)n'' \qquad [\mathrm{dB/km}]\ , \\ \phi &= (2\pi\nu/c)n' \qquad\qquad\quad [\mathrm{rad/km}] \end{aligned} \qquad (2)$$

where ν is the microwave frequency, c is the speed of light, and $10 \log e \approx 4.34294$. The dimensionless macroscopic measure of the interaction between radiation and gas molecules is a complex refractive index

$$\underline{n} = n' - jn'' \quad , \tag{2a}$$

where

$n' = n_o + \Delta n(\nu)$ is the Refraction Spectrum and

$n''(\nu)$ is the Extinction Spectrum.

Both spectra are interrelated by Kramers-Kronig integral equations, which are obeyed by the shape functions chosen (Eqs. 17, 23, 28, Table 8). This report is concerned with theoretical and analytical evaluations of the refractive index $\underline{n}$ for air over the frequency band, $\nu \approx 40$ to 140 GHz. The environmental conditions to be considered for altitudes h = 0 to 100 km are:

Dry air pressure	p(h)	[see below]	(3)
Mixing ratio of dry air components	r_k=const.	[see Table 1]	
Temperature	T(h)	[330 to 180°K]	
Water Vapor pressure	$p_w(T, h)$	[0 to 50 torr]*	
Earth's magnetic field strength	H(h and geo-magnetic coord.)	[0.2 to 0.7 gauss]*	

The field strength H decreases between h = 0 and 100 km by 4.8 percent.

Pressure changes versus altitude as shown (U. S. Std. Atm. 62):

h [km]	0	100	20	30	40
p [torr]*	760	199	41.5	9.0	2.2
h[km]	50	60	70	80	100
p[mtorr]	600	170	41	7.8	0.23

*) The units [torr] and [gauss] do not comply with recommended S. I. units. The conversions are 1 torr ≡ 133.322 pascal (N/m²) and 1 gauss ≡ 10^{-4} Wb/m².

The solution of equations (1) and (2) leads to the extinction and refraction spectra of oxygen and water vapor being defined by

$$n' = n_o + \sum_i S_i F_i' + \Delta n_n + \Delta n_w$$

and by (4)

$$n'' = \sum_i S_i F_i'' + n''_n + n''_w \quad ,$$

where

n_o is the frequency-independent refraction of air (see Sect. 2.2);

i is the label for lines of the O_2 Microwave Spectrum (see Sect. 2.3.1);

S_i are the individual line strengths (see Sect. 2.3.2 and 3);

F_i', F_i'' are the shape functions (real and imaginary parts) for individual lines (see Sect. 2.4);

n''_n and Δn_n indicates the nonresonant oxygen spectrum (see Sect. 2.4.2); and

n''_w and Δn_w indicates contributions due to water vapor (see Sect. 2.5).

2.2 Frequency-Independent Phase Delay

The non-dispersive phase delay of a millimeter wave propagating through the gaseous atmosphere is commonly expressed in **N**-units,

$$\mathbf{N} = (n_o - 1)\, 10^6 = [pR_d^\circ + p_w \cdot R_w^\bullet (T)]/T, \quad [\text{ppm}] \quad .^\dagger \qquad (5)$$

The corresponding phase delay in engineering terms is

$$\phi_o = (2\pi\nu/c) \cdot n_o \quad , \quad [\text{rad/km}] \quad .$$

---

†Pressure proportionality is indicated in general for all appropriate parameters by a superscript $^\circ$.

Table 1. Relative Concentration r of Dry Air Components (near sea level) and Refractivity R^{o} Measured for Different Air Components at $\nu = 61\,156$ MHz, $p \leq 20$ torr, $T = 280\,^{o}K$. (Liebe and Welch, 1972).

k	Component		r	$R^{o}(280)$	R^{o}/T
			ppm by vol	ppm/torr	ppm ^{o}K/torr
1	Oxygen	O_2	209 460[(a)]	0.3427	95.95
2	Nitrogen	N_2	780 840	0.3771	105.60
3	Argon	Ar	9 340	0.3562*	99.73*
4	Carbon Dioxide	CO_2	314	0.6356	178.0
5	Neon	Ne	18.2	0.08659	24.25
6	Helium	He	5.2	0.0450	12.6
7	Methane	CH_4	2	0.5672	158.8
8	Krypton	Kr	1.1	0.5428	152.0
9	Nitrous Oxide	N_2O	0.5	0.7138	199.9
	Dry Air		10^6	0.3696	103.54
	Water Vapor	H_2O	variable	6.712	1879(280^{o}K)

(a) Machta and Hughes (1970).

* Reference value; all measured R^{o} are relative to the R^{o} (Ar) - value given by Newell and Baird (1965).

The refractivity values for dry air and water vapor are

$$R_d^\circ = \sum_k r_k R_k^\circ = 103.5 \quad [\text{ppm}\,^\circ\text{K/torr}]$$

and

$$R_w^\circ = 95.5 + 499500/T \quad [\text{ppm}\,^\circ\text{K/torr}],$$

which were measured for the air components at 61.156 GHz as listed in Table 1. Similar results have been reported by Boudouris (1963) and Newell and Baird (1965).

2.3 The Microwave Spectrum of Oxygen

The following simplified explanation can be given as to the nature of the O_2-MS. The magnetic dipole moment of the O_2 molecule couples to the microwave radiation field which excites quantized changes (molecular resonances) between fine structure levels of the O_2 rotational energy states. At these resonances the molecules momentarily store (phase dispersion), absorb (attenuation), and randomly re-radiate (incoherent noise) microwave energy.

Solutions to problems of atmospheric millimeter wave transmission (Eq. 4) require detailed knowledge of the O_2 Microwave Spectrum. Parameters of the O_2-MS which originate from properties of "isolated" molecules are the line center frequencies ν_o and the strength values S.

2.3.1 Line Center Frequencies of the O_2-Microwave Spectrum

The O_2 fine structure microwave spectrum obeys the selection rule: $\Delta N = 0$, $\Delta J = \pm 1$ (N, J are the rotational and total angular momentum quantum numbers), and the transition frequencies ν_o^i can be calculated by means of (Welch and Mizushima, 1972)

$$\nu_o(N^{\pm}) = \lambda_o + \frac{1}{2}\mu_o - 4\mu_1 + (\lambda_1 + \frac{5}{2}\mu_1)(a^2 + a + 2)$$
$$\pm \{f(a) - (2a+1)[\beta(a) + \frac{2}{3}\lambda_1 - \mu_1]\} \quad , \tag{6}$$

where $a = N \pm 1$, $N = 1, 3, \ldots$ (only odd values are allowed),

$$f(a) = \sqrt{C^2 + a(a+1)D^2} \quad ,$$

$$C = (2a+1)[\beta(a) - \frac{1}{2}\mu_o - \frac{1}{2}\mu_1(a^2 + a + 4)]$$
$$- [\lambda_o + \frac{1}{3}\lambda_1(7a^2 + 7a + 4)]/(2a+1) \quad ,$$

$$D = 2[\lambda_o + \lambda_1(a^2 + a + 1)]/(2a+1) \quad ,$$

$$\beta(a) = B_o + 2B_1(a^2 + a + 1) + B_2(3a^4 + 6a^3 + 13a^2 + 10a + 4) \quad .$$

The line designation $N^{\pm}$ denotes the transitions $J = N \pm 1 \longrightarrow J' = N$. The most recent values of the molecular constants are given by Welch and Mizushima (1972) and they are in megahertz:

Rotational:	$B_o = 43100.518\ (3)$, $B_1 = -0.14492\ (9)$,
	$B_2 = 1.57\ (11) \cdot 10^{-7}$.
Spin-spin coupling:	$\lambda_o = 59501.342\ (7)$,
	$\lambda_1 = 5.847\ (3) \cdot 10^{-2}$.
Spin-rotational coupling:	$\mu_o = -252.5865\ (10)$,
	$\mu_1 = -2.464\ (20) \cdot 10^{-4}$.

For all atmospheric transmission problems, it is sufficient to consider i = 44 individual lines. The known values of ν_o^i are given in Table 2. Most of the center frequencies have been measured with high accuracy, and the few missing ones are predicted by equation (6). These predictions, for example, guided atmospheric emission measurements by Waters (1973) whereby the agreement was excellent (see Table 2).

2.3.2 Line Strengths of the O_2-Microwave Spectrum

For practical applications it is helpful to reduce molecular line shape theory and define a line strength parameter S (Liebe, 1969a) as a multiplier to a Lorentzian shape function (Sect. 2.4.1). Pressure and temperature dependences of the strength for an individual line of the O_2-MS are given by

$$S = S_i^\circ (T)\ \xi\ p\ r_1 \quad , \ [Hz] \tag{7}$$

where $r_1 = 0.20946$ (Table 1), and $\xi = 0.9976$, portion* of molecules of mass $^{16}O_2$.

The strength parameter S_i° was derived from the equation describing the transition probabilities. Assuming for the magnetic field strength H = 0 ($H \neq 0$, see Section 2.3.3) leads to the expression (VanVleck, 1947; Morgan and Ekdahl, 1966; LeFande, 1968; Wilheit, 1969)

$$S_i^\circ = \nu_o^i \cdot K \cdot f(N) \cdot f(T) \quad , \ [Hz/torr] \tag{8}$$

where $K = 69.50125 \cdot 10^{-6} \cdot k(J)\ [°K^3/torr]$ and k(J) is given in Table 3 and discussed below.

---

*The isotopic abundance of $^{17}O_2$ and $^{18}O_2$ are 0.037 and 0.204 percent respectively.

The intensity functions (Matrix elements) are

$$f(N^+) = (2N^2 + 3N) / (N + 1)$$
$$f(N^-) = (2N^2 + N - 1) / N \quad . \tag{9}$$

The temperature function is in units of $[1/ °K^3]$

$$f(T) = \left\{T^{-3} \exp[-2.06858 \cdot N(N+1)/ T\right\} \cdot [1 - (h\nu_o^i / 2kT)] \quad . \tag{10}$$

The error of the approximation $[1 - (h\nu_o^i / 2kT)] \approx 1$ is less than 1 percent for all values of interest (see Fig. 3).

The approximation made in calculating the matrix element of the magnetic dipole moment operator was that O_2 is a pure Hund's case "b" molecule. The fact that this is not exactly true was accounted for by a correction factor $k(J) \leq 1$, which is a mixing coefficient quantifying the purity of a particular state (Zimmerer and Mizushima, 1961; Wilheit, 1969). The k(J) values given in Table 3 were obtained by diagonalizing the Hamiltonian matrix with the appropriate wave functions. Equation (8) was applied to compute S_i° at T = 300°K up to $N^\pm = 43$, and the results are listed in Table 3. Figure 2 displays the strength value distribution versus the frequency positions ν_o^i for 200° and 300°K.

The temperature dependence of the strength parameter can be expressed relative to the reference temperature, $T_o = 300K$, by

$$S_i^\circ(T) = S_i^\circ(300) \cdot \vartheta(N) \quad , \tag{11}$$

with

$$\vartheta(N) = (300/ T)^3 \cdot \exp\left\{-6.89526 \cdot 10^{-3} \cdot N(N+1)[(300/ T) - 1]\right\} \quad . \tag{12}$$

The temperature function can be approximated for a small temperature interval ($\Delta T \lesssim 40$ °K) by

$$\vartheta \approx (T_o / T)^{w(N)} \quad . \tag{13}$$

Each N-pair of lines possesses its own temperature dependence $\vartheta(N)$. The values of ϑ are given in graphical form in Figure 2 for atmospheric temperatures, and numerical values are listed in Table 4 which also shows temperature exponents w(N) of equation (13) for $T_o \approx 280 \pm 20°K$. The temperature function ϑ indicates the population of energy states relative to 300°K. At low temperatures many of the lines with high N-numbers may be neglected.

2.3.3 Zeeman-Splitting of the Lines in the O_2 Microwave Spectrum

The O_2-MS is greatly complicated by Zeeman-splitting of each fine-structure line into many components under the influence of a permanent magnetic field such as the earth's. The Zeeman effect, which originates from the interaction of the molecular magnetic moment with a static magnetic field of strength H, removes the spatial M-degeneracy of the J levels, splitting each level into (2J+1) sub-levels (M-magnetic quantum number). The complete Zeeman Hamiltonian for O_2 was given by Tinkham and Strandberg (1954). In the weak field case (H < 1 gauss), however, it is sufficient to retain only the term involving the interaction of the molecular electronic spin moment with the field. Matrix elements of the spin moment, evaluated in the Hund's (case "b") representation, are given by Evenson et al.(1968) and may be used in a perturbation calculation to obtain the Zeeman transition frequencies.

The selection rule on ΔM (change in magnetic quantum number) for Zeeman transitions is derived from assumptions about the orientation between H and the microwave magnetic field component $\mathfrak{y}$ perpendicular to the direction of propagation. By a judicious choice of the orientation between H and $\mathfrak{y}$, one can selectively excite two different types of Zeeman transitions:

(1) Linearly polarized radiation "induces"

$\Delta M = 0$, called π transitions when H and $\mathcal{E}$ are perpendicular,

$\Delta M = \pm 1$, called σ transitions when H and $\mathcal{E}$ are parallel, and

in both cases H is perpendicular to the propagation direction.

(2) Circular polarized radiation "induces"

$\Delta M = +1$ or σ^+ transitions for right-handed polarization,

$\Delta M = -1$ or σ^- transitions for left-handed polarization, and

in both cases H is parallel to the direction of propagation.

The simplest pattern, the normal Zeeman effect, is exhibited by the 1^+ and 1^- lines (see Table 5), each splitting into three components whereby only the two σ components shift away from the center (Hill and Gordy, 1953). The anomalous Zeeman effect splits the lines $N = 3^{\pm}$, $5^{\pm}$, ... into $3(2J^* + 1)$ components where J^* is the smaller of the two J values involved in the transition.

The frequency of each Zeeman component is determined by

$$\nu_o^z = \nu_o + \eta(M, N) \cdot Z H \ [\mathrm{MHz}] \quad . \tag{14}$$

The shift is proportional to the external field strength H, and η (Table 5) is less than one. The factor of proportionality for $^{16}O_2$ microwave lines is $Z = 2.8026$ [MHz/gauss]. The earth's magnetic field strength, $H = 0.2$ to 0.7 gauss, produces frequency shifts for the Zeeman components of up to 2 MHz.

The line strength of each Zeeman component is given by

$$S_z^\circ = \nu_o^z \cdot K \cdot f(M, N) \cdot f(T) \quad , \ [\mathrm{Hz/torr}] \tag{15}$$

analogous to equation (8). The intensity function f(M, N) is listed for the different Zeeman components in Table 5. Summing over polarizations and over all M - degeneracies of the final state J' yields f(N). Examples for atmospheric conditions are discussed in Section 3.1.1.

Table 2. Observed and Calculated Line Center Frequencies ν_o^i of the $^{16}O_2$ Microwave Spectrum, in MHz.

i	Line N^+	Observed	Ref.	Calculated (Eq. 6)*)	i	Line N^-	Observed	Ref.	Calculated (Eq. 6)*)
1	1^+	56264.766(20)	a	56264.758	2	1^-	118750.343(10)	b	118750.330
		56264.778(10)	b						
	3^+	58446.580(10)	c	58446.580		3^-	62486.255(10)	c	62486.267
		58446.600(10)	b				62486.225(10)	b	
5	5^+	59590.978(10)	c	59590.979		5^-	60306.044(10)	c	60306.065
	7^+	60434.776(10)	c	60434.778		7^-	59164.215(10)	c	59164.211
		60434.788(10)	f						
	9^+	61150.570(10)	c	61150.567	10	9^-	58323.885(10)	c	58323.883
		61150.565(5)	f						
	11^+	61800.169(20)	a	61800.167		11^-	57611.4 (2)	d	57612.492
		61800.155(10)	c						
	13^+	62411.223(10)	c	62411.234		13^-	56968.180(20)	a	56968.214
15	15^+	62996.6 (2)	d	62997.999		15^-	56363.393(20)	a	56363.397
	17^+	63568.520(10)	c	63568.542		17^-	55783.819(20)	a	55783.805
	19^+	64127.777(20)	a	64127.790	20	19^-	55221.372(20)	a	55221.362
	21^+	64678.2 (2)	d	64678.920		21^-	54671.145(20)	a	54671.141
	23^+	65224.12 (20)	c	65224.076		23^-	54129.4 (4)	d	54129.926
							54130.2 (5)	e	
25	25^+	65764.744(20)	a	65764.760		25^-	53599.4 (8)	d	53595.682
							53595.9 (2)	e	
	27^+			66302.06		27^-	53066.9 (2)	e	53066.802
	29^+			66836.77	30	29^-	52542.4 (2)	e	52542.23
	31^+			67369.51		31^-	52021.4 (5)	e	52021.17
	33^+			67900.73		33^-			51503.02
35	35^+			68430.8		35^-			50987.3
	37^+			68960.1		37^-			50473.6
	39^+			69488.7	40	39^-			49961.8
	41^+			70016.9		41^-			49451.4
43	43^+			70544.9	44	43^-			48942.4

(---) Uncertainty of the last digits given

*) See also Welch and Mizushima (1972)

References -
a. West and Mizushima (1966)
b. McKnight and Gordy (1968)
c. Zimmerer and Mizushima (1961)
d. Mizushima and Hill (1954)
e. Waters (1973)
f. Liebe and Welch (1972)

Table 3. Line Strength $S_i^\circ(300)$ at T = 300°K (Eq. 8) and Strength Correction k(J) for the $^{16}O_2$ Microwave Spectrum.

i	Line N+	k (J)	S° (300) [Hz/torr]	i	Line N⁻	k (J)	S° (300) [Hz/torr]
1	1^+	0.9808	0.348 69	2	1^-	1	0.597 25
	3^+	0.9941	0.925 05		3^-	0.9808	0.963 36
5	5^+	0.9972	1.341 02		5^-	0.9941	1.348 70
	7^+	0.9984	1.562 63		7^-	0.9972	1.526 31
	9^+	0.9989	1.589 94	10	9^-	0.9984	1.515 04
	11^+	0.9992	1.458 82		11^-	0.9989	1.359 54
	13^+	0.9997	1.227 20		13^-	0.9992	1.120 44
15	15^+	1	0.954 01		15^-	0.9997	0.853 87
	17^+	1	0.689 76		17^-	1	0.605 61
	19^+	1	0.465 60	20	19^-	1	0.401 19
	21^+	1	0.294 21		21^-	1	0.248 87
	23^+	1	0.174 37		23^-	1	0.144 84
25	25^+	1	0.097 074		25^-	1	0.079 186
	27^+	1	0.050 820		27^-	1	0.040 717
	29^+	1	0.025 041	30	29^-	1	0.019 707
	31^+	1	0.011 621		31^-	1	0.008 985
	33^+	1	0.005 083		33^-	1	0.003 860
35	35^+	1	0.002 096		35^-	1	0.001 564
	37^+	1	0.000 815		37^-	1	0.000 598
39	39^+	1	0.000 299	40	39^-	1	0.000 216
	41^+	1	0.000 104		41^-	1	0.000 073
43	43^+	1	0.000 034	44	43^-	1	0.000 024

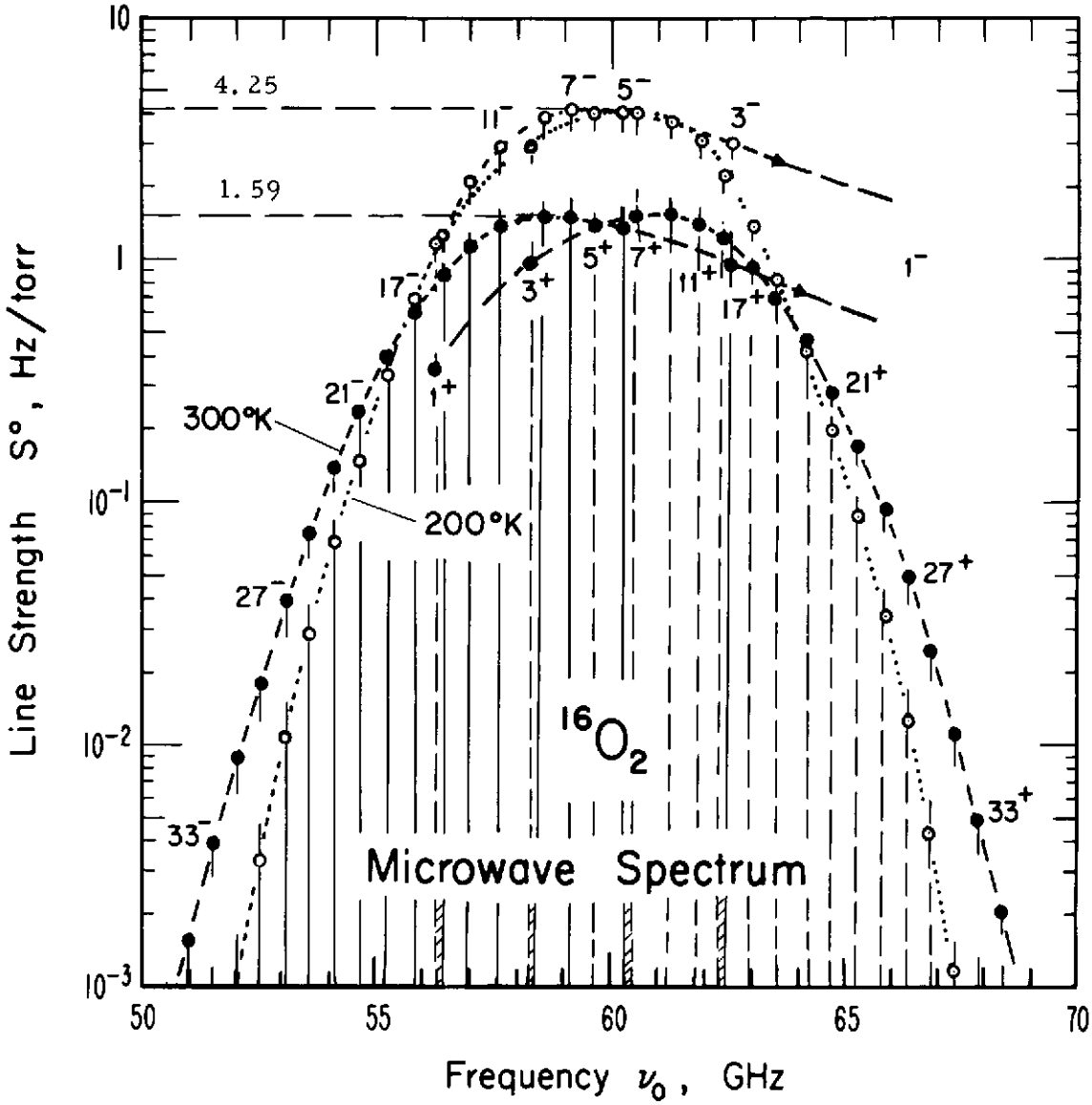

Figure 2. Line strength parameter for the O_2-MS at 200°K and 300°K. Numerical values at 300°K are listed in Table 3.

Table 4. Temperature Dependence ϑ of the Line Strength S°(300) of the O_2 Microwave Spectrum

LINE N±	Temperature T 180°K	200°K	220°K	240°K	260°K	280°K	300°K	320°K	340°K	w (280± 20°K)
1	4.5873	3.3518	2.5230	1.9464	1.5329	1.2287	1	0.8247	0.6881	2.99
3	4.3812	3.2382	2.4605	1.9131	1.5168	1.2227	1	0.8283	0.6937	2.91
5	4.0333	3.0434	2.3519	1.8547	1.4881	1.2119	1	0.8347	0.7039	2.78
7	3.5789	2.7824	2.2035	1.7734	1.4476	1.1965	1	0.8441	0.7189	2.59
9	3.0611	2.4747	2.0234	1.6724	1.3963	1.1766	1	0.8566	0.7390	2.33
11	2.5236	2.1411	1.8212	1.5556	1.3355	1.1525	1	0.8722	0.7646	2.02
13	2.0054	1.8021	1.6066	1.4272	1.2665	1.1245	1	0.8912	0.7962	1.65
15	1.5361	1.4755	1.3892	1.2914	1.1909	1.0928	1	0.9138	0.8346	1.22
17	1.1341	1.1752	1.1773	1.1525	1.1104	1.0579	1	0.9401	0.8805	.73
19	0.8071	0.9106	0.9779	1.0145	1.0265	1.0200	1	0.9706	0.9350	+ .18
21	0.5536	0.6863	0.7962	0.8808	0.9410	0.9796	1	1.0055	0.9993	- .42
23	0.3661	0.5032	0.6353	0.7542	0.8553	0.9372	1	1.0453	1.0750	-1.1
25	0.2333	0.3590	0.4969	0.6370	0.7709	0.8930	1	1.0904	1.1639	-1.8
27	0.1433	0.2491	0.3809	0.5306	0.6889	0.8476	1	1.1413	1.2684	-2.6
29	0.0849	0.1681	0.2862	0.4359	0.6104	0.8013	1	1.1988	1.3913	-3.5
31	0.0484	0.1104	0.2108	0.3532	0.5363	0.7546	1	1.2635	1.5361	-4.4
33	0.0266	0.0705	0.1522	0.2823	0.4672	0.7078	1	1.3363	1.7069	-5.3
35	0.0141	0.0438	0.1077	0.2226	0.4036	0.6613	1	1.4182	1.9091	-6.3
37	0.0072	0.0265	0.0747	0.1730	0.3457	0.6154	1	1.5103	2.1491	-7.4
39	0.0036	0.0156	0.0507	0.1327	0.2936	0.5704	1	1.6139	2.4351	-8.6
41	0.0017	0.0089	0.0338	0.1004	0.2472	0.5267	1	1.7306	2.7771	-9.8
43	0.0008	0.0050	0.0221	0.0749	0.2064	0.4844	1	1.8622	3.1877	-11

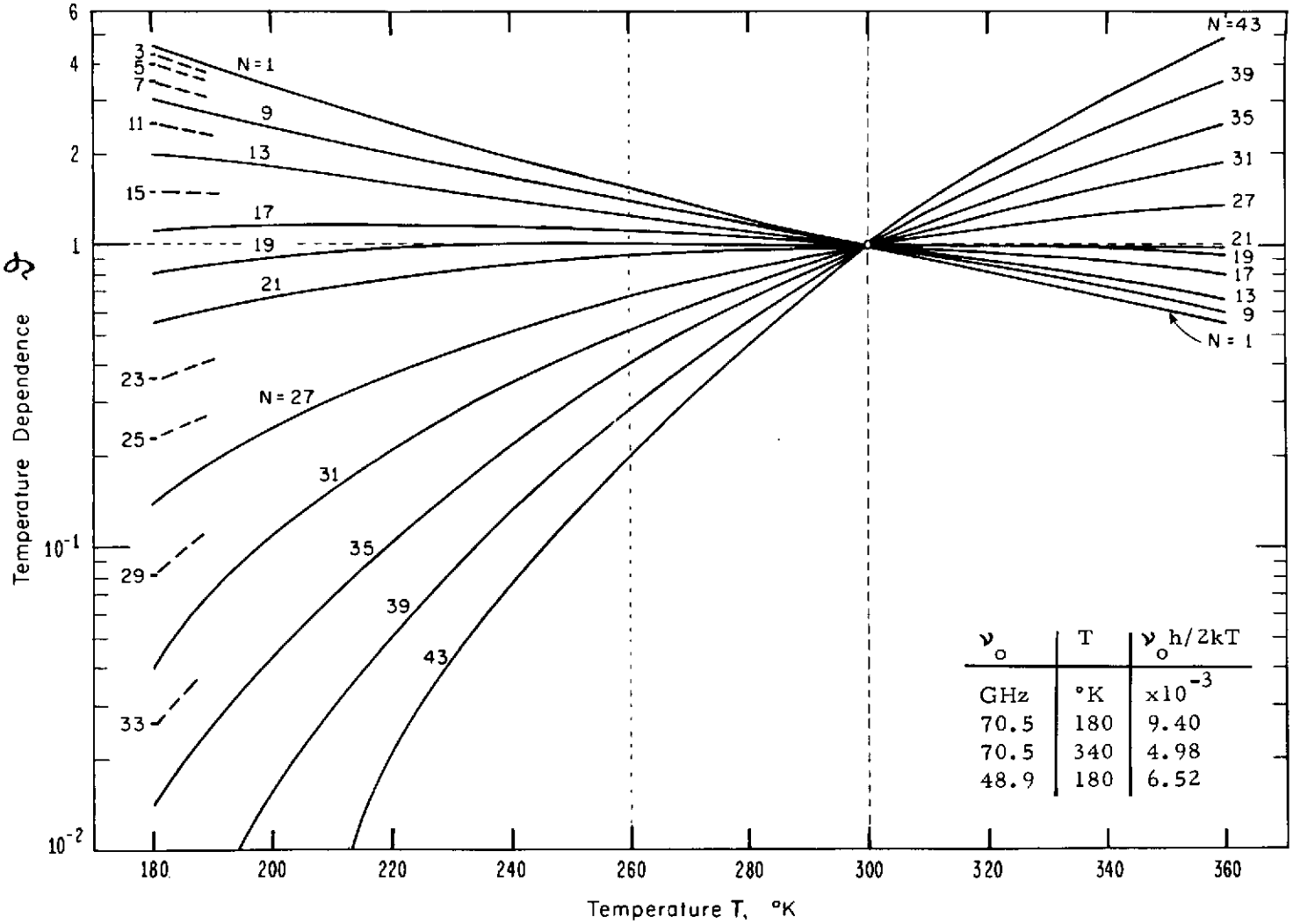

Figure 3. Temperature dependence ϑ of the line strengths S_i° (300). Numerical values are listed in Table 4.

Table 5. Frequency Shift η and Intensity Functions $f(M', N)$ for Zeeman-Components of O_2 Microwave Spectrum Lines (Eqs. 14, 15).

Initial State: N, J, $|M| \leq J$ Final State: N, J', $|M'| \leq J'$ Selection Rule: $\Delta M = M' - M$

Zeeman Transitions	Frequency Shift η (M,N)		Intensity Functions f(M',N) (Matrix Elements)	
	N^+ - Line	N^- - Line	N^+ - Line	N^- - Line
σ^+ ($\Delta M = 1$)	$\frac{M(1-N)+1}{N(N+1)}$	$\frac{M(N+2)+1}{N(N+1)}$	$\frac{3N(N+M'+1)(N+M'+2)}{4(N+1)^2(2N+1)}$	$\frac{3(N+1)(N+M')(N+M'-1)}{4N^2(2N+1)}$
π ($\Delta M = 0$)	$\frac{M(1-N)}{N(N+1)}$	$\frac{M(N+2)}{N(N+1)}$	$\frac{3N[(N+1)^2 - M'^2]}{(N+1)^2(2N+1)}$	$\frac{3(N+1)(N^2 - M'^2)}{N^2(2N+1)}$
σ^- ($\Delta M = -1$)	$\frac{M(1-N)-1}{N(N+1)}$	$\frac{M(N+2)-1}{N(N+1)}$	$\frac{3N(N-M'+1)(N-M'+2)}{4(N+1)^2(2N+1)}$	$\frac{3(N+1)(N-M')(N-M'-1)}{4N^2(2N+1)}$
	After Hill and Gordy (1954)		After Lenoir (1968)	

Example: N = 1

	$\eta(M,N)$				f(M',N)				f(N)
	M	σ^+	π	σ^-	M'	σ^+	π	σ^-	(Eq. 8)
1^+ Line	+ 1	0.5	0	0.5	+ 1	0.75	0.75	0.125	
	0	0.5	0	0.5	0	0.375	1	0.375	2.5
$J = 2 \rightarrow J' = 1$	- 1	0.5	0	0.5	- 1	0.125	0.75	0.75	
1^- Line					+ 1	1	0	0	
	0	0.5	0	0.5	0	0	2	0	2
$J = 0 \rightarrow J' = 1$					- 1	0	0	1	

2.4 Line Shapes of the Atmospheric O_2 Microwave Spectrum

The first complete theory of the atmospheric O_2-MS was given by Van Vleck (1947). As specific applications based on absorption (emission)properties of the O_2-MS evolved, the need for more detailed spectroscopic information was developed. Especially the works of Meeks and Lilley (1963), Lenoir (1968), Wilheit (1969), Waters (1970), and Westwater (1970) expanded and refined the theory of the atmospheric O_2-MS for purposes of remote sensing atmospheric temperature structures.

The molecular theory of the pressure-broadened O_2-MS was advanced by Dillon and Godfrey (1969, 1972) and Mingelgrin (1972). Both treatments are based on an intermolecular potential model for O_2-O_2, O_2-N_2, O_2-Ar interactions, and scattering calculations of the trajectories for rotational and translational motions. Dillon-Godfrey treat the rotational trajectories quantum-mechanically up to $N = 7$. Mingelgrin solves both trajectories classically up to $N = 23$, however, the approximate nature of this assumption is expected to yield width parameters which are slightly larger than the true ones (R. Gordon, private communication, 1973).

Measured high-pressure (3 to 40 ktorr) absorption rates of pure O_2 and O_2-Ar, O_2-N_2 mixtures over the 48 to 81 GHz range (Mingelgrin et al., 1972) are reproduced by the theoretical calculations. Implications of both theories to the atmospheric O_2-MS are discussed in Section 2.4.1.

In treating the intensity distribution (line shapes F', F'') of the O_2-MS it is assumed that the microwave power flux density is sufficiently low that nonlinear saturation effects are avoided. As a result, the integrated area of each absorption line is proportional to the number of possible transitions (numbers of molecules)* or, on a macroscopic

*The number of molecules per cm^3 equals $9.662 \cdot 10^{18} \cdot p/T$ (ideal gas law).

scale, to pressure. The line strengths S_i (Sect. 2.3.2) have been defined as scale factors to the area $\pi \cdot n''_o \cdot \gamma$ (Eqs. 18, 19), which is that of a Lorentzian shape (Fig. 4). While the theory of spectral properties relating to the O_2 molecule is well understood, this is not the case for the intensity distribution, especially when considering the full range of conditions specified by equation (3). The atmospheric O_2-MS for pressures above 1 torr is broadened by binary collisions (Sect. 2.4.1); for pressure below 1 torr, the gradual transition from collision-to Doppler-broadening is described by a Voigt profile (Sect. 2.4.3).

2.4.1 Pressure Broadening of the O_2 Microwave Spectrum

In the simple case of a single, pressure-broadened line, theory predicts the Lorentzian line shape to be valid when $\gamma << \nu_o$ (e.g., Dillon, 1969). The frequency, normalized to a multiple of the width γ, is

$$z = (\nu_o - \nu)/\gamma \qquad [1] \ , \tag{16}$$

yielding the shape factors in the following form:

Extinction	Dispersion
$F'' = 1/\gamma(1+z^2)$	$F' = z/\gamma(1+z^2)$. $[1/\mathrm{Hz}]$

The approximations for the wing regions ($z >> 1$) are (17)

$$F'' \approx \gamma/(\nu_o - \nu)^2 \quad \text{and} \quad F' \approx 1/(\nu_o - \nu) \ .$$

The peak extinction, for $z = 0$ ($\nu = \nu_o$) is	The peak dispersion for $z = 1$ ($\nu = \nu_o \pm \gamma$) is
$n''_o = S/\gamma$	$\Delta n_o = S/2\gamma$ (17a)

This yields the two line profiles in the form

$$n'' = n''_o/(1+z^2) \quad \text{and} \quad \Delta n = \Delta n_o \, 2z/(1+z^2) \ . \ [1] \tag{18}$$

Figure 4 gives a graphical presentation of the equations above. The linewidth γ can be expressed for atmospheric air by (Liebe, 1969a)

$$\gamma = \gamma^{\circ}(300) \left\{ m_d (300/T)^u \cdot p + m_w (300/T)^v \cdot p_w \right\} . \quad [\mathrm{MHz}] \qquad (19)$$

Table 6 shows the large body of width parameters $\gamma^{\circ}(300)$, which exists for pure oxygen ($m_d = 1$). The other quantities of equation (19) are m_d and m_w, the broadening efficiencies for dry air and water vapor, and u and v, the associated temperature dependences. The arrangement of $\gamma^{\circ}(300)$ versus the quantum number N in Figure 5 seems to support the theoretically predicted N-dependence (Dillon and Godfrey, 1972; Mingelgrin, 1972), although the experimental data (some are claimed to be accurate to ± 5 percent) are spread over a large range (± 20 percent). The uncertainties of γ are one of the largest sources of error in a reliable description of the atmospheric O_2-MS (Liebe, 1969b).

The isolated line is a good candidate for quantitative experimental work on the O_2-MS. From measured values of Δn and/or n'' one needs to determine the quantities (Eqs. 18 and 19)

$$\nu_o \quad - \quad S^{\circ}(300) \cdot \vartheta(T) \quad - \quad \gamma^{\circ} , \; m_d , \; m_w , \; u, \; v \quad .$$

Profiles of n'' and Δn close to a line center ($|\nu_o - \nu| \lesssim 10$ MHz) and at low pressures (< 1.5 torr) for different values of H can establish the validity of equations (14) and (15). O_2-MS measurements are in progress in our group using dispersion and absorption pressure-scanning spectroscopy (Liebe et al., 1973).

So far, we have measured the 9^+ line and obtained the following preliminary results (Liebe and Welch, 1972): (20)

(a) $\nu_o(9^+)$ – the value is given in Table 2. A pressure-induced shift of ν_o was not detectable (< ± 10 KHz/torr for p ≤ 50 torr) which agrees with predictions (Dillon and Godfrey, 1972).

(b) $S^{\circ}(300)\cdot\vartheta(T)$ - the agreement with calculated values (Tables 3 and 4) was within ±5 percent between 250 and 325°K. More careful work at 300°K yielded agreement within ± 1 percent.

(c) F', F'' - the shape factors were verified as being Lorentzian. The pertinent width parameters were $\gamma^{\circ}(300) = 1.81$ [MHz/torr] ± 2 percent, $m_d = 0.93$, $u = 0.87$, $m_w = 1.25$, and $v \approx 1$ (assumed).

(d) The experimental Δn_o versus $|\nu_o - \nu|$ profile at H = 0.53 [gauss] was in good agreement with "Zeeman" calculations. The responses of Δn and n'' at H = 0.53 [gauss] were undistinguishable from those measured for $H \approx 0$ for $p > 1.5$ torr and $|\nu_o(9^+) - \nu| > 10$ MHz.

(e) The comparison between air and oxygen dispersion yielded $[\Delta n_o(\text{Air})/\Delta n_o(O_2)] = 0.225$ ($\equiv r_1/m_d$ according Eqs. 18, 19).

For atmospheric O_2-MS calculations, we have arranged the relevant spectroscopic parameters in Table 7 by order of increasing frequency. The theoretical width values by Dillon-Godfrey (1972) are listed, but they have been scaled up by a factor 1.14 to match our experimental $\gamma^{\circ}(9^+)$ value. A computer summation of contributions (Eq. 4) from 44 lines of the O_2-MS for six different pressures revealed the spectra shown in figures 6 through 8. The calculation used the $S^{\circ}(300)$ values of Table 7 and $\gamma_i^{\circ} = 1.6$ MHz/torr. Pressures chosen are representative for $h \approx 30$ to 0 km. We conclude from these results that the atmospheric O_2-MS needs to be discussed separately for three pressure ranges:

I - Isolated Line Spectrum for $p < 10$ torr (Fig. 6).

II - Continuum Spectrum for $p > 300$ torr (Fig. 8), where the envelope is determined by all lines.

I/II - Mixture of I and II (Fig. 7).

In range II, the addition of individual line responses (Beer-Lampert law) may not be a valid procedure since collisions do alter the energy levels to an extent that they can interfere with each other. Mingelgrin (1972) included overlap effects in his calculations, which are compared with the pressure-linear width model (Eq. 19) in Figure 9. A substantial narrowing can be noticed above 100 torr. For standard conditions (760 torr, 298°K) the difference in peak intensity at 60 GHz is as high as +28 percent. Overlap effects between N^+ and N^- lines have been computed by Dillon (1969) and found to be insignificant for standard conditions. These contradicting predictions need to be clarified through analysis of reliable experimental continuum data.

A necessary condition for overlap in the coalescence of extinction line shapes (Eq. 17) under the influence of pressure-broadening. Table 7 reveals 8 lines where the separation ε of the centers is only about 1/5 of the normal spacings. These doublets overlap with increasing pressure first. A second condition comes from pressure-broadening theory, which predicts different sensitivities of the energy levels to mutual interferences. Approximately, one can treat the individual linewidths as being no longer proportional to pressure and formulate

$$\gamma_c(\text{range II}) \approx \gamma_i^\circ p - \delta(\varepsilon, p, N) \quad . \tag{21}$$

For example, the 760 torr attenuation profile by Mingelgrin (Fig. 9) can be fitted approximately by assuming for the doublets a linewidth of one-half of the isolated width. Thus the doublets may be responsible for most of the overlap effects of the atmospheric continuum O_2-MS. Considering only overlap factors δ for these line pairs would simplify computations of the continuum O_2 spectrum.

An empirical width model was introduced by Meeks and Lilley (1963) to reconcile atmospheric attenuation rates between the line

spectrum (I) and the continuum spectrum (II). Zenith attenuation data (see Table 10) have been fitted with this model whereby over the range of the continuum spectrum, γ was reduced to 1/2 (Carter et al., 1968) or even to 1/3 (Reber, 1972). This will be treated further in Sections 3.1 and 2.

2.4.2 Nonresonant O_2-Spectrum

In a classical picture the molecular dipole is unable to follow completely the oscillating field. Thus, after every collision there is a preferred reorientation relative to the field. Formally, collisions induce transitions between identical energy levels under the selection rule, $\Delta J = 0$ and $\Delta N = 0$. As a consequence, increasing pressure ($p > 100$ torr) adds to the O_2-MS a non-resonant contribution which is centered at $\nu = 0$ Hz and can be described by a Debye-type polarization (VanVleck, 1947; Zhevakin and Naumov, 1967) which is

$$n''_n = S_o F''_o \quad \text{and} \quad \Delta n_n = S_o F'_o \quad . \tag{22}$$

The Debye shape factors are

$$F'' = 2\nu\gamma_o / (\nu^2+\gamma^2) \quad \text{and} \quad F' = \left[\gamma_o^2 / (\nu^2+\gamma_o^2)\right] - 1 \quad . \tag{23}$$

The O_2 dispersion spectrum at 760 torr was calculated ($\nu = 0$ to 80 GHz; $N \leq 25$) by Mingelgrin (1972), and from the result, which is shown in Figure 22, we can deduce approximate values of strength and width

$$S_o \approx 5.2 \cdot 10^{-10} (300/T)^2 \cdot r_1 \cdot p \,, \qquad [1/\text{torr}] \,, \tag{24}$$

$$\gamma_o \approx 1.8 (300/T) \cdot p \,, \qquad [\text{MHz/torr}] \,.$$

The example for standard condtions at sea level (760 torr, 300°K) shows that at microwave frequencies the nonresonant part is small when

compared with the much larger resonance part and it can very well be neglected in the remainder of this report:

ν [GHz]	1.37 (γ_o)	40	90	140
α_n [dB/km]	.021	.041	.041	.042
$\Delta\phi_n$ [rad/km]	-.001	-.070	-.157	-.244

2.4.3 Transition to Doppler Broadening (Voigt Profile)

As the pressure decreases with altitude (Eq. 3), we have to consider another broadening mechanism - the Doppler effect. The transition frequency of a non-colliding molecule moving with velocity c_m in respect to the radiation field is $\nu_o[1+(c_m/c)]$. The velocity distribution of gas molecules in thermal equilibrium is Maxwellian. The resulting Gaussian intensity distribution has a linewidth γ_D which depends on temperature. The pressure-independent width γ_D makes the peak intensity proportional to pressure, thus forcing the atmospheric O_2 line spectrum to vanish. The equation for γ_D (see Table 8) yields the following values for $^{16}O_2$:

T[°K]	γ_D [kHz]		
	At ν_o = 68.49	and at	49.96 [GHz]
180	59.1		42.5
290	74.9		53.9

using

$$\gamma_D = 6.34 \cdot 10^{-8} \cdot \nu_o \cdot \sqrt{T} \quad . \quad [\text{Hz}] \qquad (25)$$

The Gaussian shape of a Doppler-broadened line is for extinction (F'') a little broader at the center but decreases much more rapidly in the wings when compared to a Lorentzian. A normalization factor,

$\sqrt{\pi \ln 2}$ is introduced for the Gaussian (area = $n''_o \cdot \gamma \cdot \sqrt{\pi / \ln 2}$) in order to match the Lorentzian (area = $n'_o \cdot \gamma \cdot \pi$) integrated strength (Table 8).

A convoluation of the two shape functions leads to a Voigt profile whereby it is assumed that the free motion of molecules is unaffected by collisions ("pressure" and "temperature" are statistically independent) which is not exactly true. The reduced mathematical expressions for the Voigt function are given in Table 8. The Voigt parameters

$$y = \gamma^\circ p / \gamma_D \quad \text{and} \quad x = \Delta\nu / \gamma_D \tag{26}$$

govern the extinction profile $u(x, y) \equiv n''/ n''_o$ and the dispersion profile $v(x, y) \equiv \Delta n / \Delta n_o$ as shown in Figure 10. For $y < 0.1$ the shape is practically Gaussian, and for $y > 10$ the shape is Lorentzian. As the pressure goes to zero ($y < 0.1$), the rate for the Lorentzian values n''_o and Δn_o to approach zero becomes $0.678\ S^\circ p / \gamma_D$ for the max. extinction n''_o and $0.610\ S^\circ p / \gamma_D$ for the max. dispersion Δn_o (see Figs. 10 and 11). Figure 11 also gives the corresponding frequency loci of Δn_o (p) and γ(p). In principle, the Voigt profile has to be applied to each Zeeman component in the presence of a magnetic field H.

2.5 Attenuation and Dispersion Due to Water Vapor

Two rotational lines of H_2O are centered on either side of the 40 to 140 GHz band. The low-frequency wing of the complete H_2O rotational spectrum and additional polarization mechanisms also contribute to atmospheric millimeter wave transmissivity. We can separate the resonance contributions from the remainder (q) and define:

$$n''_w(\nu) = \sum_{i=1}^{2} S_i F''_i + q''_w \qquad \Delta n_w = \sum_{i=1}^{2} S_i F'_i + q'_w \ . \tag{27}$$

The resonant contributions by the two H_2O lines adjacent to the frequency band under consideration can be evaluated using the following spectroscopic parameters (Liebe, 1969a)

i	1	2
ν_o [GHz]	22.235 15	183.310 12
S [Hz]	$13.9\left(\frac{300}{T}\right)^{3.5} \cdot \exp\left[2.14\left(1-\frac{300}{T}\right)\right] \cdot p_w$	$322\left(\frac{300}{T}\right)^{3.5} \cdot \exp\left[0.653\left(1-\frac{300}{T}\right)\right] \cdot p_w$
γ [MHz/torr]	$18.0\left[0.209\left(\frac{300}{T}\right)^{0.6} \cdot p + \left(\frac{300}{T}\right) \cdot p_w\right]$	$19\left[0.21\left(\frac{300}{T}\right)^{0.6} \cdot p + \left(\frac{300}{T}\right) \cdot p_w\right]$

The Gross shape was found to give a better fit of experimental data in the wings of strongly foreign-gas-broadened lines,

$$F'_G = 2\nu_o (\nu_o^2 - \nu^2)/[(\nu_o^2 - \nu^2)^2 + (2\nu\gamma)^2], \quad [1/\text{Hz}]$$
$$F''_G = 4\nu^2\gamma/[(\nu_o^2 - \nu^2)^2 + (2\nu\gamma)^2] . \quad [1/\text{Hz}] \qquad (28)$$

An example for $p_w = 10$ torr under standard conditions, $p = 760$ torr and and 300°K, yields the following resonance contributions (Eqs. 2, 27, 28)

ν[GHz]	$22^{(\nu_o)}$	40	60	80	100	120	140	$183^{(\nu_o)}$
α_w [dB/km]	.194	.016	.009	.010	.017	.038	.106	33.8
$\Delta\phi_w$ [rad/km]	.001	.026	.047	.071	.103	.153	.245	.017

These contributions are by far not enough to account for millimeter wave H_2O attenuation. Laboratory measurements at two frequencies produced results shown in Figure 12. Experimental uncertainties are on the order of 10 percent. A tentative fit of the data was

accomplished by (Liebe et al., 1973)

$$\alpha(q''_w) \approx \left\{3\, p_w \left(\frac{\nu}{61}\right)\left(\frac{300}{T}\right)^{2.4} + 0.8\, p_w^2 \left(\frac{\nu}{61}\right)^{2.6} \cdot \left(\frac{300}{T}\right)^{10}\right\} \cdot 10^{-3}, \quad [\mathrm{dB/km}] \tag{29}$$

where the frequency ν is in gigahertz.

The term linear with p_w indicates roughly the contribution expected from the residual water vapor attenuation due to the low frequency wing of the rotational spectrum. VanVleck (1947) estimated for this term the following amount (Liebe, 1969a)

$$\alpha \approx 1.9 \cdot 10^{-9} \cdot \nu^2 \cdot p_w / T^{2.5} \quad , \quad [\mathrm{dB/km}] \quad ,$$

which yields at 61 GHz and 300°K the value $4.5 \cdot 10^{-3}$ [dB/km torr].

The p_w^2 term, however, points to pressure-induced polarization effects such as dimerization. Noteworthy are the temperature dependence. An Arrhenius plot, $\log \alpha$ versus T^{-1}, yields a "binding energy" of 4.5 [kcal/mole] ± 10%. The p^2 term gives rise to abnormal high attenuation when saturation (p_S) is approached. A similar p^2 response was measured for the dispersion $q'_w = n'(\nu_1) - n'(\nu_1/2)$ for ν_1 at 61.2 GHz (T = 280 and 325°K). The sketchy experimental evidence of unaccounted, pressure-induced polarization in water vapor certainly warrants a more careful study of $\alpha(q''_w)$ and q'_w over a wider rang of millimeter wave frequencies and close to saturation pressures $p_S(T)$. Such experiments can shed light on the fact that the theory of the rotational H_2O spectrum does yield atmospheric attenuation values in the wings of the two microwave spectral lines which are too low when compared with measured data.

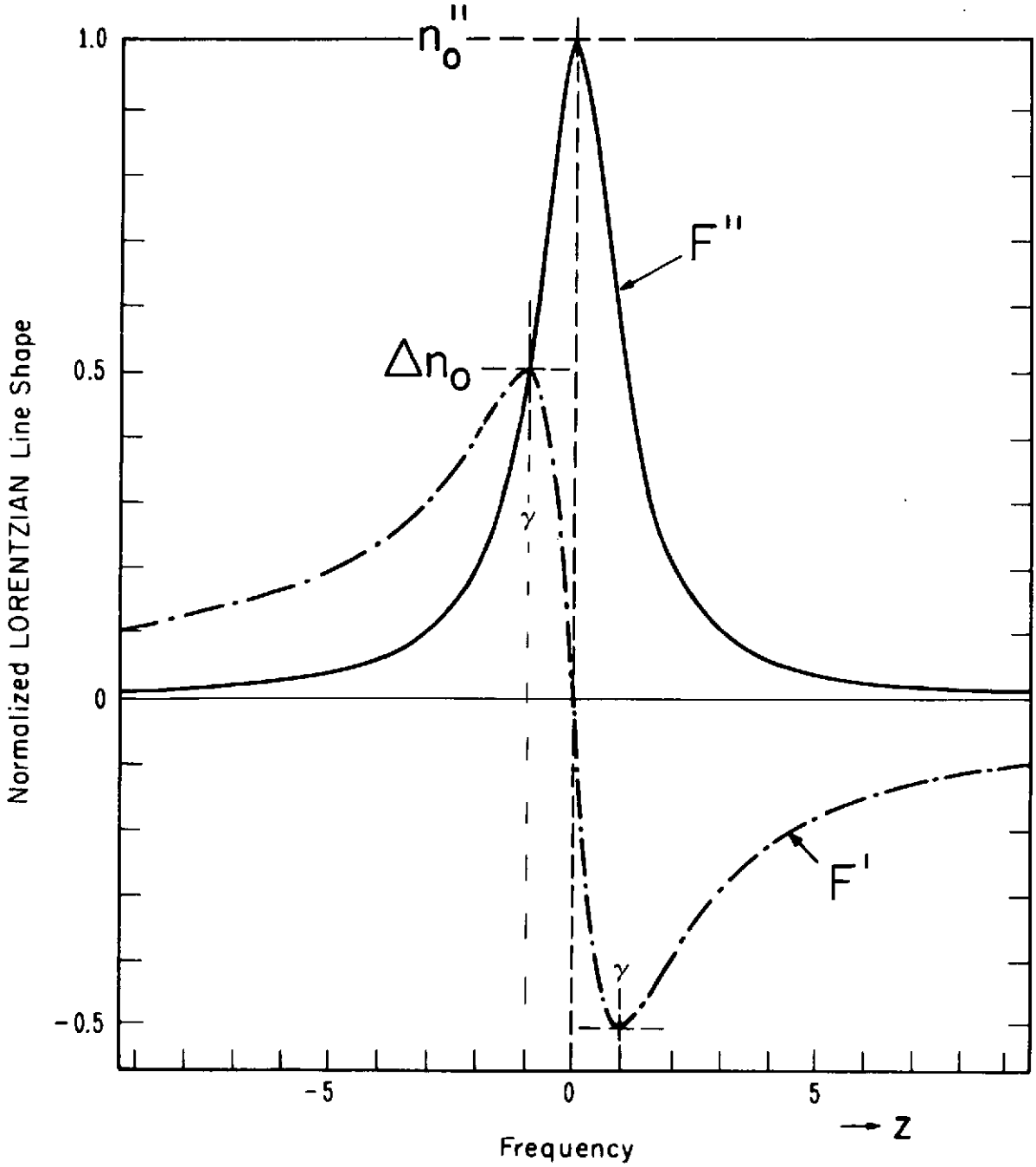

Figure 4. Normalized ($S = \gamma$) Lorentzian shape of an isolated pressure-broadened line for dispersion (F') and extinction (F''). The normalized frequency z indicates multiples of the width γ.

Table 6. Reported width parameters $\gamma^{o}(300)$ and their temperature dependency u for self-pressure broadened lines of the O_2 Microwave Spectrum.

N±	$\gamma^{o}(300)$ in MHz/torr Theory (a)	Theory (b)	Experiment (c)	Experiment (d)	Experiment (e)	Experiment (f)	Experiment (h)	Experiment (i)	Experiment (k)	Experiment (l)	u (b)	u (c)	u (d)	u (e)	u (k)	u (f)
1+	2.37	2.015				-		2.20	-	1.96	.80				-	-
-		1.870				1.90[g]		-	1.97	-					.90	
3+	2.35	1 682				1.86[x]	1.96	2.23	2.07	1.71	.81				.85	2
-		1.680				--	1.96	-	-	1.92					-	-
5+	2.05	1.611				1.72[x]	1.56	1.96[x]	1.80	1.86	.79				.88	2
-						1.98[x]	1.60	1.99[x]	-	-					-	2
7+	2.10	1.592				1.73[x]	1.68	1.92[x]	-	2.05	.79				-	2
-						1.53[x]	1.70	1.82[x]	2.01	-					.84	2
9+	1.95	(1.59)	1.81			1.78[x]	1.42	1.93[x]	-	-		.85			-	2
-			-			1.48[x]	1.64	2.00[x]	1.94	1.97					.71	2
11+	1.95	(1.59)		1.88	1.79	1.56[x]	1.60	-		1.97			1.0	0.85		2
-						--	--	1.97		-						-
13+	1.91	(1.59)				Reduced from	1.54	-		-						
-							-	1.86[x]		1.87						
15+	1.71	(1.59)				310 to 300°K	-	-		1.77						
-							-	1.99		-						
17+	1.73	(1.59)					1.50	-		-						
-								-		1.76						
19+	1.58	(1.59)						-		1.58						
-								1.92		1.62						
21+	1.60	(1.59)								-						
-						x ± 5 percent rms				1.26						
23+	1.52	(1.59)								1.26						
-										1.29						

References: (a) Mingelgrin (1972)
(b) Dillon (1969)
Dillon & Godfrey (1972)
(c) Liebe & Welch (1972)
(d) Reber (1972)
(e) Carter et al. (1968)
(f) Stafford & Tolbert (1963)
(g) Schulze & Tolbert (1963)
(h) Zimmerer & Mizushima(1961)
(i) Artmann & Gordon (1954)
(k) Hill & Gordy (1954)
(l) Anderson et al. (1952)

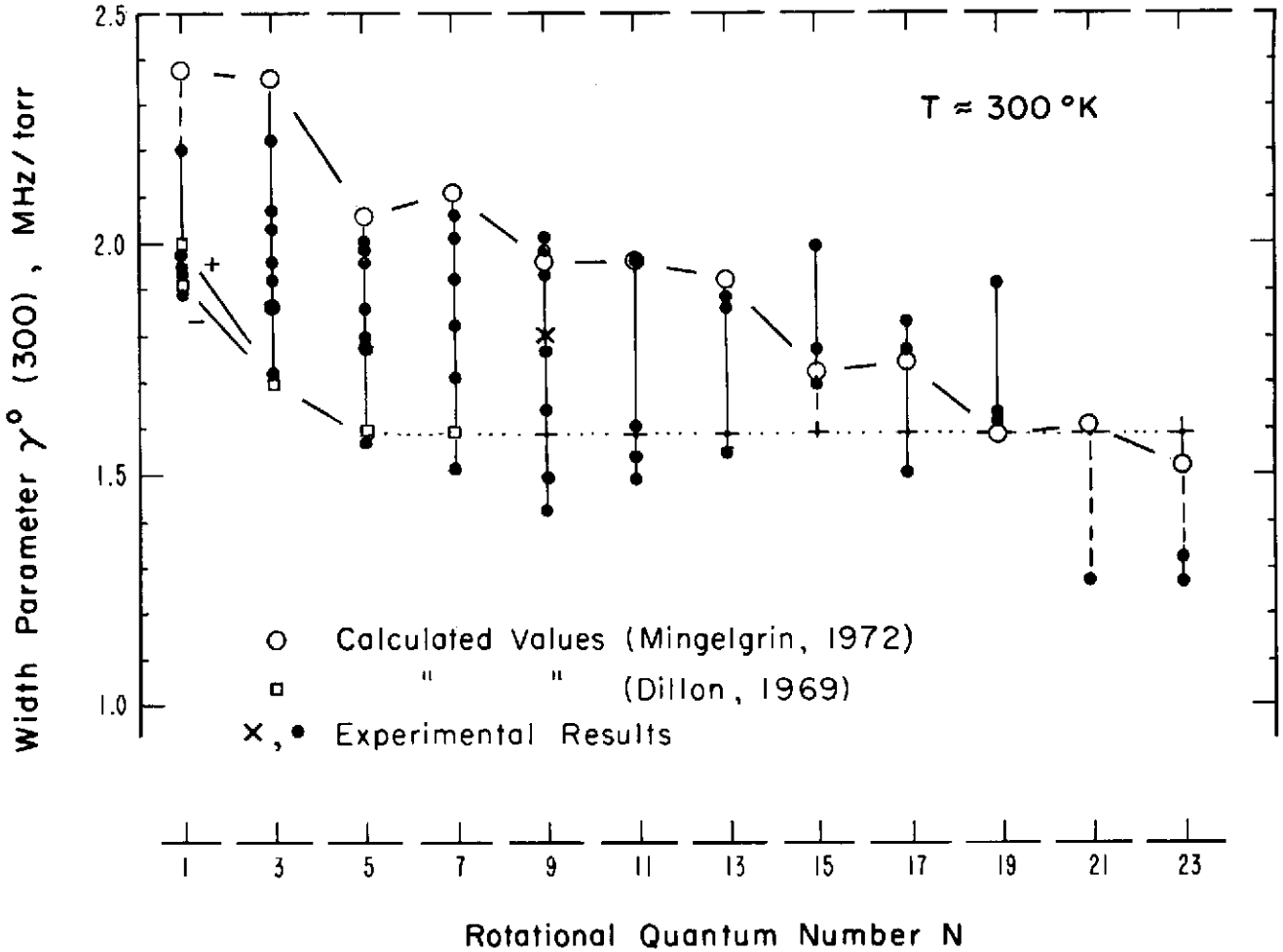

Figure 5. Reported line width parameter $\gamma^{o}(300)$ for the self-pressure broadened O_2 Microwave Spectrum (see Table 6) versus the quantum number N for end-over-end rotational angular momentum.

Table 7. Spectroscopic parameters of the O_2 microwave spectrum used for computations of this report.

i	ν_o	N +	N −	T = 300° K S°(300)	T = 300° K γ°(300)	Remarks
				[1/torr]	[MHz/torr]	Nonreson.
0	0	1 to 25		$5.2 \cdot 10^{-10}$	1.8	Spectrum
	[GHz]			[Hz/torr]		
1	48.942 4		43	.000 024	1.81	
	49.451 4		41	.000 073	1.81	
	49.961 8		39	.000 216	1.81	
	50.473 6		37	.000 598	1.81	
5	50.987 3		35	.001 564	1.81	
	51.503 02		33	.003 860	1.81	
	52.021 17		31	.008 985	1.81	
	52.542 23		29	.019 707	1.81	
	53.066 80		27	.040 717	1.81	
10	53.595 68		25	.079 186	1.81	
	54.129 96		23	.144 84	1.81	
	54.671 145 (20)		21	.248 87	1.81	
	55.221 372 (20)		19	.401 19	1.81	ε
	55.783 819 (20)		17	.605 61	1.81	[MHz]
15	56.264 778 (10)	1		.348 69	2.29	Doublet
	56.363 393 (20)		15	.853 87	1.81	98.62
	56.968 180 (20)		13	1.120 4	1.81	
	57.612 49		11	1.359 5	1.81	
	58.323 885 (10)		9	1.515 0	1.81	Doublet
20	58.446 580 (10)	3		.925 05	1.91	122.72
	59.164 215 (10)		7	1.526 3	1.81	
	59.590 978 (10)	5		1.341 0	1.83	
	60.306 044 (10)		5	1.348 7	1.83	Doublet
	60.434 776 (10)	7		1.562 6	1.81	128.74
25	61.150 565 (5)	9		1.589 9	*1.81	
	61.800 169 (10)	11		1.458 8	1.81	
	62.411 223 (10)	13		1.227 2	1.81	Doublet
	62.486 255 (10)		3	.963 36	1.91	75.03
	62.998 00	15		.954 01	1.81	
30	63.568 520 (10)	17		.689 76	1.81	
	64.127 777 (20)	19		.465 60	1.81	
	64.678 92	21		.294 21	1.81	
	65.224 120 (20)	23		.174 37	1.81	
	65.764 744 (20)	25		.097 074	1.81	
35	66.302 06	27		.050 820	1.81	
	66.836 77	29		.025 041	1.81	
	67.369 51	31		.011 621	1.81	
	67.900 73	33		.005 083	1.81	
	68.430 8	35		.002 096	1.81	
40	68.960 1	37		.000 815	1.81	
	69.488 7	39		.000 299	1.81	
	70.016 9	41		.000 104	1.81	
	70.544 9	43		.000 034	1.81	
44	118.750 343 (10)		1	.597 25	2.13	Isolated Line

*Experimental value (Liebe et al., 1973)

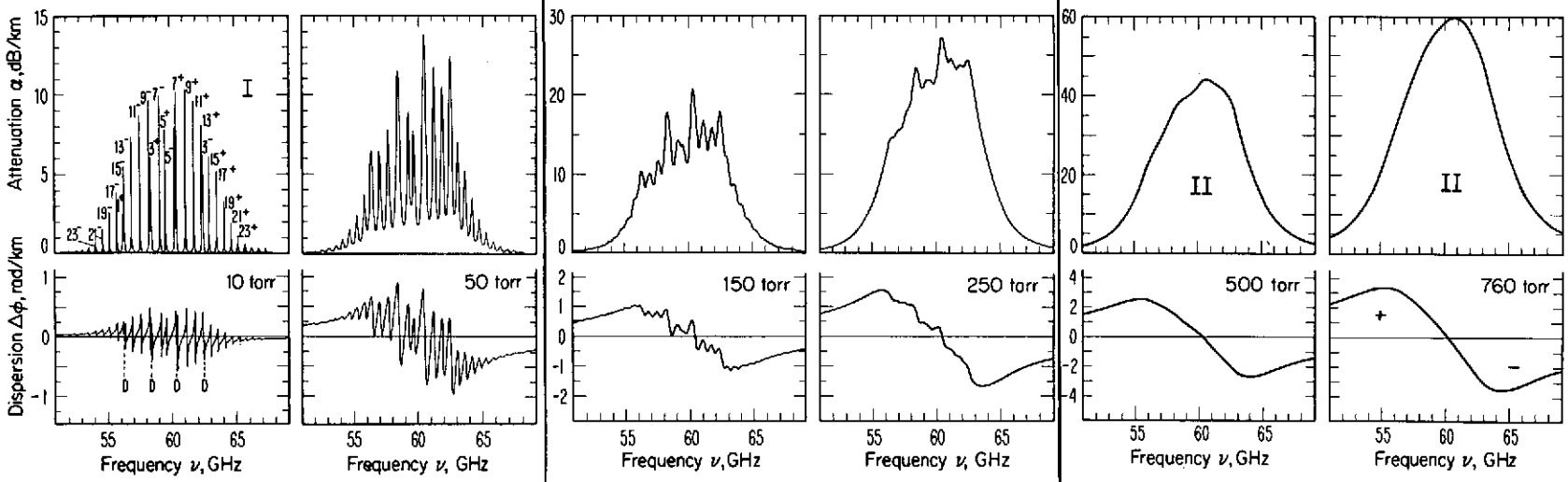

D-Doublet (Table 7)

Figure 6

Figure 7

Figure 8

Figure 6 - 8. Computer plots of the pressure-broadened O_2 Microwave Spectrum for six different pressures (10 to 760 torr) corresponding to altitudes between $h \approx 30$ and 0 km. The model of linear addition of individual Lorentzians was used ($T = 300°K$, $\gamma_i^\circ = 1.6$ MHz/torr).

For analysis of atmospheric conditions see Figures 14 through 17.

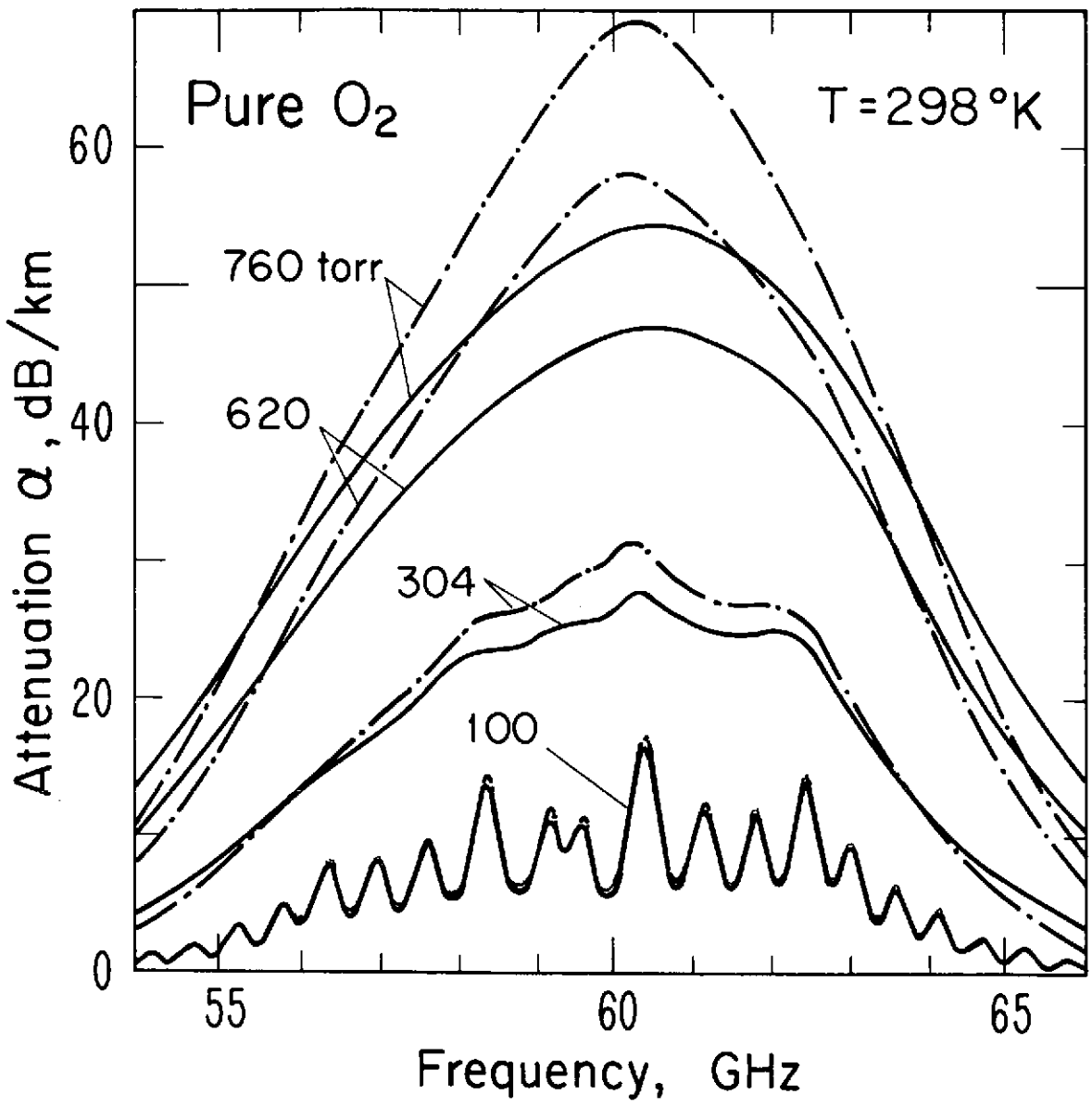

Figure 9. Attenuation of oxygen between 54 and 66 GHz at four different pressures.
Solid lines: Linear addition of Lorentzians (see Figs. 6-8) using Mingelgrin's width parameters (Table 6).
Dashed lines: Scattering calculation by Mingelgrin (1972).

Table 8. Shape Function for an Isolated Spectral Line

Line Profile	Broadening Mechanism	Refraction Spectrum	Extinction Spectrum
LORENTZIAN (See Fig. 4)	Pressure p (Collisions) $\gamma = \gamma^{\circ} p$	$F' = \left(\frac{z}{1+z^2}\right)\frac{1}{\gamma}$	$F'' = \left(\frac{1}{1+z^2}\right)\frac{1}{\gamma}$
		"Frequency" $z = (\nu_o - \nu)/\gamma$	
VOIGT (See Fig. 10, $y \neq 0$)	Convolution between Gaussian and Lorentzian	$v(x,y) = \int_{-\infty}^{\infty} \frac{e^{-(x')^2}(x-x')}{(x-x')^2 + y^2}\,dx'$	$u(x,y) = y\int_{-\infty}^{\infty} \frac{e^{-(x')^2}}{(x-x')^2 + y^2}\,dx'$
		"Frequency" $x = (\nu_o - \nu)/\gamma_D$	
		"Pressure" $y = \gamma/\gamma_D$	
GAUSSIAN (See Fig. 10, $y = 0$)	Doppler Effect due to T (Velocity distribution). Doppler width, $\gamma_D = (\nu_o / c)\sqrt{2\,kT/M}$ M - molecular mass	$F' = \frac{4\sqrt{\ln 2}}{\gamma_D} \exp[-\ln 2 x^2] \int_o^{x\sqrt{\ln 2}} \exp (x')^2\,dx'$ Dawson's Function[a]	$F'' = \frac{\sqrt{\pi \ln 2}}{\gamma_D} \exp(-\ln 2 x^2)$

(a) Miller and Gordon (1931).

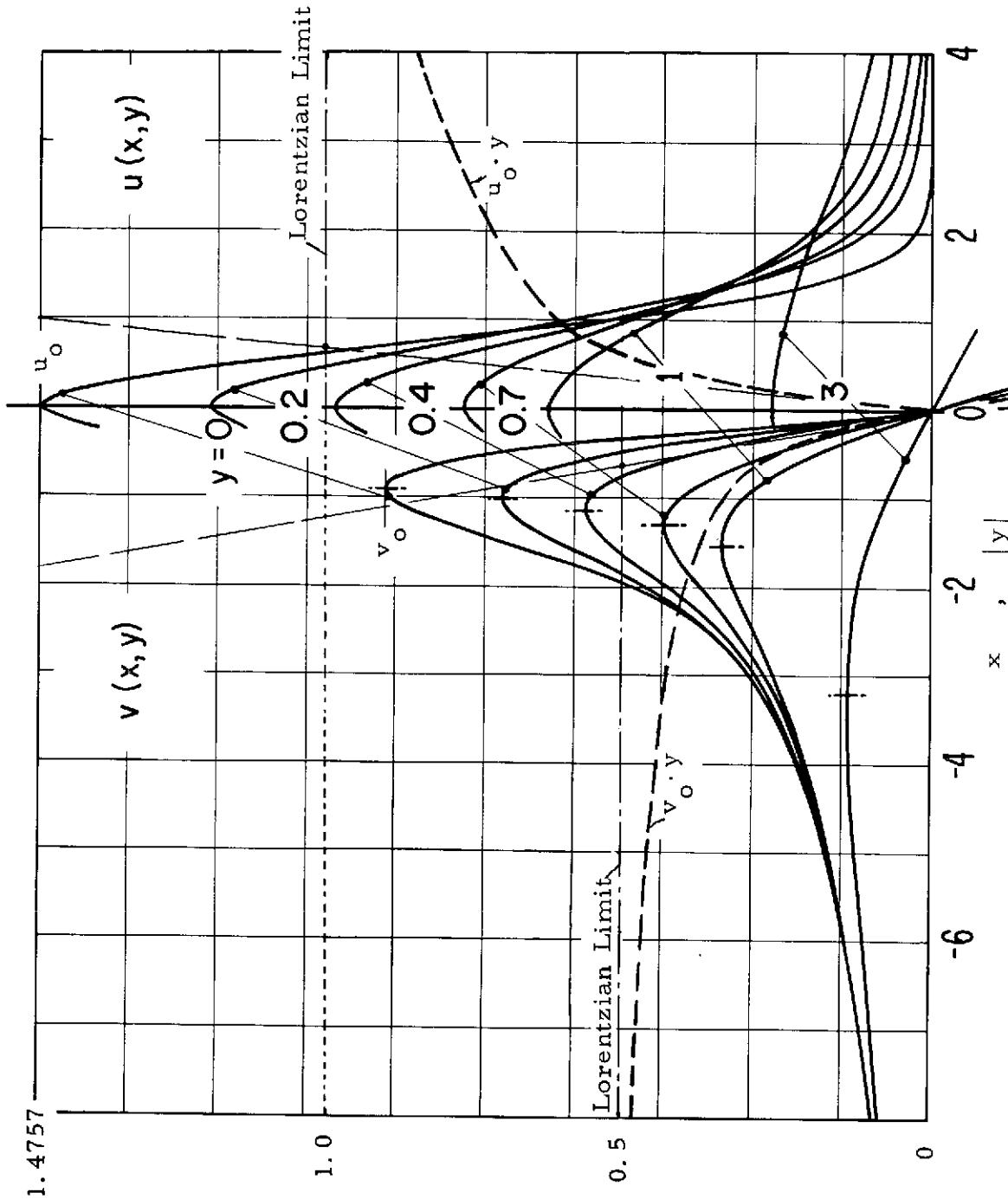

Figure 10. Normalized Voigt profiles for dispersion $v(x,y)$ and extinction $u(x,y)$ (Faddeyea and Terent'ev, 1961). The mathematical functions are given in Table 8.
"Frequency" $x = (\nu_o - \nu)/\gamma_D$, solid-line curves.
"Pressure" $y = \gamma^o\, p/\gamma_D$, dashed-line curves.

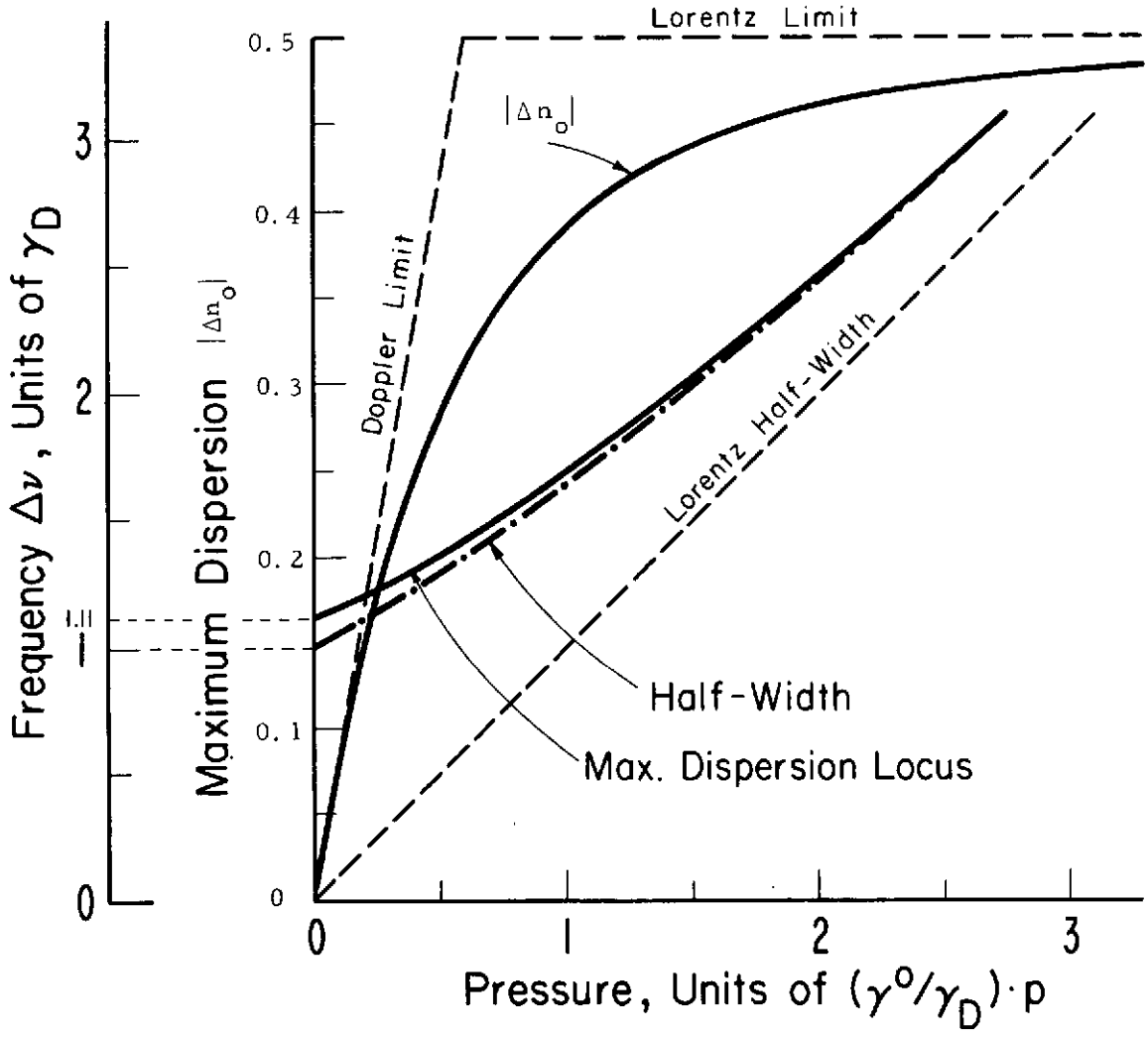

Figure 11. Frequency loci of the maximum dispersion $|\Delta n_o|$ and line half-width (γ) for a Voigt profile. Also shown is the normalized amount of $|\Delta n_o|$. The ordinate is in normalized pressure units (y).

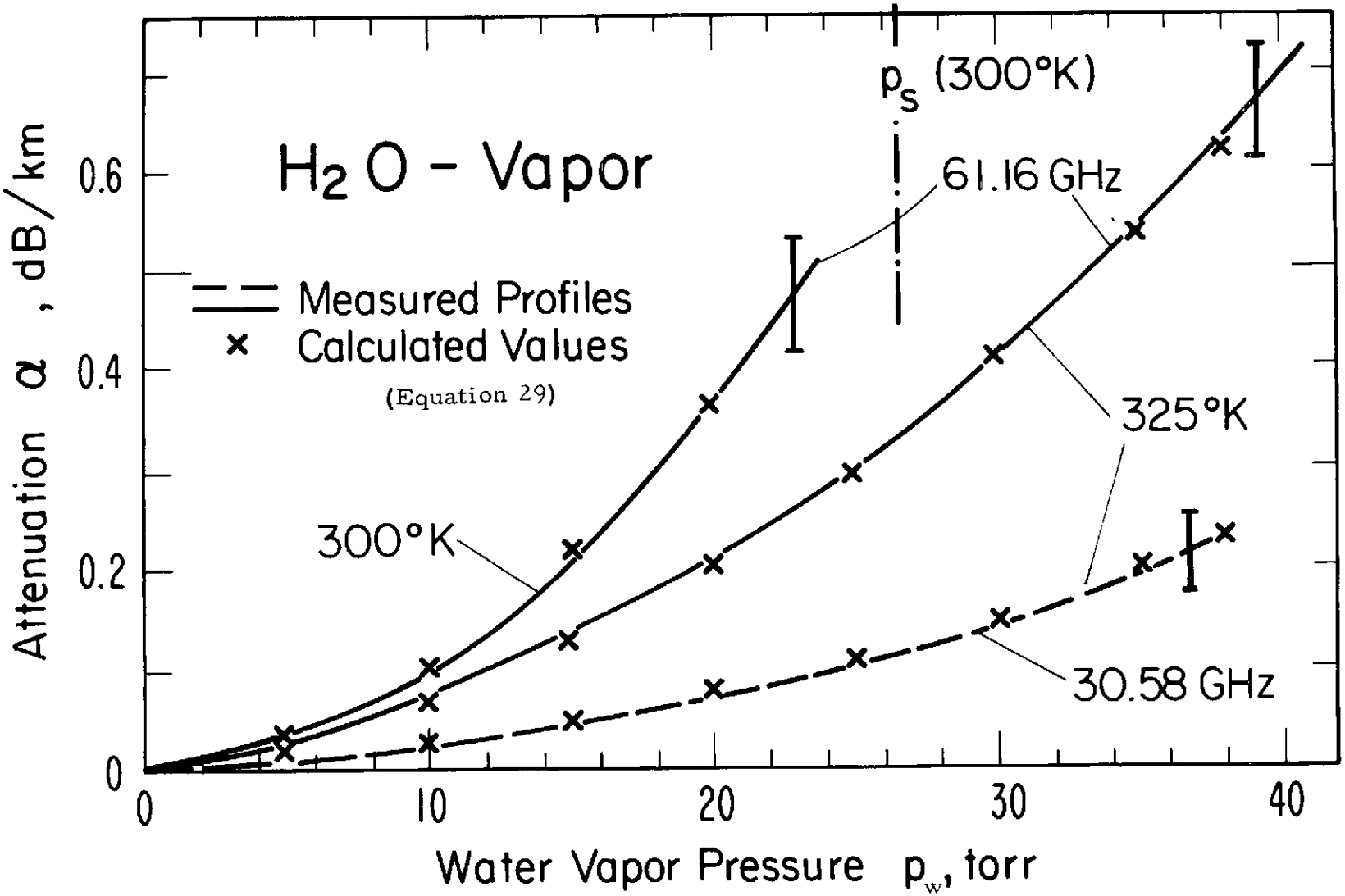

Figure 12. Pure water vapor attenuation as a function of the vapor pressure for two different temperatures at 61.16 GHz, and at 30.58 GHz.

3. COMPUTER ANALYSIS OF ATMOSPHERIC PATH MODELS

3.1 Homogeneous Path Transmissivity at Various Altitudes

Before applying theoretical results of Section 2 to actual atmospheric conditions, it seems appropriate to establish their validity. A serious test of the theory is possible by comparison with experimental results of sufficient accuracy which in turn can only be obtained under controlled laboratory conditions.

The O_2 Line Spectrum

One experiment yielded quantitative attenuation data for eight isolated lines around 60 GHz (Stafford and Tolbert, 1963) and the single line at 119 GHz (Schulze and Tolbert, 1963). The conversion of peak attenuation α_o and linewidth $\gamma°$ to a strength parameter (Eq. 11) is accomplished by means of (Eqs. 2, 18)

$$S° = 5493\, \alpha_o\, \gamma° / \nu_o \quad [\text{Hz/torr}] \tag{30}$$

where ν_o is in megahertz (from Table 7). This is illustrated by the tabulation below

$N^{\pm}$	α_o O_2 (Air) [dB/km]		$\gamma°$ Exp. [MHz/torr]	$\gamma°$ Table 7 [MHz/torr]	T [°K]	$S°$ Exp. [Hz/torr]	$S°_{Th}$ (Eq. 11) [Hz/torr]	$(S°/S°_{Th}) - 1$ Exp. [%]	$(S°/S°_{Th}) - 1$ Table 7 [%]
	(±12.2%)		(±5%)						
9^-	7.58	D	1.39	1.76	310	.993	1.406	-29 ?	-10
3^+	4.73		1.74	1.86	"	.774	.846	- 9	- 2
7^-	6.50		1.43	1.76	"	.864	1.407	-38 ?	-24 ?
5^+	5.94		1.61	1.78	"	.880	1.230	-29 ?	-21 ?
5^-	8.58	D	1.86	1.78	"	1.46	1.237	+18 ?	+12
7^+	8.63		1.62	1.76	"	1.27	1.441	-12	- 4
9^+	8.85	(1.97)	1.67	1.76	"	1.33	1.475	-11	- 5
11^+	7.70	(1.97)	1.46	1.76	"	1.00	1.366	-27 ?	-11
1^-	6.50	(1.60)	1.99	2.07	300	.598	.597	0	+ 3
9^+ (Eq. 20)			1.81		300	1.59	1.5899	0	

The difference between S° and S°_{Th} is for five lines larger than the combined experimental uncertainties. The fit improves when the linewidth parameters of Table 7 are applied. The discrepancies are probably due to insufficient control of experimental conditions, incorrect assumptions in reducing the data to 310°K ($u = w = 2$!), and baseline ($\alpha = 0$) problems. This, together with our experimental results for the 9^+ line (Eq. 20), leads us to believe that the theoretical line strengths are valid as given by equations (7), (11), (12), and Table 7.

The other important parameter of the isolated O_2 line spectrum is the correct width. Ab initio calculations of $\gamma^\circ(300)$ by Mingelgrin (1972) and Dillon-Godfrey (1972) are sensitive to the intermolecular potential parameters which are obtained from data unrelated to the O_2-MS. Results from both theories differ by about 20 percent as do the experimental values (Table 6, Fig. 5). Confidence in the measured $\gamma^\circ(9^+)$ parameter (Eq. 20) and support by other experiments of an N-dependence for the width (Fig. 5), made us use the 1.81 MHz/torr value to "calibrate" the Dillon-Godfrey widths.

The atmospheric transfer function versus frequency above an altitude of about 25 kilometers resembles a string of individual O_2-MS lines. The analysis of the O_2 line spectrum seems to be in fairly good shape. Uncertainties are connected with the width parameters γ°, m_d, u, m_w, and v (Eq. 19) for other lines than the 9^+. Further experimental work with the dispersion spectrometer (Liebe et al., 1973) will hopefully provide the missing information. A guide to treatments of the line spectrum in this report with respect to practical applications can be found in the overview on the next page

Guide to Treatments of the Atmospheric Oxygen Line Spectrum (h > 25 km)

Altitude h Line Broadening Line Shape		> 25 km Pressure p Lorentzian			> 40 km Magnetic Field H Lorentzian - Voigt			> 60 km Temperature T Voigt		
		Eq.	Table	Fig.	Eq.	Table	Fig.	Eq.	Table	Fig.
Transfer Fct.	$\underline{\tau}$	1, 2		6, 17	1, 2		18, 19			
Refract. Index	$\underline{n}$	4, 18			4			4		10, 11
Line Centers	ν_o	6	2, 7		14	5		14	5	
Strengths	S°	7, 11	3, 7	2	15	5		15	5	
Temper. Fct.	ϑ	12, 13	4	3	12, 13			12, 13		
Shape Fct.	$\underline{F}$	17		4			10		8	10
Widths	γ	19	6, 7	5, 13	19	7	13	25		13

The complete O_2-MS and detailed insight into its transfer properties require a good deal of theory. Therefore, it is important to test theoretical results by as many reliable experiments as possible.

Interesting properties of isolated lines are their markedly different temperature dependences. The peak attenuation α_o varies approximately as (Eqs. 2, 13, and 18)

$$\alpha_o \sim (T_o / T)^{w-u} \quad . \tag{31}$$

Looking at Table 4 and assuming $u = 0.9$, we find that α_o of the two $N = 15$ lines is almost independent of temperature and thus a good candidate as an atmospheric pressure sensor (from a satellite). One can also pick lines with inversely linear ($N = 11$) and square-law ($N = 3$) dependences as well as linear ($N = 15$), square-law ($N = 23$), and higher order temperature dependences. The high rotational lines are very sensitive functions of temperature (Waters, 1973). For example, a 1 percent (+1.8 °K) raise at 280 °K produces for $N = 27$ lines a 3.5 percent increase in α_o, and at 220 °K the increase is even 5.1 percent.

The O_2 Continuum Spectrum

One early experiment (Artman and Gordon, 1954) provided attenuation data (± 10 percent) at 25 frequencies between 52 and 61 GHz under controlled laboratory conditions ($p = 760$, 380, 190 torr; $T = 300$ °K). Several workers (e.g., Meeks and Lilley, 1963; Westwater, 1970) used these data, different line shape functions, and theoretical line strengths to deduce the pressure-broadening line parameters. It was found that the isolated width parameter (assumed equal for all lines) needs to be reduced by 30 to 50 percent (see Eq. 12) to fit more or less the continuum spectrum, and in all cases it was stated clearly that future laboratory measurements are needed to

remove the encountered uncertainties. Since such experiments have not been reported up to now, we have had to rely upon measurements made in the atmosphere.

Results of field measurements contain information not only about the O_2-MS but also about the structure of the atmosphere. Many of the uncertainties in present knowledge of the transfer function cannot be distinguished from uncertainties in pressure and temperature distributions which makes field data an unsatisfactory alternative to laboratory measurements.

Once the O_2-MS is completely understood it is an easy task to use spectroscopic properties as a probe of (dry) atmospheric conditions. Right now, however, we have to content with an empirical linewidth model introduced by Meeks and Lilley (1963) which determines the individual width from (γ_i applied to all lines except the 1^-)

$$\gamma_i(p) \approx G(h)\,(p/760)\,(300/T)^u \qquad \text{and} \qquad (32)$$

$$\gamma_i(h) \approx \sqrt{\gamma_i^2(p) + \gamma_D^2} \quad . \qquad (33)$$

Carter et al. (1968) and Reber (1972) measured oxygen attenuation of the atmosphere by the zenith angle technique using the sun as a source. Their ground level results are given in Table 10. Carter et al. accomplished a ± 8.8 percent fit (squared deviations) to their data which include airplane measurements (taken between h = 2.6 and 12.2 km) by the following scheme for G(h):

h [km]	G(h) [MHz]	u	p [torr]	$\gamma_i^\circ(300)$ [MHz/torr]
0 to 8	640	0.85	>180	0.84
8 to 25	640 to 1357, linear with h	"	-	-
> 25	1357	"	< 20	1.79

With these values, equation (32) becomes the "CMR-Model" which is used for the analysis described in the remainder of the report.

Another approximation, equation (33), is introduced to take care of the transition to Doppler-broadening (Section 2.4.3). The Lorentzian shape is assumed for the vanishing O_2-MS, and the transition to a Gaussian shape (Voigt profile) is not done. At h = 50 km this approximation was found to be indistinguishable over the strongest 90 percent of a line from the more correct Voigt profile (Waters, 1970). Equation (33) is sufficient in the context of analyzing cumulative effects through the atmosphere (Sect. 3.2), but for a calculation of the line profile over a homogeneous path above h = 60 km the Voigt profile has to be applied.

3.1.1 Analysis of Attenuation and Dispersion for Dry Air Between 49 and 72 GHz.

The analysis includes all lines with rotational quantum numbers N = 1 to 43 (Table 7), which omits lines with strengths less than about $2 \cdot 10^{-5}$ of that of the strongest line. This cutoff is sufficient even for computations of transmission over long paths. The assumptions made for the computer analysis of homogeneous attenuation and dispersion rates (Eq. 2) were:

(a) The U. S. Standard Atmosphere (1962) models the distribution of pressure p and temperature T versus altitude h.

(b) The atmosphere is dry, $p_w = 0$.

(c) The sum of 44 O_2 lines (Eq. 4) is the only source of attenuation and dispersion over the frequency band considered.

(d) The intensity distribution of each line is a Lorentzian (Eq. (Eq. 17), and the theoretical strength values (Table 7, Eqs. 7, 11, 12) are valid.

(e) The individual widths are the same for each line. They are given by the "CMR-Model" (Eqs. 32, 33) whose approximate (empirical) nature provides at best analytical estimates of transfer properties. The altitude dependence of the width is shown in Figure 13.

Results of the calculation are given in Figures 14 through 19. Only the graphical presentation provides an overview of the structure of the transfer function at different altitudes. Numerical results (computer print-outs) for any given set of conditions are available upon request.

At h = 0 km, figure 14 shows a continuum spectrum (II). The envelope is not a sensitive function of the width parameter: (1) γ° = 0.876 MHz/torr plus arbitrary variations of ± 25 percent (CMR-Model); (2) γ° = 1.27 MHz/torr, a value obtained by Westwater from fitting Artman and Gordon's (1954) data. Atmospheric attenuation for sea level conditions was reported at 21 frequencies between 40 and 120 GHz (Thompson, et al., 1972, Fig. 3).

At h = 10 and 20 km, figures 15 and 16 show a mixture of continuum (II) and line (I) spectra. The influence of the width becomes more pronounced as the lines gain identity. At h = 30 km (Fig. 17), we have a pressure-broadened line spectrum.

At h = 50 km, figures 18 and 19 show the effects of Zeeman splitting of two individual (9^+ and 27^-) lines. Figure 18 gives changes in transmissivity for the case of linearly polarized radiation. Each of the 19 π- or 38 σ-components (Eq. 14) is treated as a pressure-broadened line of Lorentzian shape (Eq. 17) with a width determined by equations (32) and (33). The line strengths are calculated using equation (15). The contributions from each Zeeman component are summed up over frequency (Eq. 4). The 9^+ line widens under the influence of H = 0.53 gauss while the peak attenuation is reduced by

20 to 36 percent, respectively, for the π - and σ -envelopes. The σ -envelope splits for circular-polarized radiation depending on the orientation. The two halves are shown in the example for the 27^- line in figure 19. The individual Zeeman components are not resolved in both cases. A consequence of the Zeeman effect is that above $h \geq 40$ km the atmosphere becomes a medium with polarization dependent anisotropic transfer properties.

The evaluation of a practical case requires the determination of the type of polarization for the propagating radiation. The next step is to define the orientation between the direction of H and the microwave field component ψ. Lenoir's (1968) transfer function in tensor form does this in general form for geomagnetic coordinates. Croom (1971) discussed 24 possible "pure" constellations between H and ψ for the case of emission from the 1^- line where ψ takes the role of the radiometer antenna polarization.

The simple Zeeman pattern of the 1^- and 1^+ lines eases considerably the interpretation of emission (attenuation) measurements in the vicinity of these lines. Such emissions can be picked up from satellite-born radiometers and then converted to mesospheric temperature structures and magnetic field (H) data on a global basis (Lenoir, 1968; Croom, 1971). At these heights the 1^+ line is well isolated from its 15^- satellite. The peak attenuation of both lines (Eqs. 2, 7, 18, and Table 7) have for T = 300 °K the values

$$\alpha_o(1^+) = .351 \text{ and } \alpha_o(1^-) = 1.36^* \text{ [dB/km]}$$

*Croom (1971) gives at h = 0 for 288 °K a value $\alpha_o(1^-) = 3.8$ dB/km which is wrong since the overlap-reduced width (Eq. 32) was used. At 288 °K we calculate 1.54 dB/km (Eqs. 2, 11, 12, 18, 19, and Table 7). This error reduces the zenith attenuation, which should be closer to $A_o(1^-) \approx 110$ dB (0.7 · 1.5 · 100 km) instead of 266 dB as given by Croom.

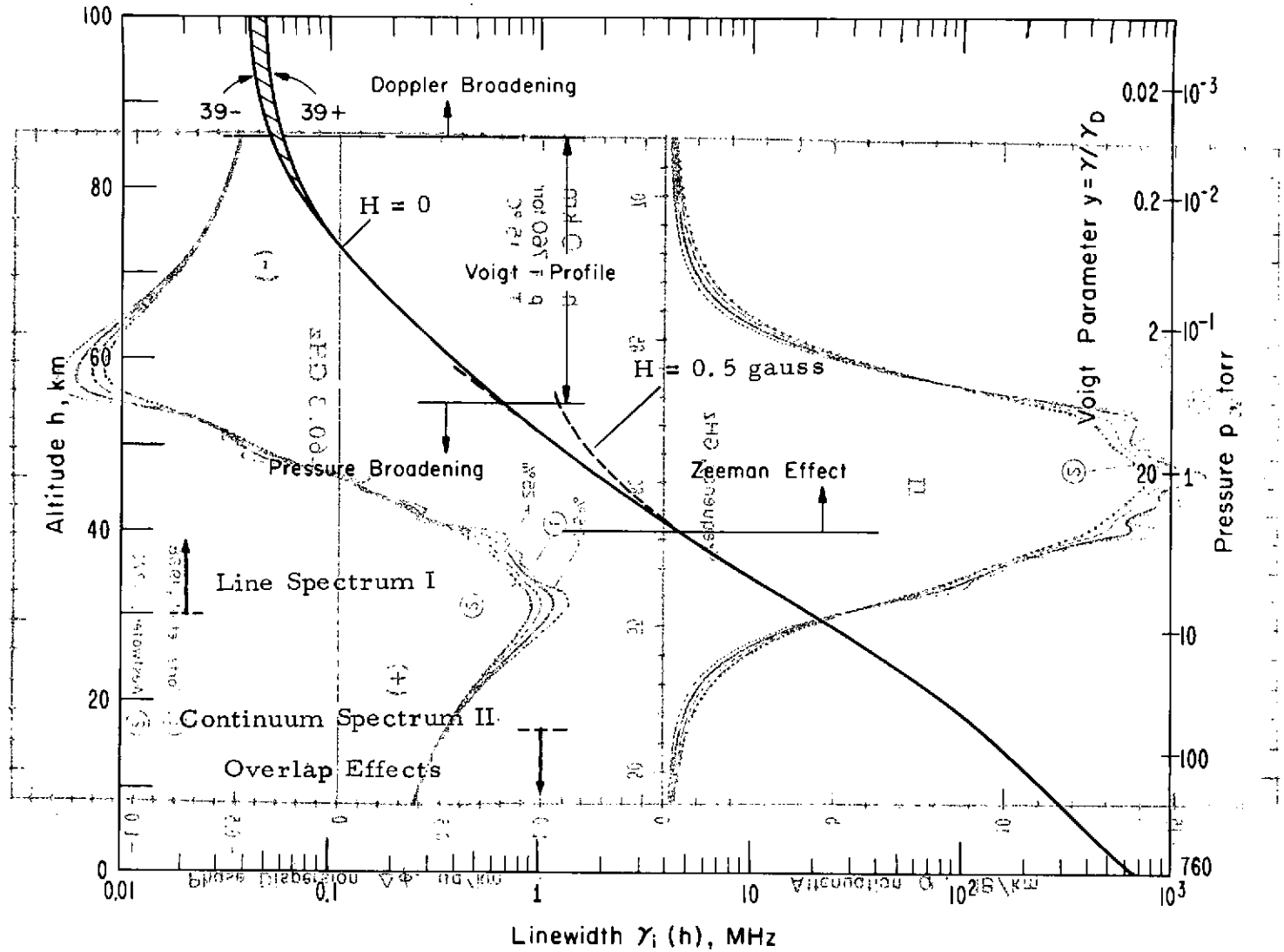

Figure 13. Linewidth γ_i (same for all lines of O_2 - MS) versus altitude h and pressure p as obtained from the CMR-model (Carter et al., 1968).

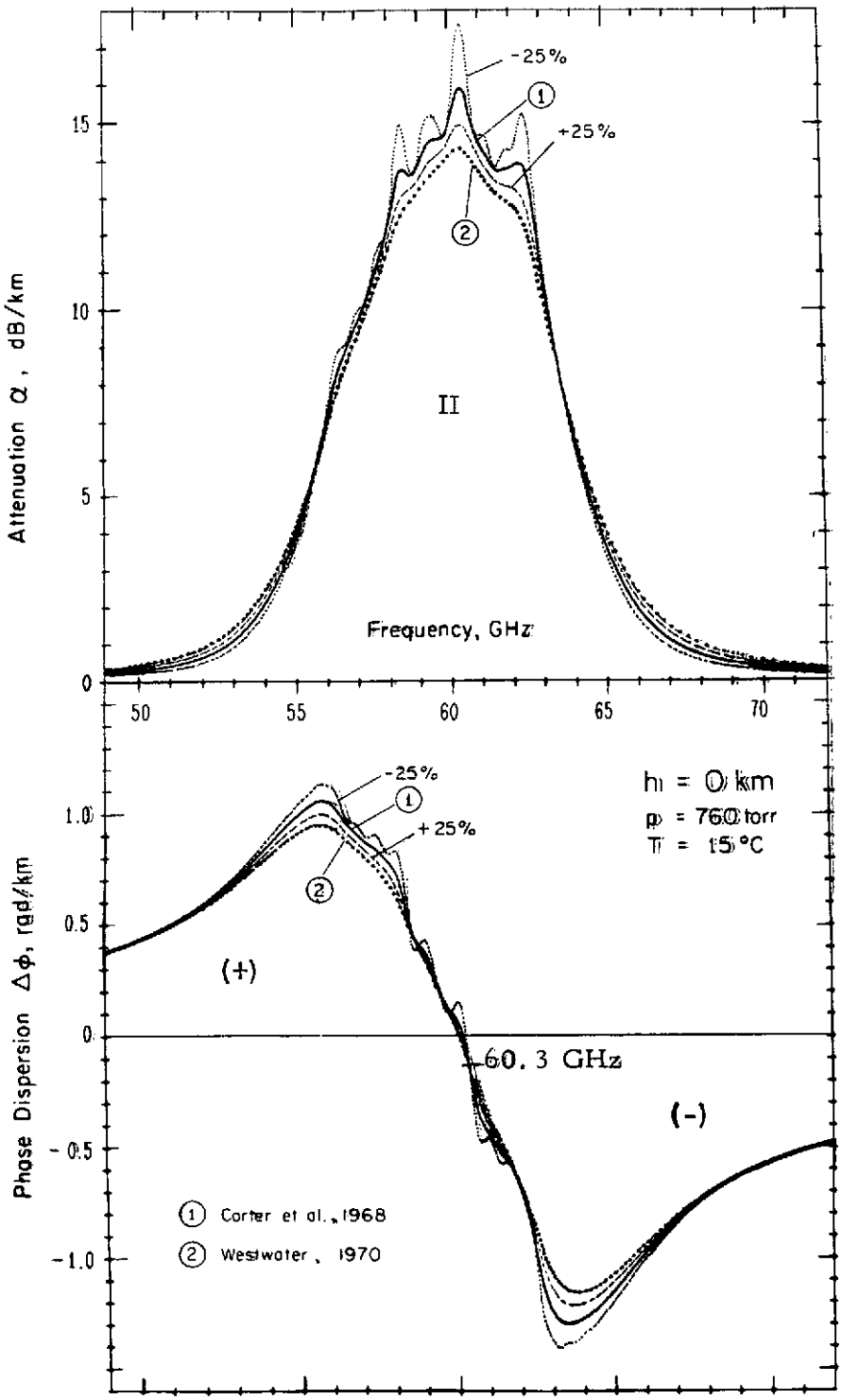

Figure 14. Horizontal (homogeneous) transmissivity at sea level, h = 0 km. Variations are shown due to different linewidth values : ① γ_i = 666 MHz ± 25%, ② γ_i = 968 MHz.

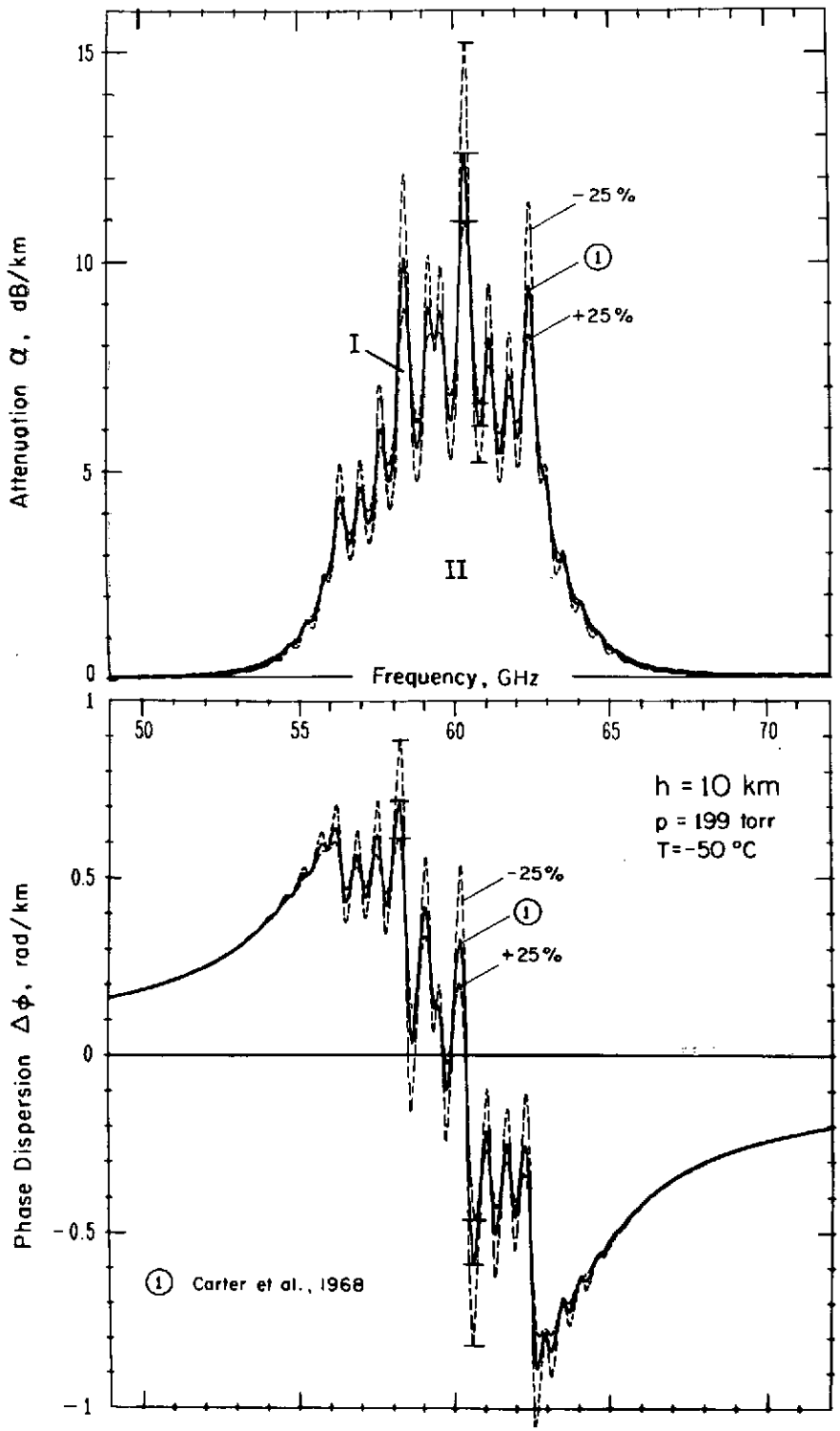

Figure 15. Horizontal (homogeneous) transmissivity at h = 10 km (U.S. Std. Atm. 62). Variations are shown due to different line-width values : ① γ_i = 255 MHz ± 25%.

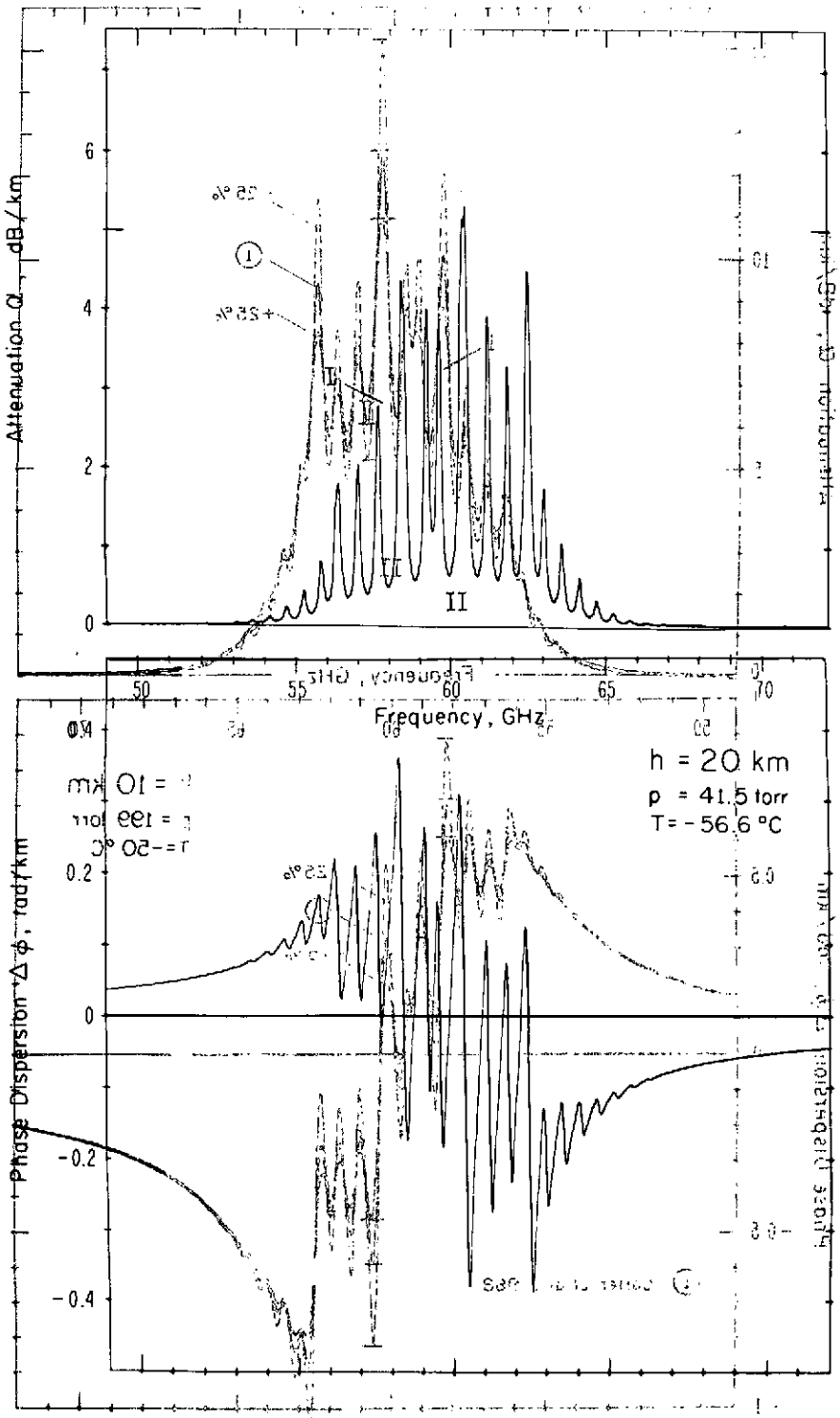

Figure 16. Horizontal (homogeneous) transmissivity at h = 20 km (U.S. Std. Atm. 62). The linewidth values are, γ_i = 86.6 MHz.

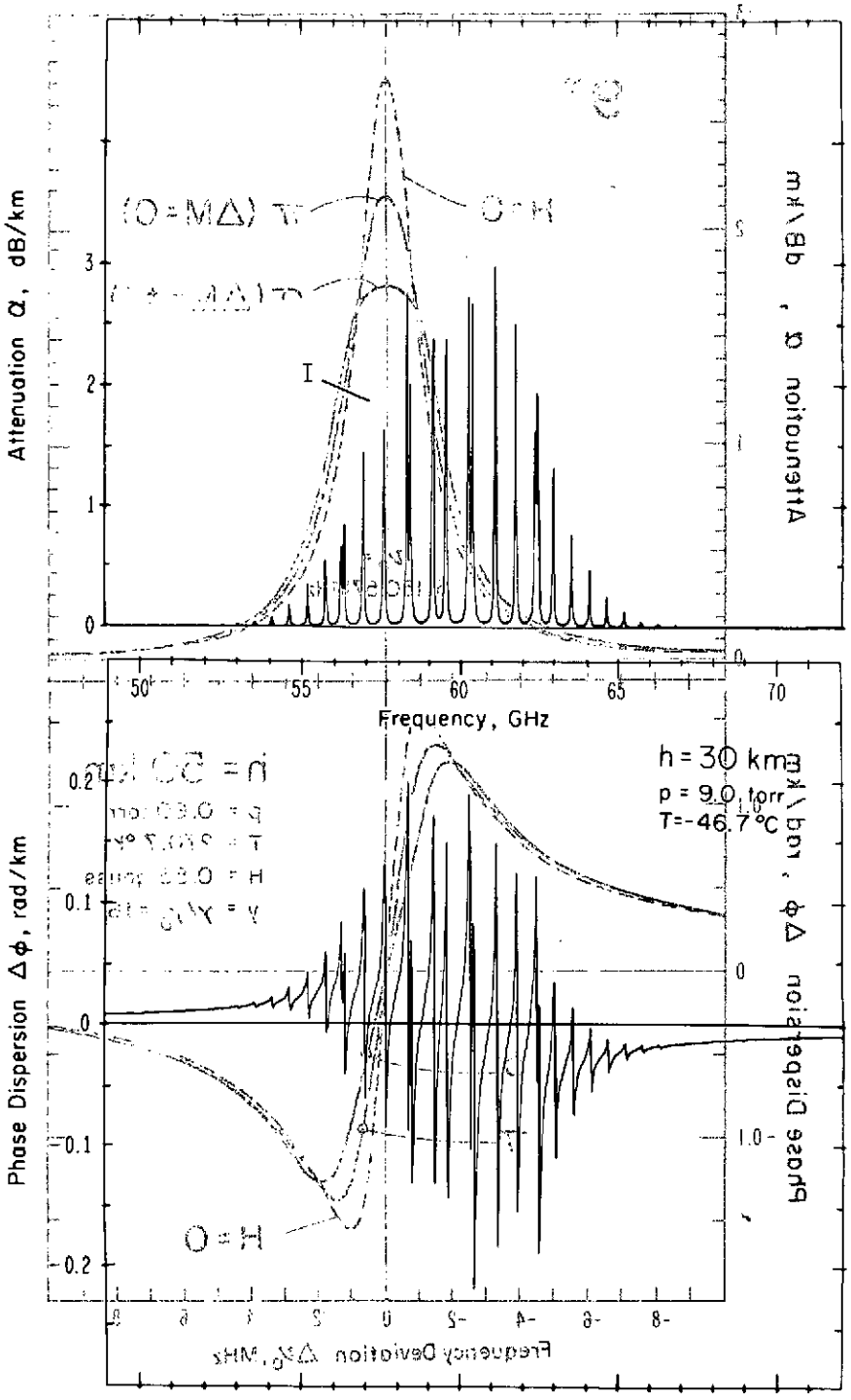

Figure 17. Horizontal (homogeneous) transmissivity at h = 30 km (U.S.Std.Atm.62). The linewidth values are, γ_i = 21.2 MHz.

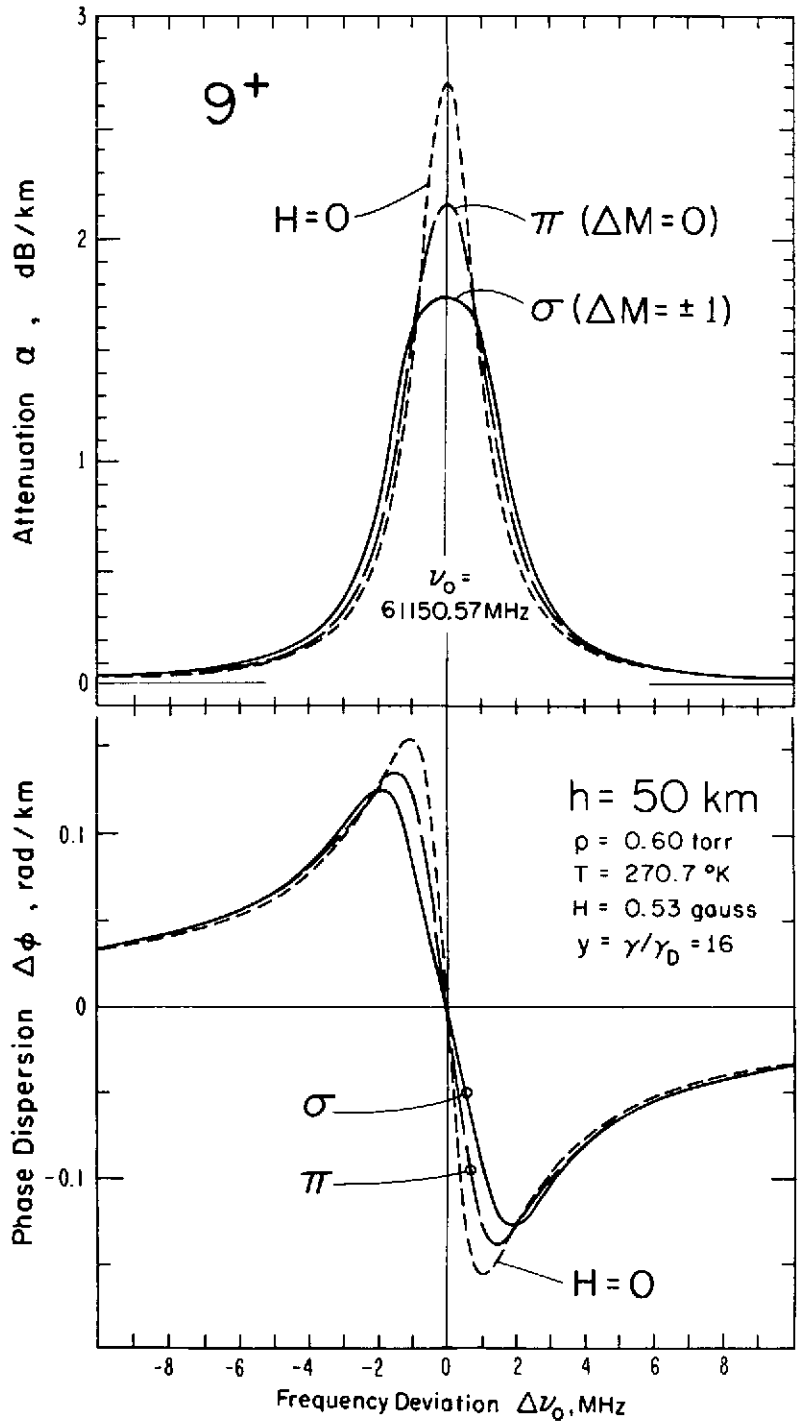

Figure 18. Effect of Zeeman-splitting upon the horizontal (homogeneous) transmissivity at h = 50 km (U.S. Std. Atm. 62) in the vicinity of the 9^+ line of the O_2-MS for linearly polarized radiation with $\mathcal{E} \perp H$ (π) or $\mathcal{E} \parallel H$ (σ).

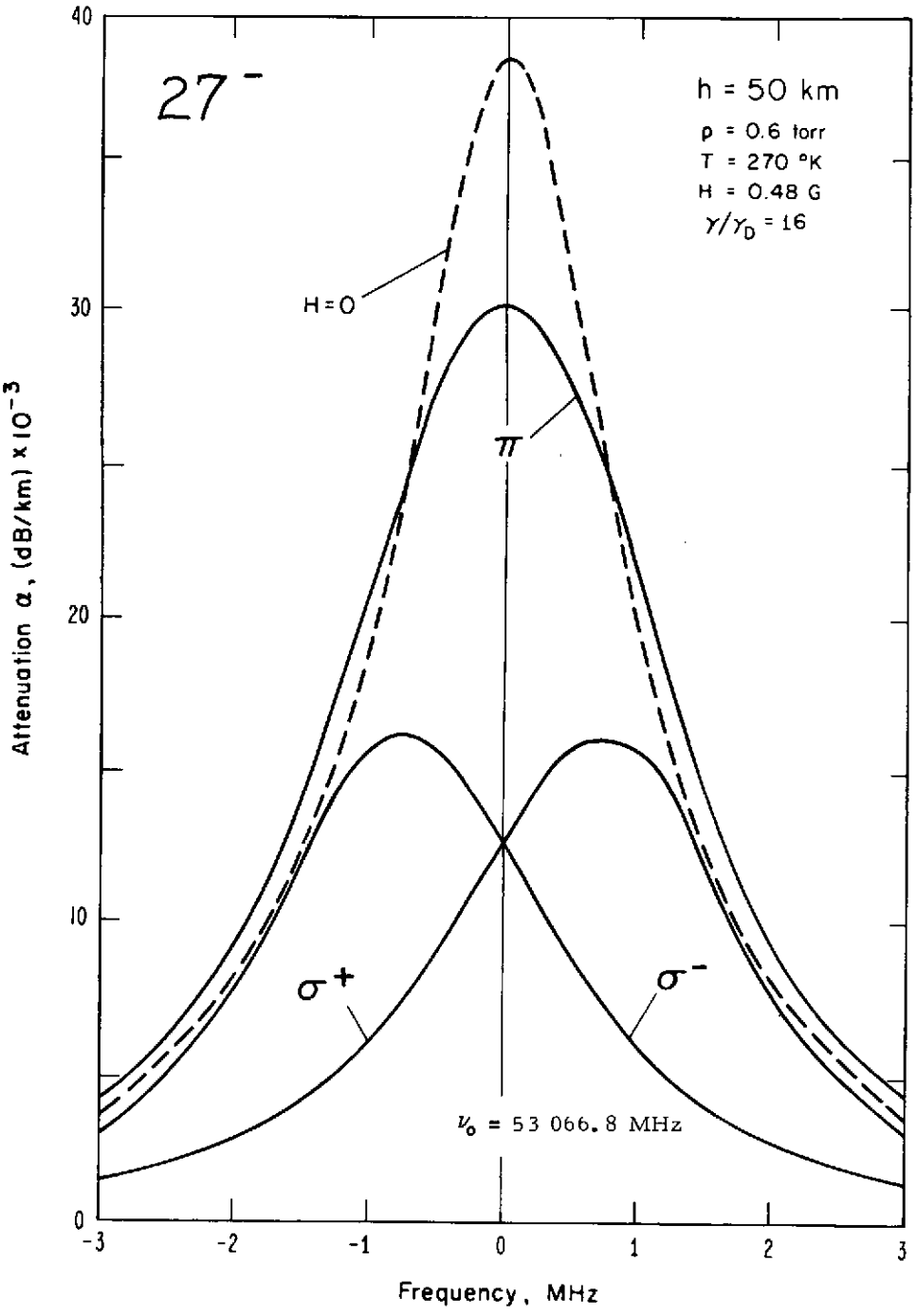

Figure 19. Effect of Zeeman-splitting upon the horizontal (homogeneous) transmissivity at h = 50 km (U.S.Std.Atm.62) in the vicinity of the 27^- line of the O_2-MS (after Waters, 1970) for linearly polarized radiation with $\vec{E} \perp H(\pi)$ or for circularly polarized (right-, left-handed) radiation (σ^+, σ^-).

The intensities of both lines differ by about 1 to 4, but technology at 56 GHz (1^+) is more advanced. The NIMBUS 5 radiometer, for example is working well in space at 60 GHz (D. Staelin, private communication, 1973).

3.1.2 Phase Dispersion Between 10- and 140- GHz

While attenuation (or emission) is the subject of all papers dealing with applications of the O_2-MS, data on phase dispersion are not readily available. In general, the complete transfer function $\underline{T}(\alpha, \phi)$ (Eq. 1) is required for an evaluation of atmospheric limitations imposed on system performances. The phase term has particular relevance for broadband communication and for various disciplines of microwave measurements. For example, phase dispersion limits the useable, phase-coherent channel bandwidth of a broadband system (Morgan and Ekdahl, 1966); propagation delay and its fluctuations determine the accuracy of clock synchronization via satellite (Levine, 1970), the resolution of long-baseline interferometers (Schaper et al., 1970), the accuracy of radio range measurements (e.g., Thompson, 1968), etc.

The atmosphere delays radio signals causing an apparent increase ΔL in the geometric path length L. The propagation time

$$t = (L + \Delta L)/ c \qquad [s] \tag{34}$$

is determined for refractive indices $n' \geq 1$ by the phase velocity c/n' and for $n' < 1$ by the group velocity cn'.

The case $n' < 1$ exists for the O_2-MS only under special circumstances when the negative resonance dispersion $\Delta n(\nu)$ of an isolated line (Fig. 4) is larger than the non-dispersive refraction n_o (Section 2.2). This case occurs at frequencies up to several megahertz above a line center (Liebe et al., 1973, Fig. 4), but it will not be considered in the following discussion.

We define

$$\Delta L = \int_L (n' - 1)\, dl = \int_L [\mathbf{N} \cdot 10^{-6} + \Delta n(\nu)]\, dl \qquad [m] \qquad (35)$$

where the integration is taken along the ray path. For example, the additional electrical length of a zenith path from sea level to outer space is typically $\Delta L \approx 2$ meters (Schaper et al., 1970). Extreme values of zenith path length changes due to O_2-MS dispersion are only +12 millimeters at 58.3 GHz and -14 mm at 62.6 GHz. The extreme values for $\Delta L(\nu)$ from different initial altitudes are listed in Table 9. The calculation procedure of these results will be described in Section 3.2.

System engineers express dispersion effects of the homogeneous atmosphere by a phase change in radians per unit distance:

$$\Delta\phi(\nu) = (2\pi\nu/c)\, \Delta n(\nu) \qquad [rad/km] \quad . \qquad (36)$$

Calculations of $\Delta\phi$ over the 49 to 72 GHz range (O_2-MS attenuation) have been described in Section 3.1.1, and various examples for h = 0 to 50 km display the O_2-MS dispersion spectrum (Figs. 14 through 18). It is evident that the molecular resonance dispersion extends over a much larger frequency range. The reason lies in the shape function F' whose wing intensity decreases with $|\nu_o - \nu|$ as compared to $|\nu_o - \nu|^2$ for F'' (Eq. 17 and Figs. 4, 10).

The calculations are extended to cover the frequency range 10 to 140 GHz for h = 0 and 10 km, and the graphical results are shown in figure 20. The dispersion of the 22 GHz H_2O line puts a "wrinkle" into the dry air phase response. At h = 0, we calculate (Eqs. 27, 28, 36): $(\Delta\phi_w)_{max} = \pm 1.2 \cdot 10^{-3}$ rad/km per torr of water vapor at 19.2 and 25.3 GHz respectively, while the O_2-MS dispersion over the same frequency range is $+ 25 \cdot 10^{-3}$ rad/km.

The dispersion $\Delta n(\nu)$ of the O_2-MS was first calculated for $h = 0$ by Zhevakin and Naumov (1967). The complete oxygen dispersion spectrum including overlap and nonresonant dispersion (Sect. 2.4) was recently evaluated by Mingelgrin (1972), and his result at $h = 0$ km for $\nu = 0$ to 80 GHz is shown in figure 21. The peak value span (7.87 ppm) of O_2 translates for air into 2.11 rad/km, which agrees well with the value of (2) in figure 14. Another dispersion calculation for dry air at h = 0 km was performed by Sullivan and Richardson (MITRE, 1965). They predicted a dispersion of 0.4 ppm between 45 and 90 GHz while our calculated value is 0.381 ppm. A broadband system operating on the ground close to the O_2-MS attenuation band, e.g., in the 45 or 75 GHz bands, does experience phase dispersion on the order of ± 0.03 rad/km per gigahertz.

Dispersion measurements are difficult in the laboratory because the small effect is heavily masked by instrumental instabilities. A few measurements have been made in our laboratory using a differential microwave refractometer (Thompson and Vetter, 1968) similar to the one described by Liebe et al. (1973). The difference of the refractivity at 26 and at (26/3) GHz was measured at 610 torr and 300°K in dry air to be 0.12 ± 0.03 ppm (M. J. Vetter, private communication, 1968). The calculated value for the same conditions is (0.394 - 0.261) = 0.133 ppm.

In another experiment we measured the difference in refractivity between 23.6 and (23.6/2) GHz (Liebe, unpublished results, 1969). In dry air from p = 50 to 600 torr at 300°K, the following result was obtained $(1.25 \pm 0.3) \cdot 10^{-4} \cdot p$, while the calculated response is $(6.03 - 4.55) \cdot 10^{-4} \cdot p = 1.48 \cdot 10^{-4} \cdot p$ [ppm/torr].

These two experiments provide a rough (± 25 percent) confirmation of O_2-MS dispersion outside the 60 GHz attenuation band where the dispersion is nearly independent of the widths γ (Eqs. 19, 21).

Atmospheric refraction limits the accuracy of such systems as electronic distance meters and tracking radars. The measurement of distance is based on determining the propagation time t (Eq. 34), whereas the deviation of the vertical tracking angle is proportional to the gradient dn' / dh. These errors can be reduced if pertinent atmospheric parameters of the propagation path are known. The dispersion of the O_2-MS offers a means of evaluating the refractive index $\overline{n'}$ of dry air averaged along an atmospheric path. Systems operating at two (or more) phase-coherent frequencies can extract path conditions from the difference in phase shifts experienced by the signals when travelling the same path (MITRE, 1965; Thompson, 1968; Liebe, 1969b).

The potential of a differential phase measurement is analyzed for signal frequencies in the wings of the O_2-MS. Two different signal pairs are chosen for short and long operating ranges in the following example

Master Frequ.	Multipl. Factor X	Signal Freq. ν	Phase Difference ϕ	Temperature Sensitivity of ϕ	Pressure Sensitivity of ϕ	Operating Range L
			At 20°C, 760 torr	(20 ± 20)°C See Fig. 22	(600±200) torr	$\alpha \lessapprox 40$ dB
[GHz]		[GHz]	[rad/km]	[rad/km °K]	[rad/km torr]	[km]
11 11	5 6	55 66	1.93	$-11.8 \cdot 10^{-3}$	$9.3 \cdot 10^{-4}$	$\lessapprox 10$
10.2 10.2	5 7	51.0 71.4	0.98	$-4.3 \cdot 10^{-3}$	$4.7 \cdot 10^{-4}$	$\lessapprox 100$

The phase shifts $\theta_{1,2}$ experienced by each signal over a path length L are (Eqs. 35, 36)

$$\theta_1 = [2\pi\nu_1 (1 + \bar{N} \cdot 10^{-6})/c + \Delta\phi(\nu_1)] \cdot L$$

and (37)

$$\theta_2 = [2\pi\nu_2 (1 + \bar{N} \cdot 10^{-6})/c - \Delta\phi(\nu_2)] \cdot L \quad ,$$

when the signal frequencies are chosen so that $|\Delta\phi(\nu_1)| \approx |\Delta\phi(\nu_2)|$ (see Fig. 22) and $\bar{N}$ is the refractivity averaged along the path. The averaged refractivity can be separated into a "dry" and a "wet" term,

$$\bar{N} = \bar{N}_d + \bar{N}_w \quad . \tag{38}$$

Assuming (a) a straight line-of-sight ray path (no reflections or bending), (b) a perfect correlation of time-varying phase changes (mainly due to water vapor density fluctuations), and (c) a common frequency $\bar{\nu} = (\nu_1 + \nu_2)/2$ (e.g., by heterodyning ν_1 and ν_2 and then multiplying each IF by the opposite factor X) one can measure at the receiving end the difference

$$\theta_1 - \theta_2 = \phi L = \left\{\Delta\phi_1(\bar{\nu}) + |\Delta\phi_2(\bar{\nu})|\right\} \cdot L \qquad [\text{rad}] \tag{39}$$

and the sum

$$\theta_1 + \theta_2 \approx 2\pi (\nu_1 + \nu_2) (1 + \bar{N}\, 10^{-6})\, L/c \quad [\text{rad}] \quad . \tag{40}$$

The O_2-MS dispersion ϕ can be tabulated in terms of dry air density, $\rho_d = 464\, p/T\ [g/m^3]$. Approximate pressure and temperature sensitivities are listed on the previous page. For the path length L, first the uncorrected value can be used with some possible later iterations. Thus the value $\bar{\rho}_d$ found through a measurement of ϕ determines the dry term refractivity (Eqs. 5, 39)

$$N_d = 0.223\, \bar{\rho}_d \qquad [\text{ppm}] \quad . \tag{41}$$

Table 9. Extreme values of zenith phase dispersion ΔT and electrical path length change $\Delta L(\nu)$ with associated frequency ν and attenuation **A** for different initial altitudes, h_1 (CMR-Model).

h_1	See Figure	Number of Integrat. Layers	Maximum Values				Minimum Values			
			ΔT	$\Delta L(\nu)$	ν	A	ΔT	$\Delta L(\nu)$	ν	A
km			rad	mm	MHz	dB	rad	mm	MHz	dB
0	25	151	14.7	12.0	58260	179	-18.3 (-11.9)	-13.9 (-9.4)	62580 60500	160 (216)
5	27	101	11.5	9.4	58280	130	-13.4 (-10.4)	-10.2 (-8.2)	62540 60480	119 (177)
10	29	81	8.5	6.9	58300	94	-9.2 (-8.4)	-7.0 (-6.6)	62520 60460	81 (143)
15	31	71	6.1	5.0	58300	56	(-6.3) -6.5	(-4.8) -5.1	62500 60460	(621) 113
20	33	61	4.5	3.7	58320	30	(-4.3) -4.9	(-3.3) -3.8	62500 60440	(36) 65
25	35	56	3.6	2.9	58320	14.3	(-3.0) -3.9	(-2.3) -3.1	62500 60440	(19) 27
30	37	51	3.0	2.5	58320	5.2	(-2.0) -3.2	(-1.5) -2.5	62500 60440	(8.8) 15

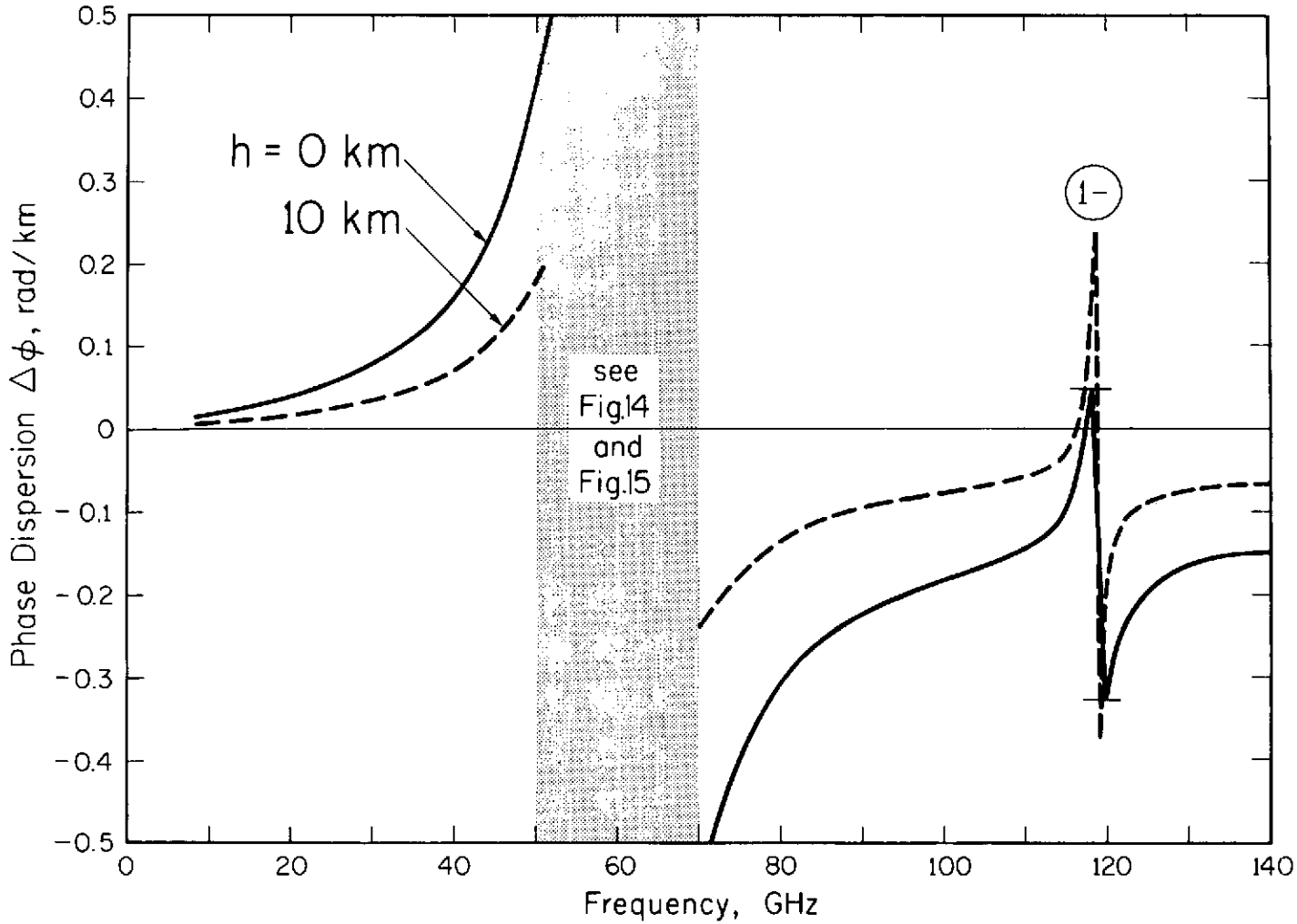

Figure 20. Phase dispersion in dry air due to the microwave spectrum of O_2 for horizontal paths at h = 0 (760 torr, 15°C) and h = 10 km (199 tor, -50°C) using the linear model (sum of Lorentzians).

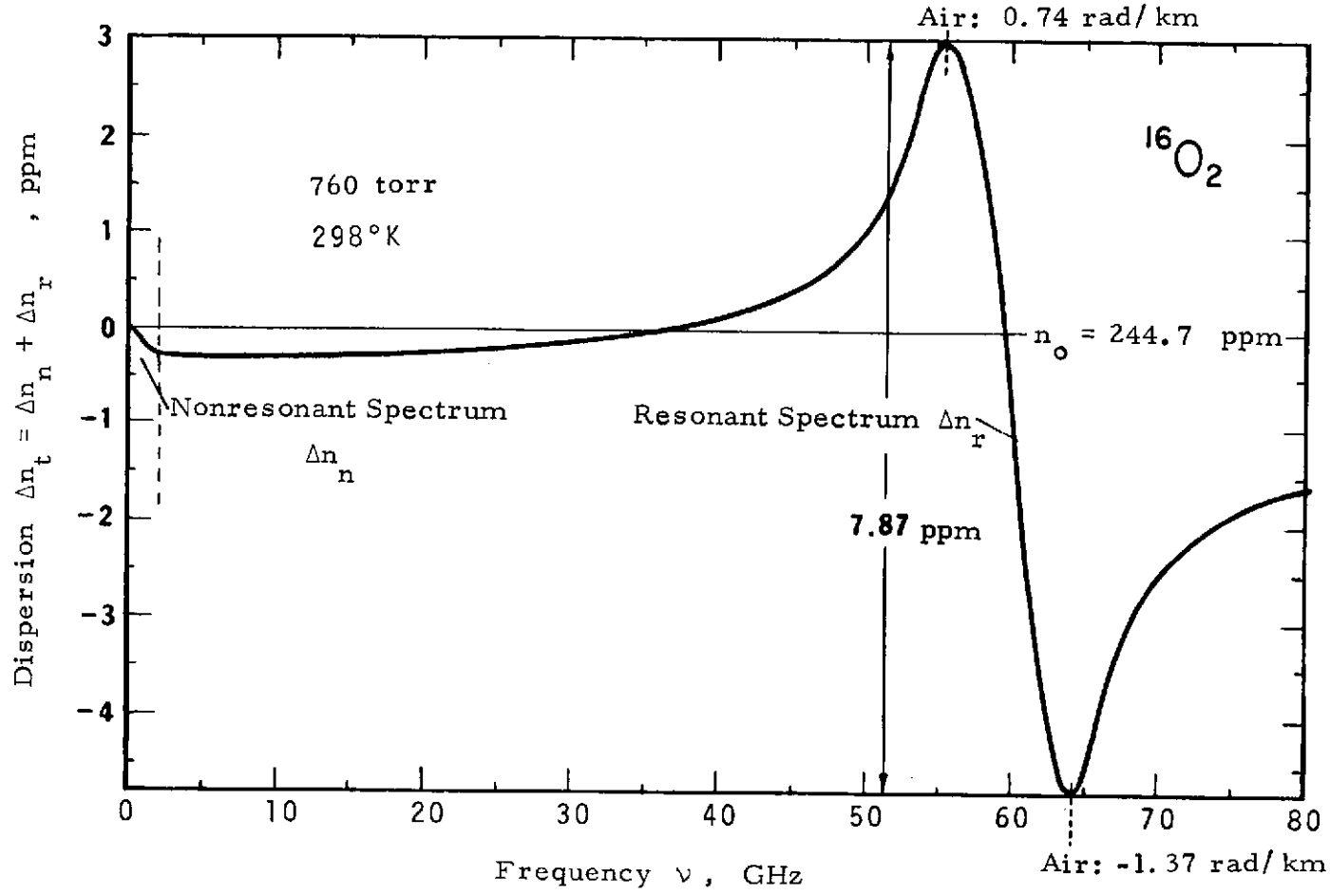

Figure 21. Total dispersion Δn_t of the O_2 Microwave Spectrum for 760 torr and 298°K as obtained for pure oxygen using scattering calculations (Mingelgrin, 1972). The associated attenuation is shown in Figure 9.

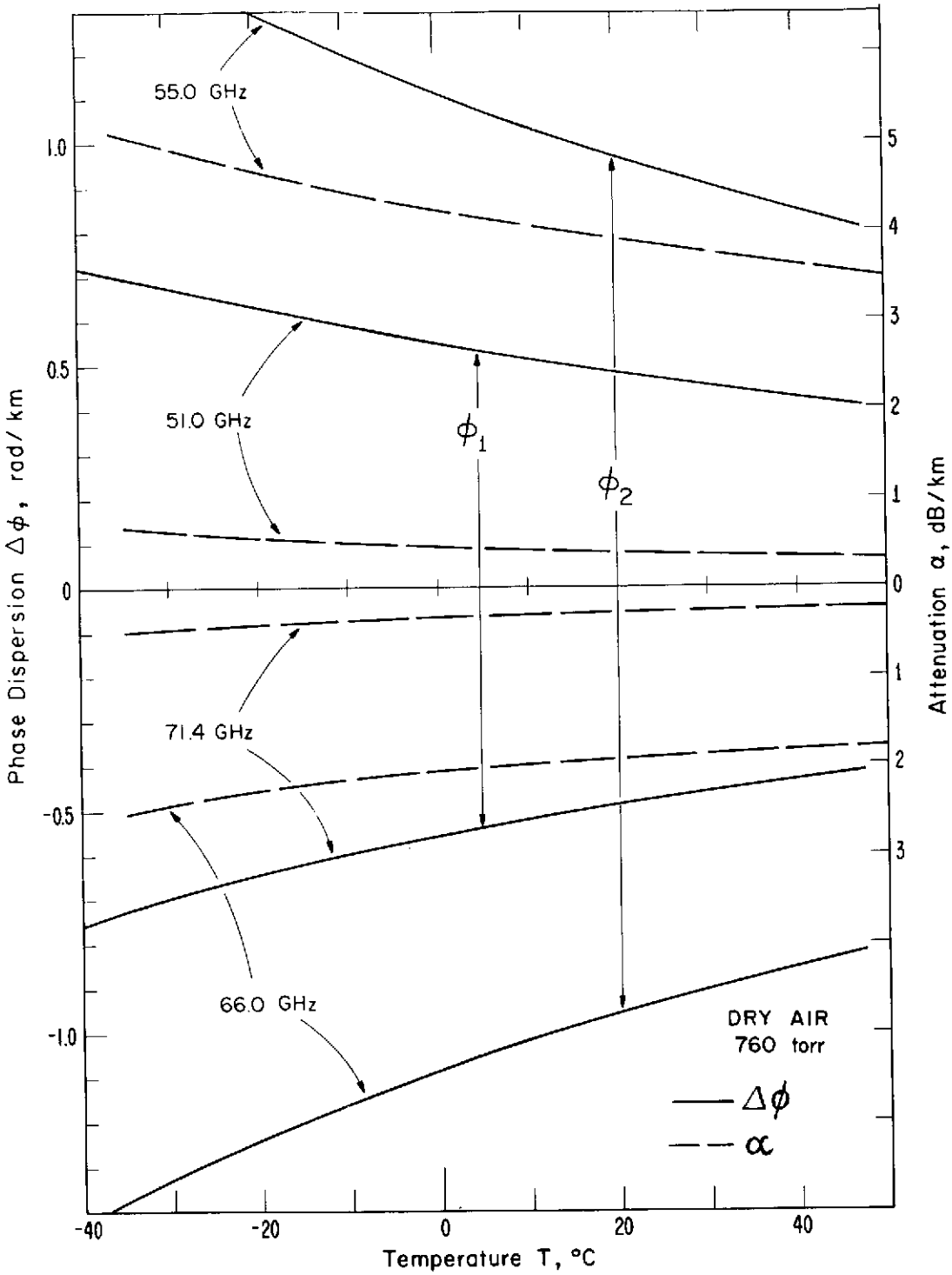

Figure 22. Phase dispersion $\Delta\phi$ and associated attenuation α versus temperature T for two different harmonious frequency pairs in dry air at sea level using the linear model (sum of Lorentzians). $\phi_{1,2}$ - differential dispersion between 51.0/71.4 and 55/66 GHz.

The wet term refractivity $\bar{N}_w$ originates from the water vapor within the path. With equation (5) and $\rho_w = 288.8\, p_w / T$ [g/m^3] one obtains

$$\bar{N}_w \approx 1.73 \cdot 10^3 \cdot \bar{\rho}_w / T \qquad [\text{ppm}] . \qquad (42)$$

It is possible to solve for the average water vapor density along the path, $\bar{\rho}_w$ using the measured sum of phase shifts (Eqs. 40, 38, 41, 42).

The proposed measurement principle offers the potential to follow air and water vapor density fluctuations separately in real time as they occur as spatial averages along a line-of-sight path. This information is also a wanted correction term (Eqs. 34, 35) for radio distance measurements.

3.2 Slant Path Transmissivity

3.2.1. Calculation Procedure and Critical Comments

Computations of non-turbulent transfer properties through the first 100 kilometers of the atmosphere depend on the exact functional form of $\alpha(h)$ and $\Delta\phi(h)$ [Sect. 2], on the model atmosphere which determines p(h) and T(h) [U. S. Stand. Atm. 1962], on the mixing ratio distribution $r_k(h)$ [Fig. 23], on the ray path geometry [Fig. 24], and on the refractivity distribution N(h) [Eq. 5]. Cumulative transmissivity along a ray path is defined by

$$A = \int_{h_i}^{\infty} \alpha(\ell)\, d\ell \quad \text{and} \quad \Delta T = \int_{h_i}^{\infty} \Delta\phi(\ell)\, d\ell , \qquad (43)$$

where $d\ell$ is the increment of the ray path and h_i is the initial altitude. The atmosphere has only a weak dependence on geographic coordinates and in the first approximation it can be considered as a layered homogeneous medium which does not change with time. The numerical method used for the evaluation of equation (43) consisted of assuming a spherically

stratified atmosphere which was divided into slabs of thickness Δh. The altitude increments Δh were chosen so that each layer was quasi-homogeneous ($\Delta p < 10$ torr and/or $\Delta T < 5°K$ across each slab) amounting to a number of n = 151 for h = 0 to 100 km (see Table 9). Attenuation α and dispersion $\Delta\phi$ were calculated for each slab as described in Section 3.1.1. The clean, dry atmosphere sustains a constant mixing ratio up to h > 90 km for all gases which might have a measurable ($r_k > 10^{-6}$) influence upon transfer properties (Fig. 23). An exception is ozone (and possible air pollutants), which is discussed briefly in Section 3.2.3. The correct evaluation of a path trajectory would include refractive ray bending commonly expressed by Snell's law (e.g., Blake, 1972). The effect is most severe for a horizontal starting angle ($\theta = 90°$) defining a tangential path and is zero for a vertical starting angle ($\theta = 0$) defining a zenith path. We assume a straight line slant path with the increment $d\ell(\theta) \approx \Delta\ell(\theta)$ determined by the algorithm given in figure 24. Finally, a numerical integration based on Simpson's rule was employed to compute the integrals of (43); i.e.,

$$A \approx \sum_n 0.5\,(\alpha_n + \alpha_{n+1})\,\Delta\ell_n(\theta)$$

$$\Delta T \approx \sum_n 0.5\,(\Delta\phi_n + \Delta\phi_{n+1})\,\Delta\ell_n(\theta) \quad . \tag{44}$$

A word of caution regarding these calculations should be noted at this point. Results obtained by the method described above can only qualify as analytical estimates allowing an overview on altitude-dependent transfer properties of the O_2-MS. The following key-words underline the approximate nature: (a) empirical linewidth model, (b) straight line ray path, (c) numerical integration, (d) neglect of water vapor, (e) neglect of temporal variations of p and T, and (f) a more or less representative model atmosphere. The climate dependence of the

O_2-MS is not too strong. The attenuation peaks of A , for example, decrease by about 10 percent in a tropical climate and increase by about 20 percent in an arctic climate when compared with results (Figs. 25, 17) for the U. S. Std. Atm. 62 (Reber et al., 1970). Values for A and ΔT are, however, consistent in themselves, and the spectra could be scaled to results of reliable experiments.

3.2.2 Zenith and Tangential Path Transmissivities Between 49 and 72 GHz at Various Altitudes

A computer program was developed for evaluations of equation (44). The routine was tested for the two extreme (zenith and tangential) cases of a slant path. We present examples of results in the form of computer plots in Figures 25 through 39. The print-outs are too lengthy for reproduction here, but Table 11 gives an example of the format. Such listing can be made available upon request for any given set of variables. The path transmissions between a given initial altitude and outer space are obtained by summing the contributions of 44 O_2-MS lines, integrating over height, and finally integrating over frequency. For example, the computation of the results shown in figure 25 require for frequency increments of 20 MHz about $23 \cdot 10^6$ individual calculations to cover the 49 to 72 GHz band which takes about 5 minutes on a CDC 3800 machine.

The zenith path spectra are labeled by the initial altitude h_I which was varied between h = 0 and 30 km in increments of 5 km. The tangential spectra are calculated for a straight-line path through the total atmosphere (satellite-to-satellite) and they are labeled by the height h_o, marking the closest approach of the tangent to sea level. Factors that determine tropospheric path loss are not only molecular attenuation but also stratification and path geometry which can introduce

multipath, diffraction, and ground reflection effects. To avoid considering these problems, we limited $h_o \geq 5$ km. The peak values of a zenith and a tangential path for $h_1 = h_o$ differ by about 1 to 30. The tangential spectra were extended to $h_o = 50$ and 75 km (Figs. 38, 39) to gain insight into the problem how deep a satellite-satellite link can penetrate the atmosphere. At these altitudes there is still appreciable attenuation at the line centers due to the long path length, but in between are many "clear" channels with bandwidths on the order of 400 MHz.

A few experimental results are available on zenith attenuation from h = 0 (Table 10). Carter et al. (1968) also reported some aircraft measurements for different altitudes between $h_1 = 2.6$ and 13.7 km. Their data points for $h_1 = 9.1$ km are shown in figure 29. Figure 25 illustrates the degree of agreement obtained between experiment and the CMR-Model analysis (Eqs. 32, 33) which is on the order of $\pm$ 10 percent. Table 10 gives the numerical values.

Reber (1972) published recently more extensive data for A on both sides of the O_2-MS (Table 10). Special care was taken to eliminate water vapor attenuation, being typically on the order of < 1 dB total at zenith. The dry air data were fitted by yet another linewidth model (R-Model) which consists of a two-piece linear pressure dependence for the width γ of the 60 GHz line complex excluding the 1^- line --

$$\begin{aligned} &\text{Range 1, } \gamma < 52.7 \text{ MHz}, \\ &\qquad \gamma = 1.88\, p\, (300/T) \quad [\text{MHz}] \\ &\text{Range 2, } \gamma \geq 52.7 \text{ MHz } (p_1 = 20.7 \text{ torr at } T = 222\,^\circ\text{K}), \\ &\qquad \gamma = 52.7 + (1,88/3)\,(p-p_1)\,(300/T) \quad [\text{MHz}]. \end{aligned} \tag{45}$$

We substituted the R-Model (Eq. 45) into the computer routine and, as expected, got a good fit to the Reber data. Both empirical width models (Eqs. 32, 45) are a somewhat arbitrary discription of an intensity distribution which deviates from a linear addition of individual shapes.

The experimental zenith data (Table 10) strongly suggest overlap effects in the O_2 continuum spectrum (Sect. 2.4.1), especially when compared with A-values which have been calculated using the pressure-linear linewidth model (Eq. 19). The experimental values, however, are only wing data and as such not really representative of the O_2 continuum spectrum.

Center data cannot be obtained by the radiometric technique since the band between 55 and 65 GHz is practically opaque for any source in space. Reliable experimental information on the pressure dependence of the intensity distribution of the O_2 continuum spectrum can be obtained by a controlled laboratory experiment. An analysis of continuum data is based on the accurate knowledge of the O_2 line spectrum and overlap effects as shown by the theoretical treatments of Mingelgrin (1972) and Dillon (1969).

The O_2-MS offers between 55 and 65 GHz one feature not found at any lower frequency; namely, high attenuation and phase dispersion values related to the fairly stable dry part of the lower atmosphere. This affords shielding of satellite-satellite links against ground interferences. The first 100 km of the atmosphere present a fairly complicated "natural" filter which can be used to advantage in special system applications. The strong frequency dependences of $A(\alpha)$ and $\Delta T(\Delta\phi)$ permit frequency diversity techniques and signal preprocessing such as phase-keying. Figures 25 through 39 demonstrate that the atmosphere, which is opaque close to sea level, becomes transparent at higher altitudes in 16 channels each possessing a bandwidth of several hundred megahertz. One such channel is centered around 58.8 GHz, and for a tangential path geometry the loss due to the O_2-MS varies as follows

h_o [km]	5	10	15	20	25	30	50	75
A_t [dB]	5240	2760	835	203	46.5	9.8	.54	$1.5 \cdot 10^{-4}$

The curves presented in figures 25 through 39 for cumulative transmission and zenith ray path properties are for one-way radio communication cases. The distinction between the highly-structured line spectrum (I) and the smooth continuum spectrum (II) can clearly be made within each cumulative spectrum.

Aircraft can communicate with one another or with satellites between the O_2-MS lines when flying above 10 kilometers while being shielded against the ground. Several atmospheric channels might be combined to increase the bandwidth by means of frequency transposition. The cumulative phase dispersion, ΔT, in the pass band centered at 58.8 GHz varies for a zenith path from -5.7 rad per 350 MHz at h_1 = 15 km, to -4.5 rad per 680 MHz at h_1 = 30 km.

3.2.3. Some Spectroscopic Properties of Ozone and Other Minor Atmospheric Gases.

The mixing ratio for the main constitutents of clean, dry air is constant up to $h \gtrapprox 90$ km for all $r_k \geq 10^{-5}$ (Fig. 23). Several minor constituents and gaseous pollutants exhibit, in addition to O_2 and H_2O, spectral lines over the 40 to 140 GHz band (Table 12). These lines are part of rotational spectra due to molecular electric dipole moments. Linear rotor molecules (N_2O, CO) exhibit an almost harmonic spacing of lines, while asymmetric rotors with three different principle moments of inertia (H_2O, SO_2, NO_2, CH_2O) display an irregular line pattern. Although the absorption coefficients of electric dipole transitions are considerably larger than those for O_2, these spectra are of no importance to transfer properties of the lower ($h < 20$ km) atmosphere.

Trace concentrations and strong foreign-gas-broadening essentially "wash-out" these resonances.

Ozone is practically the only molecule which causes some concern. The line shape is altered according to the manner in which the gas is distributed throughout the atmosphere. The increase of the O_3-mixing ratio with height produces line profiles of several megahertz width. Waters (1970) calculated 48 O_3-lines between 39.426 and 142.172 GHz of which 14 lines are masked by the O_2-MS. The 7 strongest O_3 lines are listed in Table 12, and the maximum values for the total zenith attenuation indicate that the vicinity of these lines probably should be avoided by ground-to-satellite links. On the other hand, one could "tune-in" on these resonances and use phase or amplitude variations of a transmitted signal as tracer for high-altitude ozone activity.

3.2.4 Atmospheric Noise Due to Molecular Attenuation.

Atmospheric noise reaching an antenna as a function of orientation and frequency is, as derived from radiative transfer theory, an integral over the temperature $T(\ell)$ and the attenuation rate $\alpha(\ell)$ along a ray path (see Sect. 3.2.1). A ground-based antenna "sees" the noise temperature (e.g., Blake, 1972)

$$T_A = \int_0^\infty T(\ell)\,\alpha(\ell)\,\exp.\,\left[-\int_0^\ell \alpha(s)\,ds\right] d\ell \qquad [°K] \quad . \tag{46}$$

The tropospheric O_2-MS attenuation between about 55 and 65 GHz is so high (opaque atmosphere), that most of the noise originates from the lowest layers. The noise temperature equals approximately the surface temperature since the integrand of (46) is large at $\ell = 0$ and rapidly approaches zero for $\ell > 0$. At the band edges of the O_2-MS, the atmosphere becomes semi-transparent, and T_A starts to drop when $A \lesssim 30$ dB (Eq. 43).

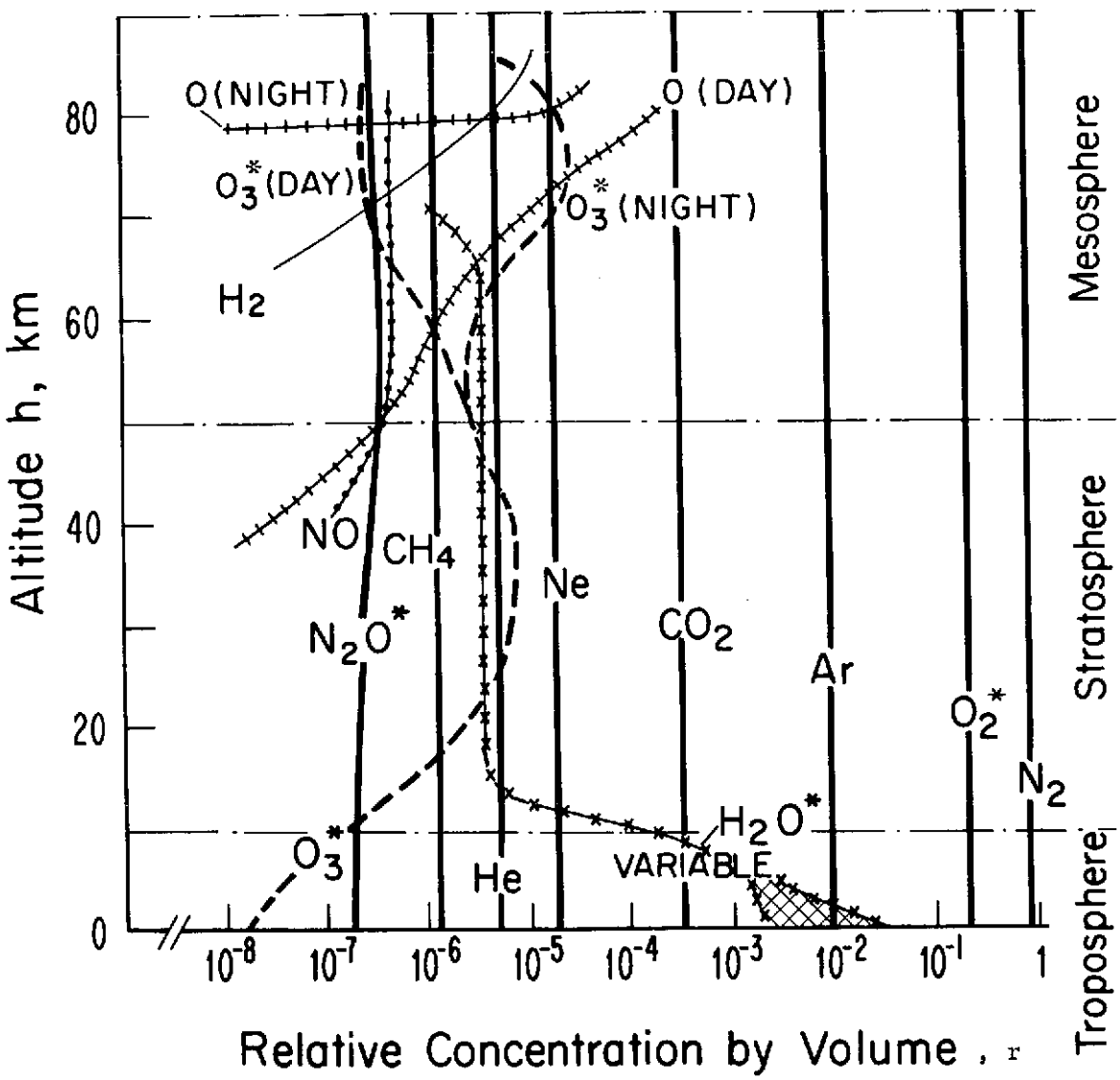

Figure 23. Model profiles of atmospheric constituents showing their relative concentrations versus altitude up to h = 90 km (after Waters, 1970). * denotes molecules with resonance spectra below 140 GHz (Tables 7, 12 and Sect. 2.5). Numerical values see Table 1.

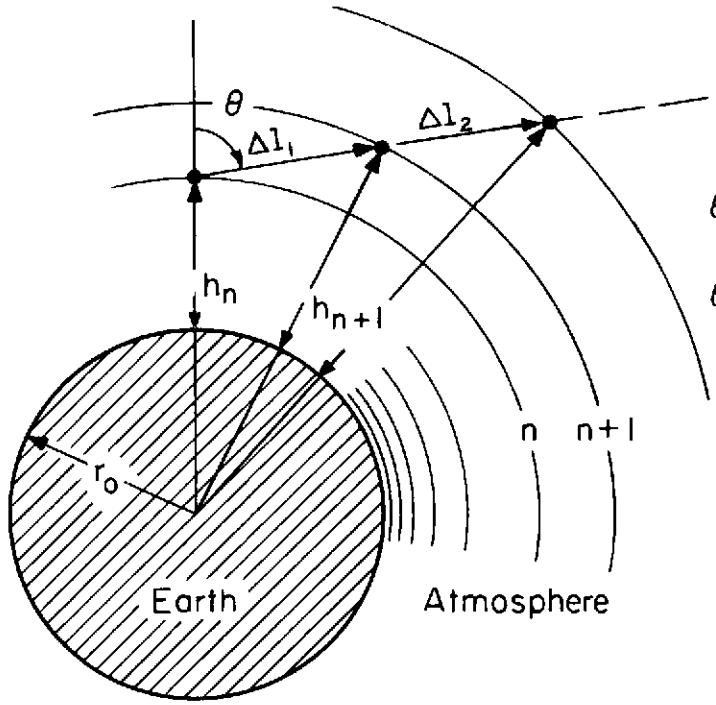

$\theta = 0°$ Zenith Path

$\theta = 90°$ $\frac{1}{2}$(Tangential Path)

$\overline{r}_o = 6368$ km

$$(r_o + h_n)\cos\theta \equiv \eta$$

$$\Delta l_1 = \sqrt{\eta^2 + (h_{n+1} - h_n)(h_{n+1} + h_n + 2r_o)} - \eta$$

$$\Delta l_2 = \sqrt{\eta^2 + (h_{n+2} - h_n)(h_{n+2} + h_n + 2r_o)} - (\eta + \Delta l_1)$$

$$\Delta l_3 = \sqrt{\eta^2 + (h_{n+3} - h_n)(h_{n+3} + h_n + 2r_o)} - (\eta + \Delta l_1 + \Delta l_2)$$

$$\Delta l_4 = \ldots\ \text{etc.}$$

Figure 24. Algorithm used for the calculation of the differential slant path length Δl_n between two shells of a spherically stratified atmosphere. θ - starting angle against zenith (n = 151 for h = 0 to 100 km).

Table 10. Zenith Oxygen Attenuation A from Sea Level.

Frequency ν ± 1 MHz	Measured Values a)		No. in Fig. 25	No. of Samples	RMS-Error ± $\delta\bar{A}$	$\bar{A}$	Calculated Values R-Model A [a)]	CMR-Model A [a)]	Linear Model A
[GHz]					[%]	[dB]			
50.000	W	1957	2	-	15	1.3	1.26	1.55	3.17
	R	1972		228	7.1	1.12			
50.200	R	"		130	9.9	1.31	1.33	1.64	3.36
50.700	R	"		120	6.3	1.58	1.57	1.92	3.90
51.250	R	"		226	12.6	1.98	1.93	2.35	4.67
51.750	R	"	7	638	11.1	2.43	2.41	2.91	5.62
52.220	R	"		171	4.8	2.92	3.07	3.67	6.81
52.500	SW	1969	6	33	≈20	5.1	3.73	4.37	7.76
53.400	CMR	1968	1	125	5.2	7.16	6.88	7.10	12.18
	R	1972		123	3.0	7.06			
53.500	SW	1969	6	8	≈20	9.3	7.74	7.82	13.0
	CMR	1969		110	6.7	7.82			
	R	1972		60	4.0	8.05			
	R	1972		43	2.9	7.84			
53.811	CMR	1968	1	129	5.4	10.20	9.37	10.52	15.33
	R	1972		120	5.9	9.59			
54.352	CMR	1968	1	26	1.4	15.39	14.53	15.98	21.17
	CMR	"	1	57	2.8	15.62			
	R	1972		44	3.9	13.91			
54.895	CMR	1968	1	50	5.6	23.35	22.50	24.35	29.57
	R	1972		20	4.1	20.89			
66.056	R	"		122	7.3	8.61	8.92	10.25	16.00
66.565	R	"		43	0.5	6.23	6.28	7.37	12.46
67.016	R	"		230	6.3	4.64	4.79	5.71	10.21
67.696	R	"		144	4.2	3.08	3.36	4.09	7.82
68.144	R	"	7	402	5.1	2.58	2.79	3.42	6.71
68.680	R	"		81	3.0	2.04	2.31	2.85	5.70
65 to 69	TS	1963	3	-	-	18 to 2.8	-	-	-
69.216	R	1972		154	13.5	1.71	1.97	2.43	4.92
69.732	R	"		81	7.7	1.46	1.71	2.12	4.33
70.0	C	1958	4	-	16	1.9	1.62	2.00	4.07
70.260	R	1972	7	447	10.2	1.37	1.51	1.88	3.85
72.0	H	1964	5	-	25	1.45	1.08	1.34	2.75

a)
W - Whitehurst et al., 1957
R - Reber, 1972
SW - Snider and Westwater, 1969
CMR - Carter et al., 1968
TS - Tolbert and Straiton, 1963
C - Coates, 1958
H - Hayes, 1964

A survey of measured values of clear sky zenith attenuation for the frequency range 15 to 140 GHz has been made by Thompson III (1971; Fig. 9-11).

Table 11. Tangential Attenuation
Tangential Phase Dispersion

CMR-Linewidth Model
U. S. Standard Atmosphere 1962

Frequency, MHz	Minimum Altitude h_o 30KM	30KM	20KM	20KM	10KM	10KM	00KM	00KM
49000	3.4978+000 rad 7.0181-003 rad/km	4.6284-002 dB 1.3202-004 dB/km	1.7364+001 rad 3.5285-002 rad/km	9.7340-001 dB 2.6840-003 dB/km	8.3808+001 1.5952-001	1.4701+001 Total Attenuation, dB 3.5778-002 Attenuation Rate, dB/km at h_o		
49020	3.5064+000 7.0353-003	4.6490-002 1.3262-004	1.7407+001 3.5371-002	9.7801-001 2.6969-003	8.4012+001 1.5991-001	1.4771+001 3.5948-002		
49040	3.5150+000 7.0525-003	4.6706-002 1.3324-004	1.7449+001 3.5457-002	9.8269-001 2.7100-003	8.4217+001 1.6030-001	Total Phase Dispersion, rad Phase Dispersion Rate, rad/km at h_o		
49060	3.5237+000 7.0699-003	4.6927-002 1.3387-004	1.7492+001 3.5544-002	9.8740-001 2.7232-003	8.4423+001 1.6069-001			
49080	3.5323+000 7.0873-003	4.7152-002 1.3451-004	1.7535+001 3.5631-002	9.9215-001 2.7365-003	8.4630+001 1.6108-001	1.4983+001 3.6466-002	3.7731-001 rad/km	2.3341-001 dB/km
49100	3.5411+000 7.1047-003	4.7379-002 1.3516-004	1.7578+001 3.5718-002	9.9693-001 2.7499-003	8.4837+001 1.6148-001	1.5055+001 3.6641-002	3.7826-001	2.3461-001
49120	3.5499+000 7.1223-003	4.7608-002 1.3581-004	1.7621+001 3.5805-002	1.0017+000 2.7633-003	8.5046+001 1.6188-001	1.5127+001 3.6818-002	3.7922-001	2.3582-001
49140	3.5587+000 7.1399-003	4.7840-002 1.3647-004	1.7665+001 3.5894-002	1.0066+000 2.7767-003	8.5255+001 1.6228-001	1.5200+001 3.6995-002	3.8018-001	2.3704-001
49160	3.5675+000 7.1576-003	4.8073-002 1.3713-004	1.7708+001 3.5982-002	1.0114+000 2.7902-003	8.5465+001 1.6268-001	1.5273+001 3.7175-002	3.8114-001	2.3827-001
49180	3.5764+000 7.1754-003	4.8309-002 1.3780-004	1.7752+001 3.6071-002	1.0163+000 2.8037-003	8.5677+001 1.6308-001	1.5347+001 3.7355-002	3.8211-001	2.3951-001
49200	3.5854+000 7.1932-003	4.8546-002 1.3848-004	1.7796+001 3.6161-002	1.0213+000 2.8173-003	8.5889+001 1.6348-001	1.5421+001 3.7537-002	3.8308-001	2.4077-001
49220	3.5943+000 7.2112-003	4.8786-002 1.3916-004	1.7840+001 3.6250-002	1.0263+000 2.8310-003	8.6102+001 1.6389-001	1.5496+001 3.7720-002	3.8405-001	2.4203-001
49240	3.6033+000 7.2292-003	4.9029-002 1.3985-004	1.7885+001 3.6340-002	1.0313+000 2.8448-003	8.6316+001 1.6430-001	1.5572+001 3.7905-002	3.8504-001	2.4330-001
49260	3.6124+000 7.2473-003	4.9274-002 1.4054-004	1.7929+001 3.6431-002	1.0363+000 2.8587-003	8.6531+001 1.6471-001	1.5648+001 3.8091-002	3.8602-001	2.4458-001

Captions for Figures 25 to 39

—Computer Plots—

a)

Figure	h_1 [km]
25	0 (sea level)
27	5
29	10
31	15
33	20
35	25
37	30

Total attenuation A and phase dispersion $\Delta\Upsilon$ due to the O_2-MS between 49 and 72 GHz for a zenith path through the U. S. Standard Atmosphere (1962) from different initial altitudes h_1 to outer space. p_o and T_o identify the pressure and temperature conditions at h_1 (CMR-Model for γ_i - Eqs. 32, 33).

b)

Figure	h_o [km]
26	5
28	10
30	15
32	20
34	25
36	30
38	50
39	75

Total tangential attenuation A_t and dispersion $\Delta\Upsilon_t$ due to the O_2-MS between 49 and 72 GHz for a straight-line path (see Fig. 24) through the total U. S. Standard Atmosphere (1962) for different minimum altitudes above ground h_o (CMR-Model for γ_i - Eqs. 32, 33).

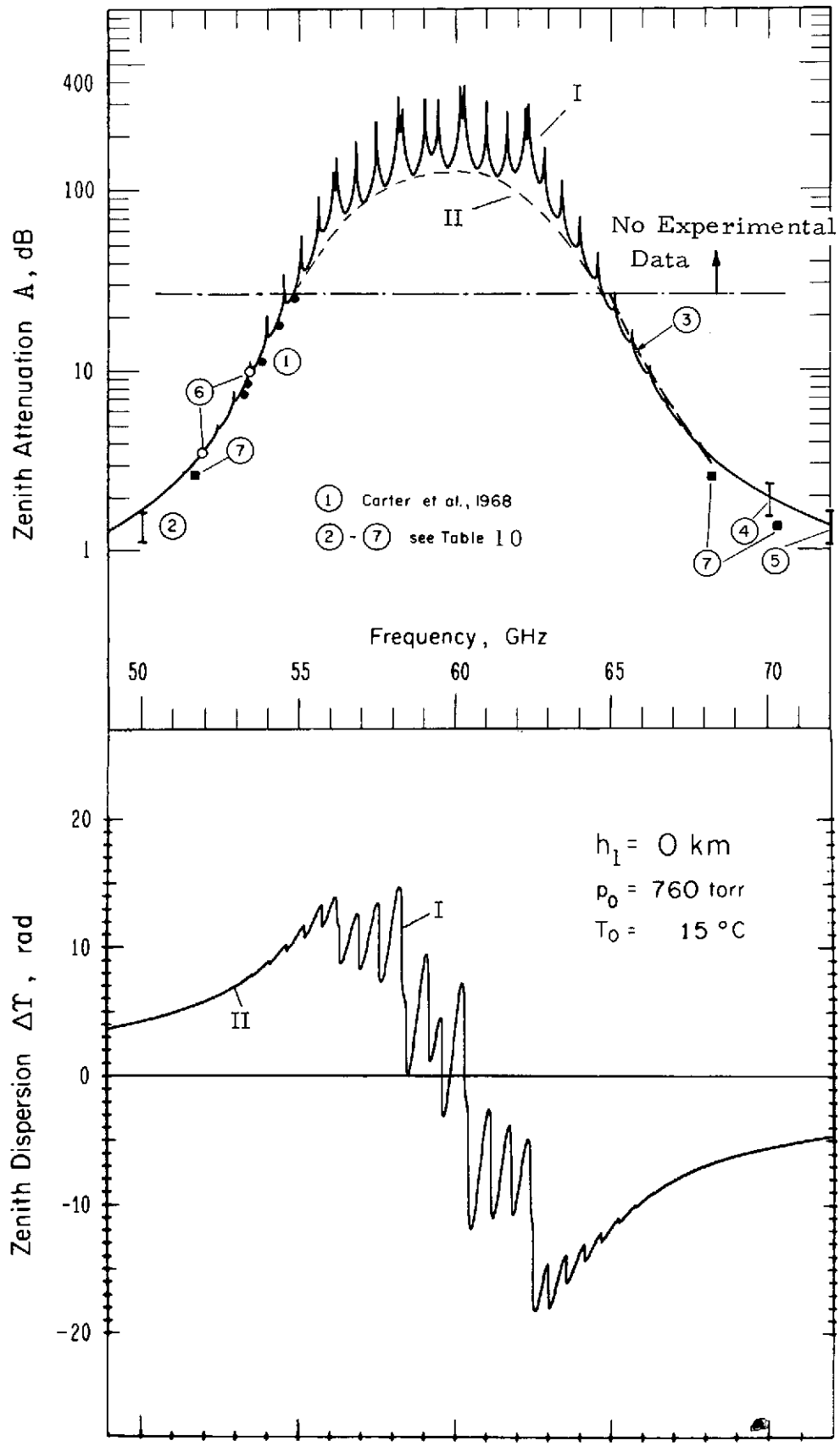
Zenith Attenuation A, dB
400
100
10
1
I
II
No Experimental Data
1 Carter et al., 1968
2 - 7 see Table 10
Frequency, GHz
50
55
60
65
70
Zenith Dispersion ΔT, rad
20
10
0
-10
-20
h_1 = 0 km
p_0 = 760 torr
T_0 = 15 °C

Figure 25.

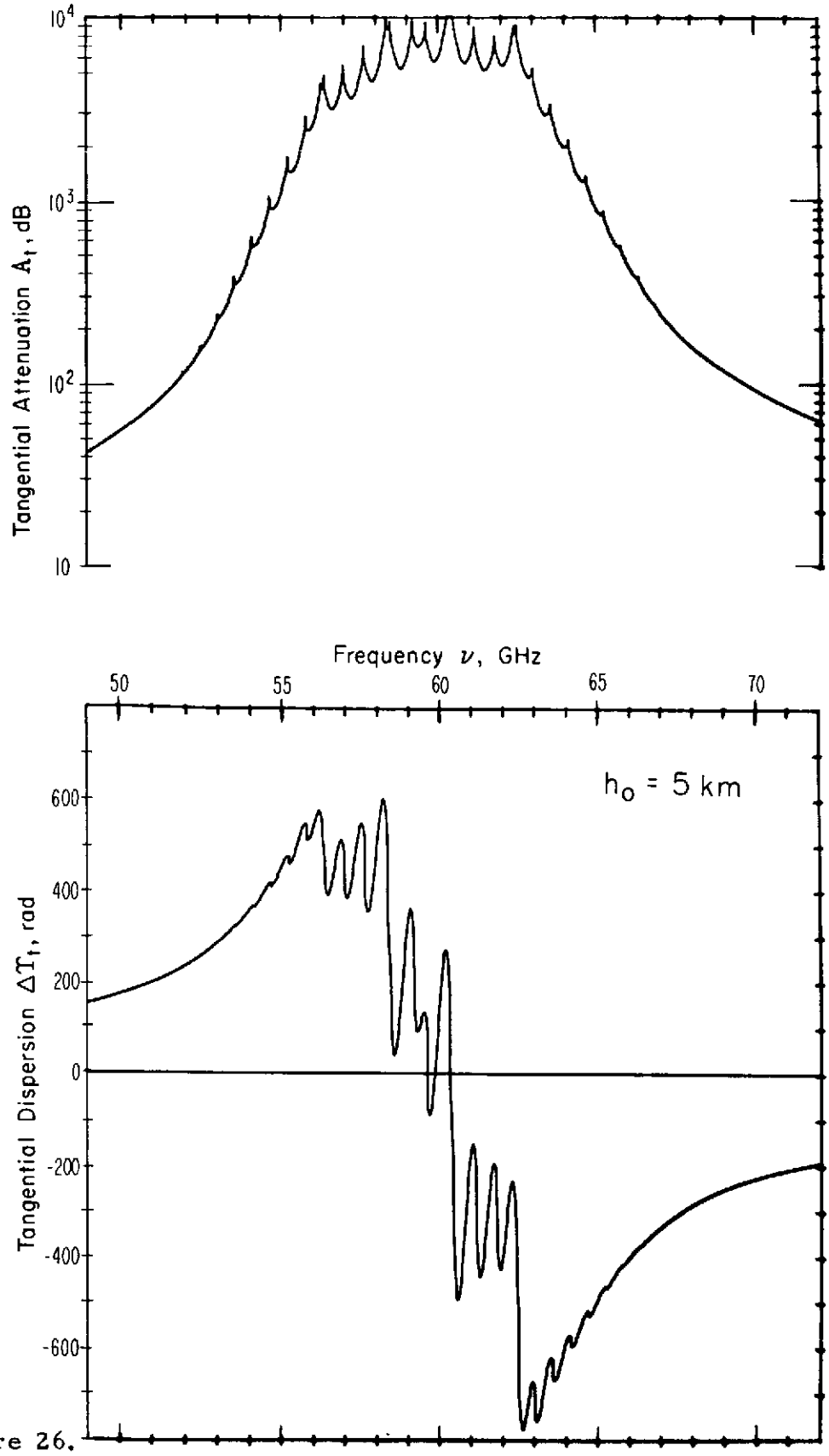
Tangential Attenuation A_t, dB
10^4
10^3
10^2
10
Frequency ν, GHz
50
55
60
65
70
h_o = 5 km
Tangential Dispersion ΔT_t, rad
600
400
200
0
-200
-400
-600

Figure 26.

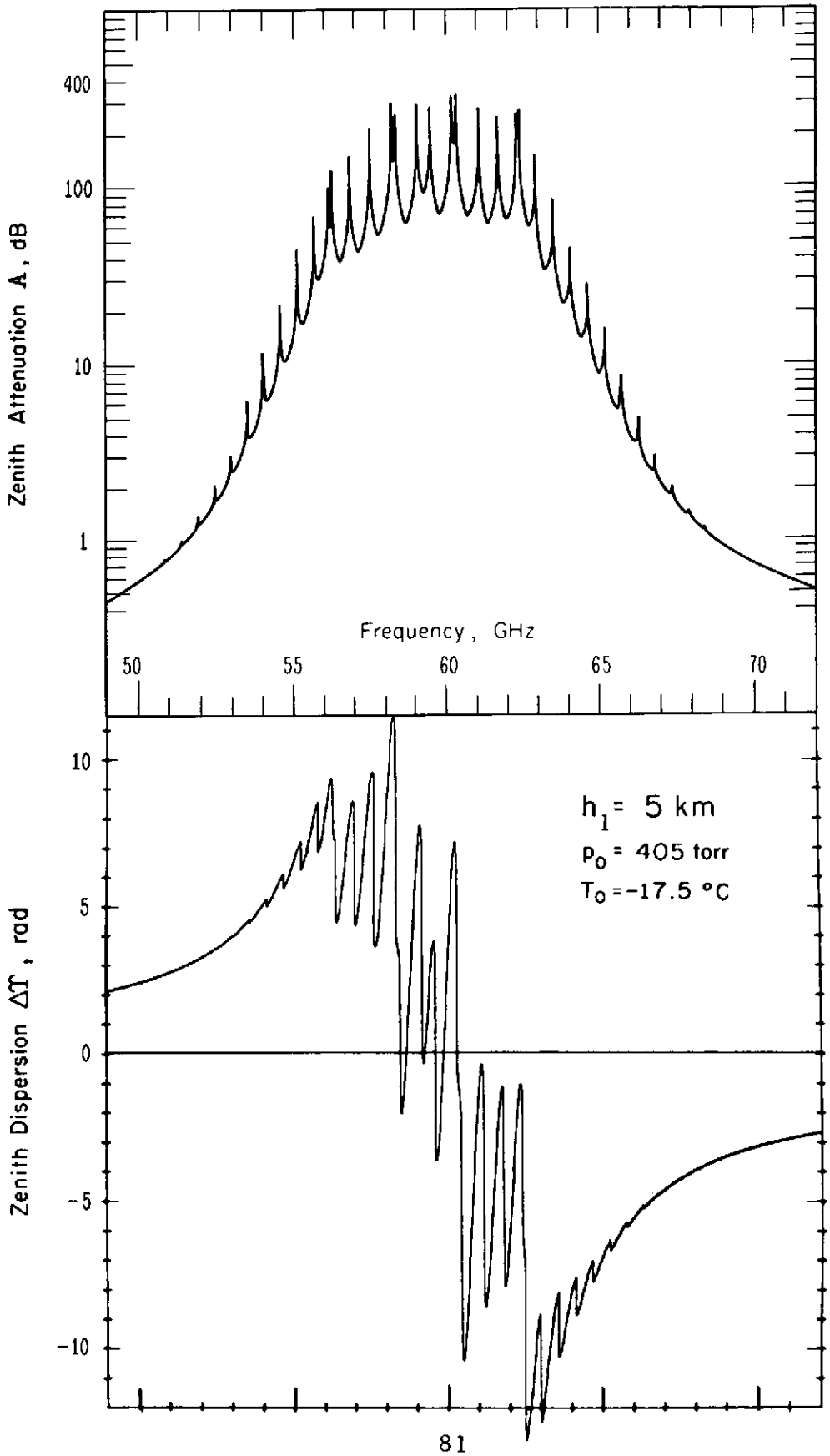
Zenith Attenuation A, dB
400
100
10
1
Frequency, GHz
50
55
60
65
70
Zenith Dispersion ΔΤ, rad
10
5
0
-5
-10
h_1 = 5 km
p_o = 405 torr
T_o = -17.5 °C

Figure 27.

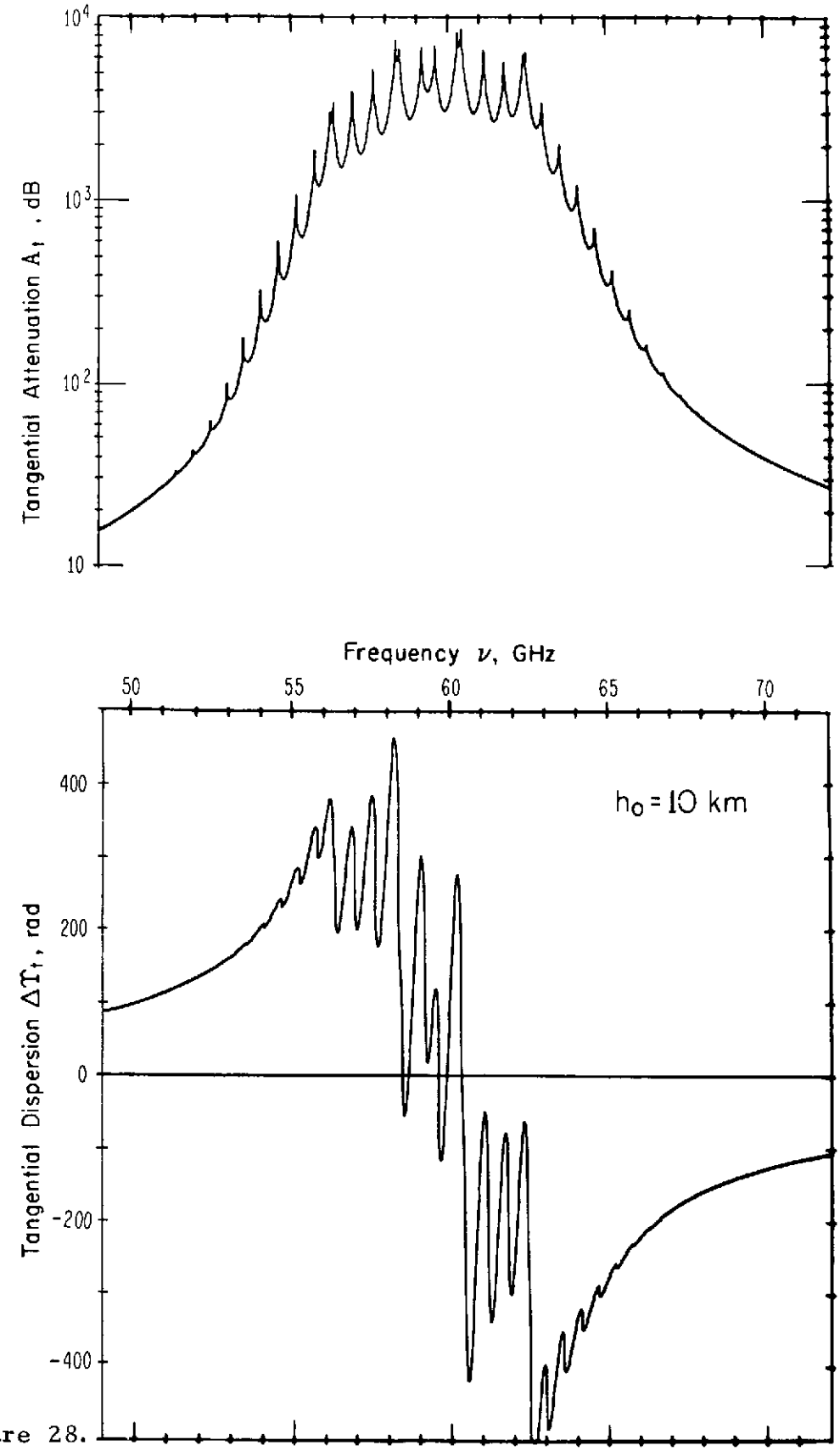
Tangential Attenuation A_t , dB
10^4
10^3
10^2
10
Frequency ν, GHz
50
55
60
65
70
h_o = 10 km
Tangential Dispersion ΔT_t, rad
400
200
0
-200
-400

Figure 28.

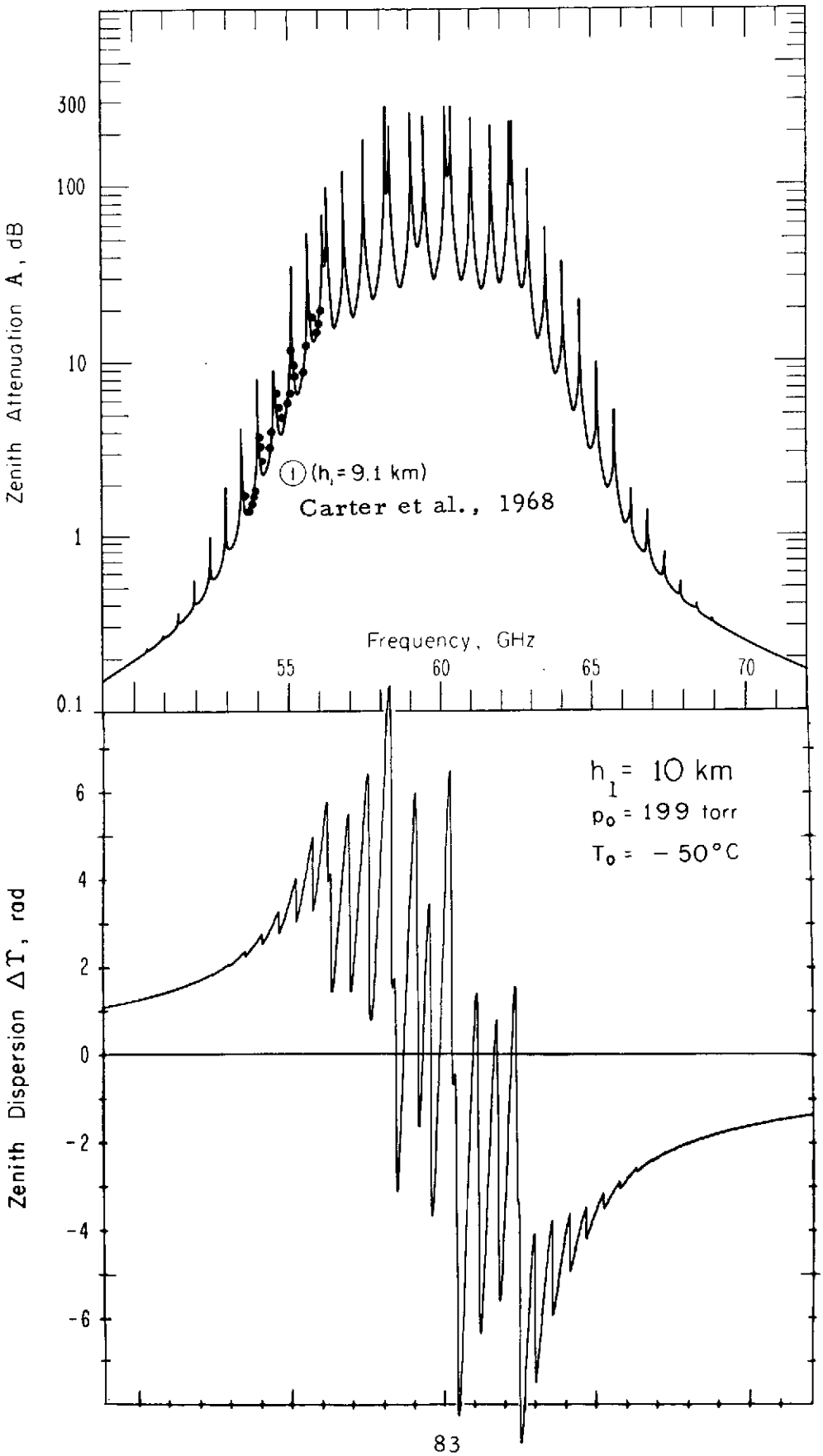
Zenith Attenuation A, dB
300
100
10
1
0.1
(1) (h_l = 9.1 km)
Carter et al., 1968
Frequency, GHz
55
60
65
70
Zenith Dispersion ΔT, rad
6
4
2
0
-2
-4
-6
h_l = 10 km
p_o = 199 torr
T_o = −50°C

Figure 29.

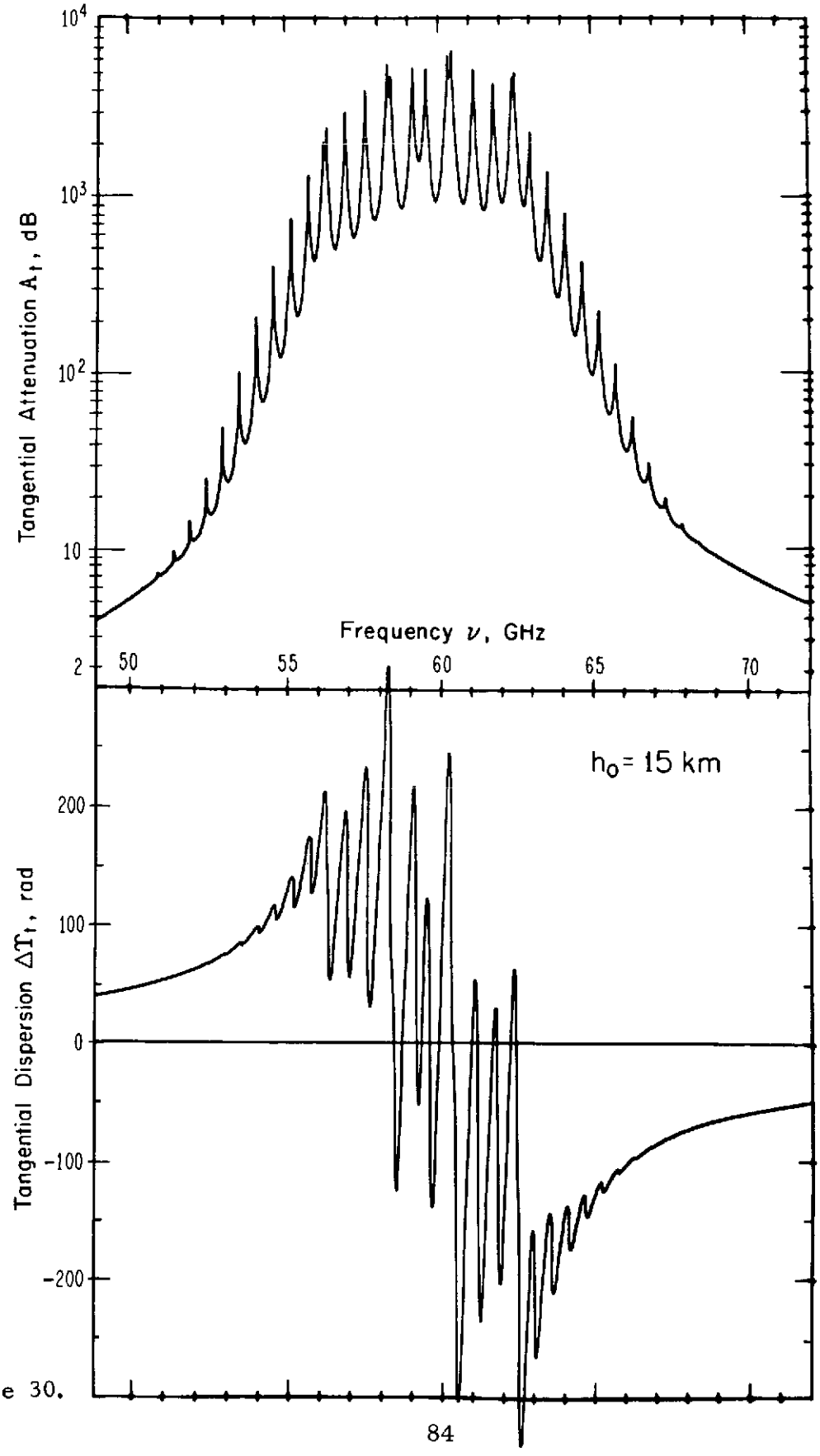
10^4
10^3
10^2
10
2
Tangential Attenuation A_t, dB
Frequency ν, GHz
50
55
60
65
70
h_o = 15 km
200
100
0
-100
-200
Tangential Dispersion ΔT_t, rad

Figure 30.

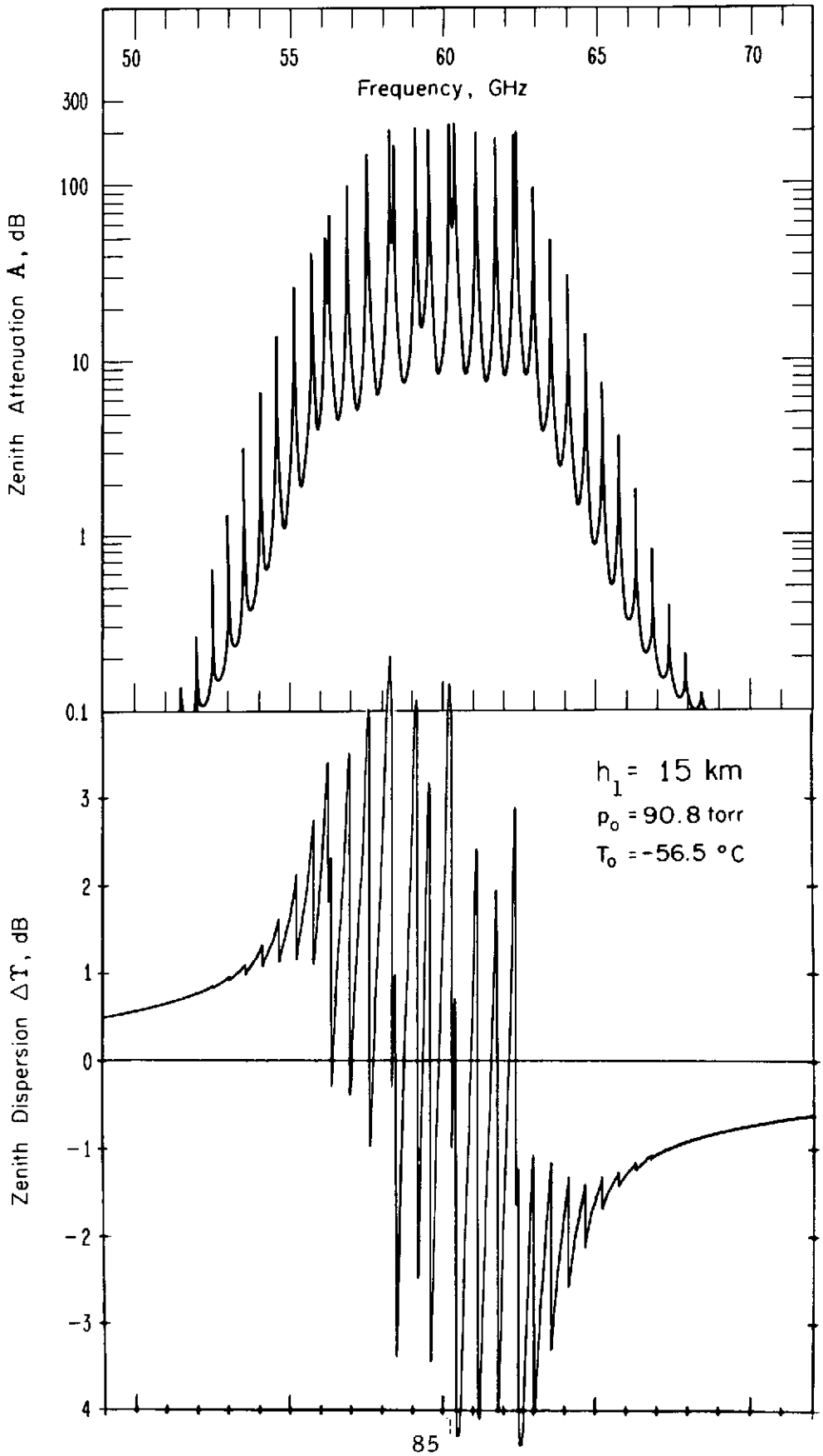
50
55
60
65
70
Frequency, GHz
300
100
10
1
0.1
Zenith Attenuation A, dB
h_1 = 15 km
p_o = 90.8 torr
T_o = -56.5 °C
3
2
1
0
-1
-2
-3
4
Zenith Dispersion ΔΤ, dB
85

Figure 31.

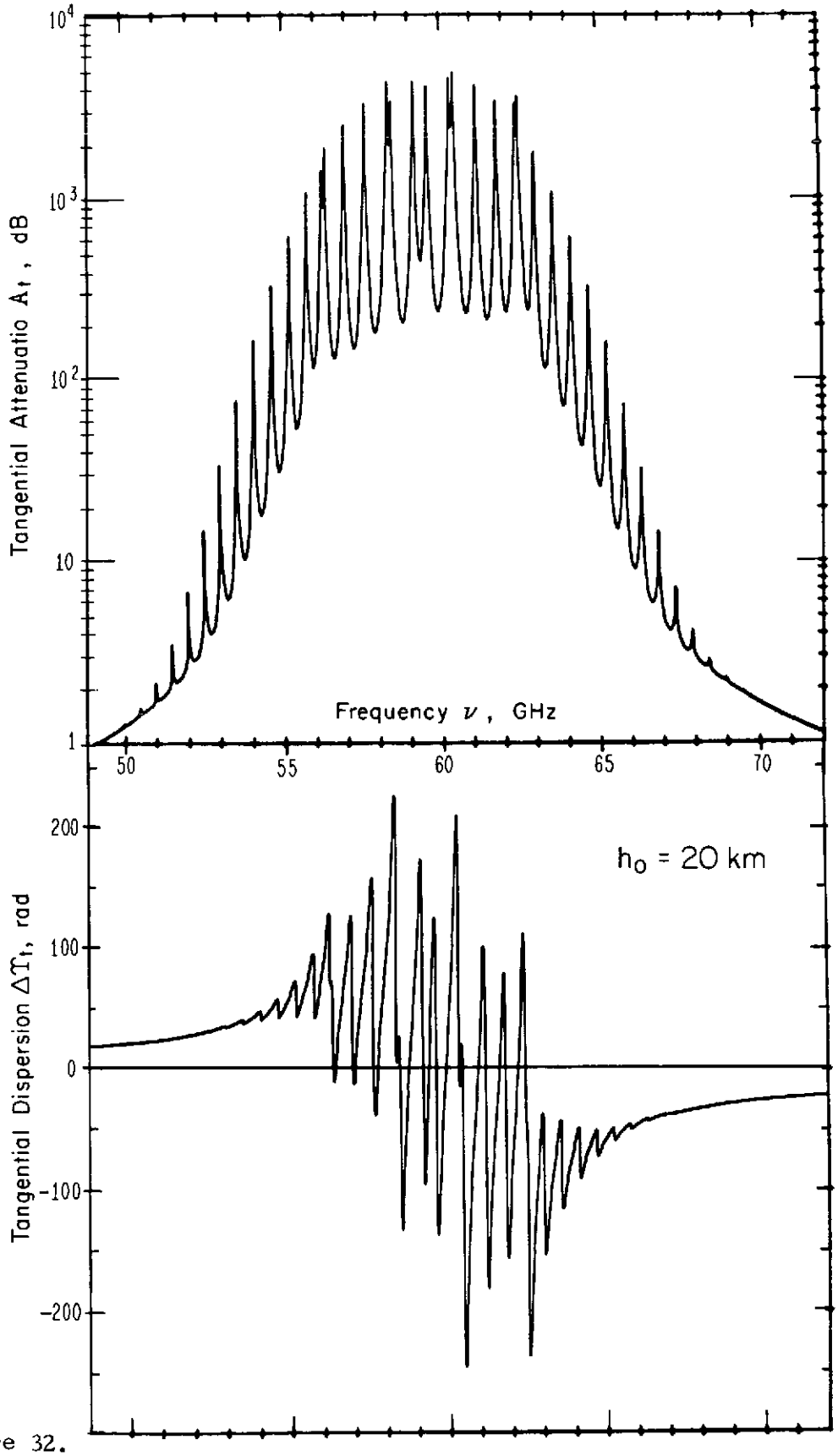
Tangential Attenuatio A_t , dB
10^4
10^3
10^2
10
1
Frequency ν , GHz
50
55
60
65
70
Tangential Dispersion ΔT_t, rad
200
100
0
-100
-200
h_o = 20 km

Figure 32.

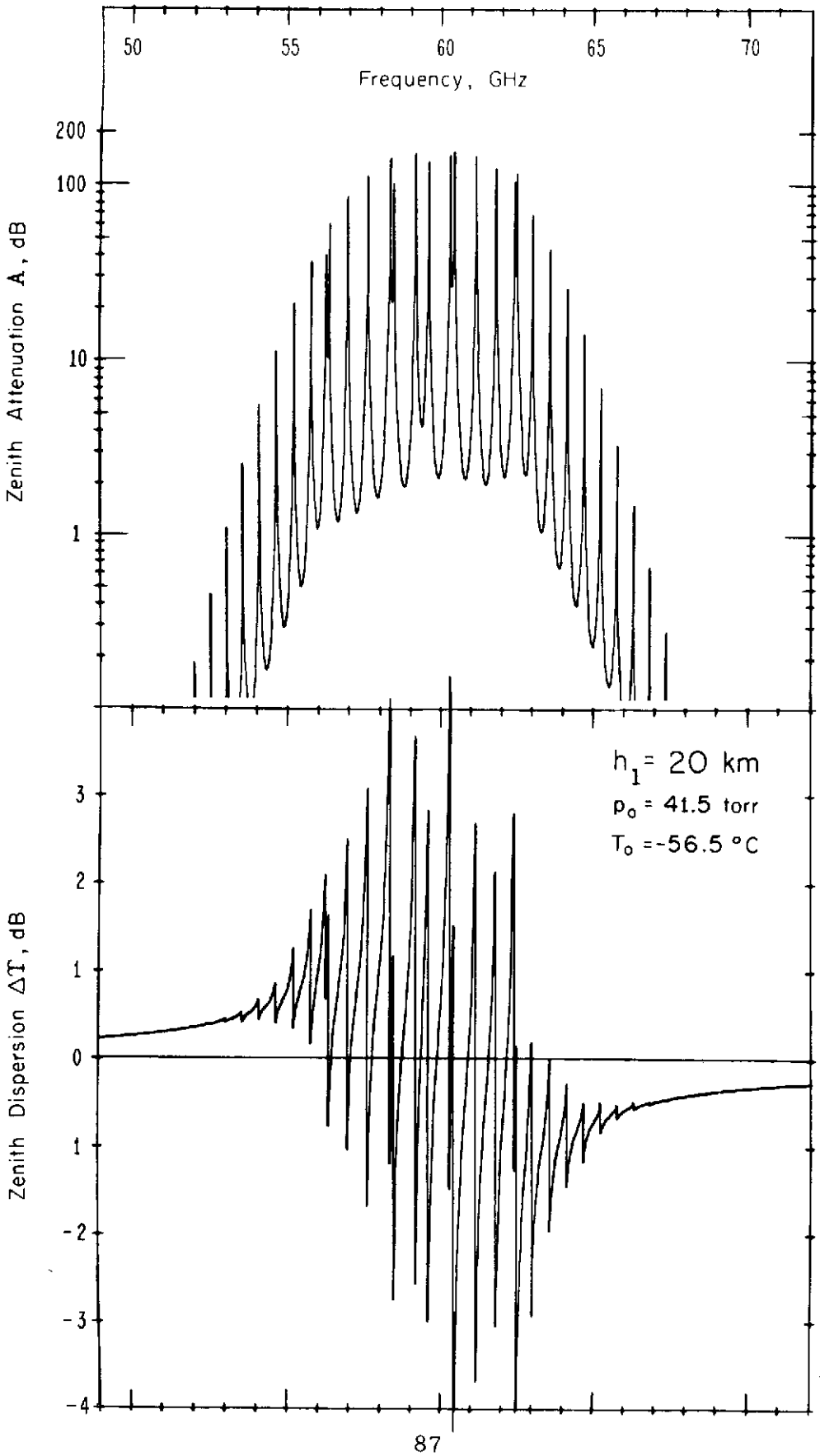
50
55
60
65
70
Frequency, GHz
200
100
10
1
Zenith Attenuation A, dB
h_1 = 20 km
p_o = 41.5 torr
T_o = -56.5 °C
3
2
1
0
1
-2
-3
-4
Zenith Dispersion ΔT, dB

Figure 33.

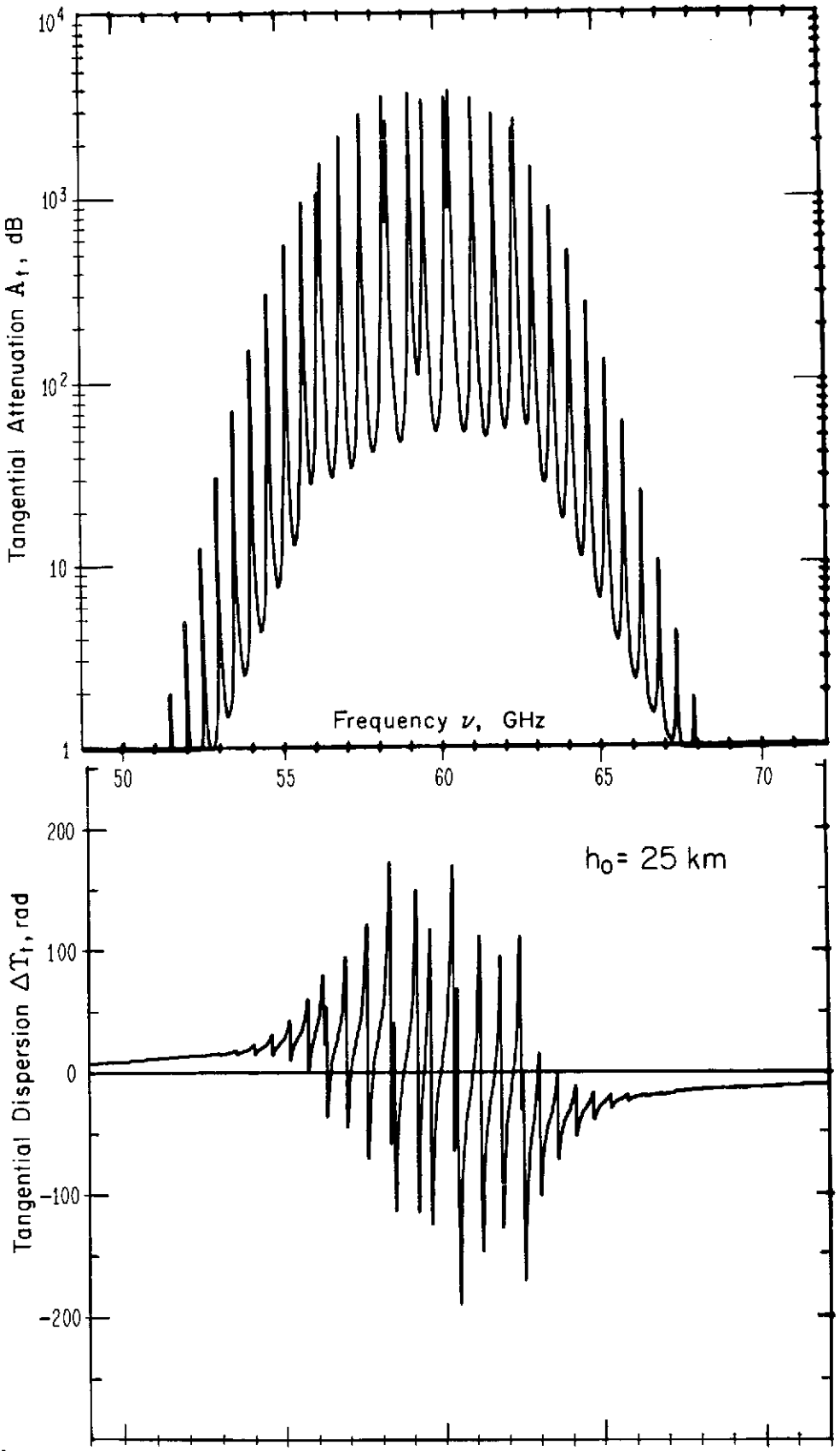
Tangential Attenuation A_t, dB
10^4
10^3
10^2
10
1
Frequency ν, GHz
50
55
60
65
70
Tangential Dispersion $\Delta\Upsilon_t$, rad
200
100
0
-100
-200
h_0= 25 km

Figure 34.

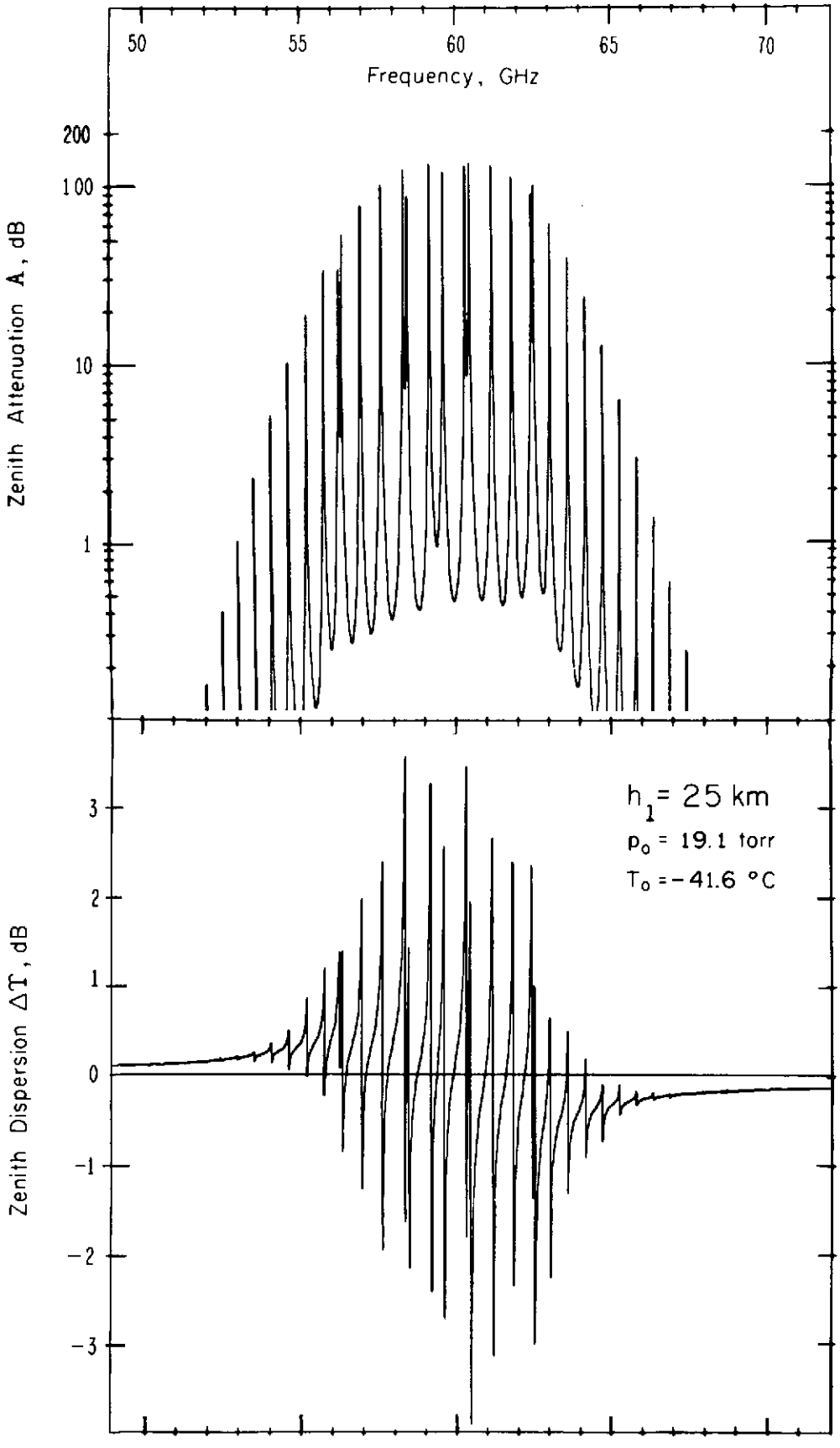
50
55
60
65
70
Frequency, GHz
200
100
10
1
Zenith Attenuation A, dB
h_1 = 25 km
p_o = 19.1 torr
T_o = -41.6 °C
3
2
1
0
-1
-2
-3
Zenith Dispersion ΔT, dB

Figure 35.

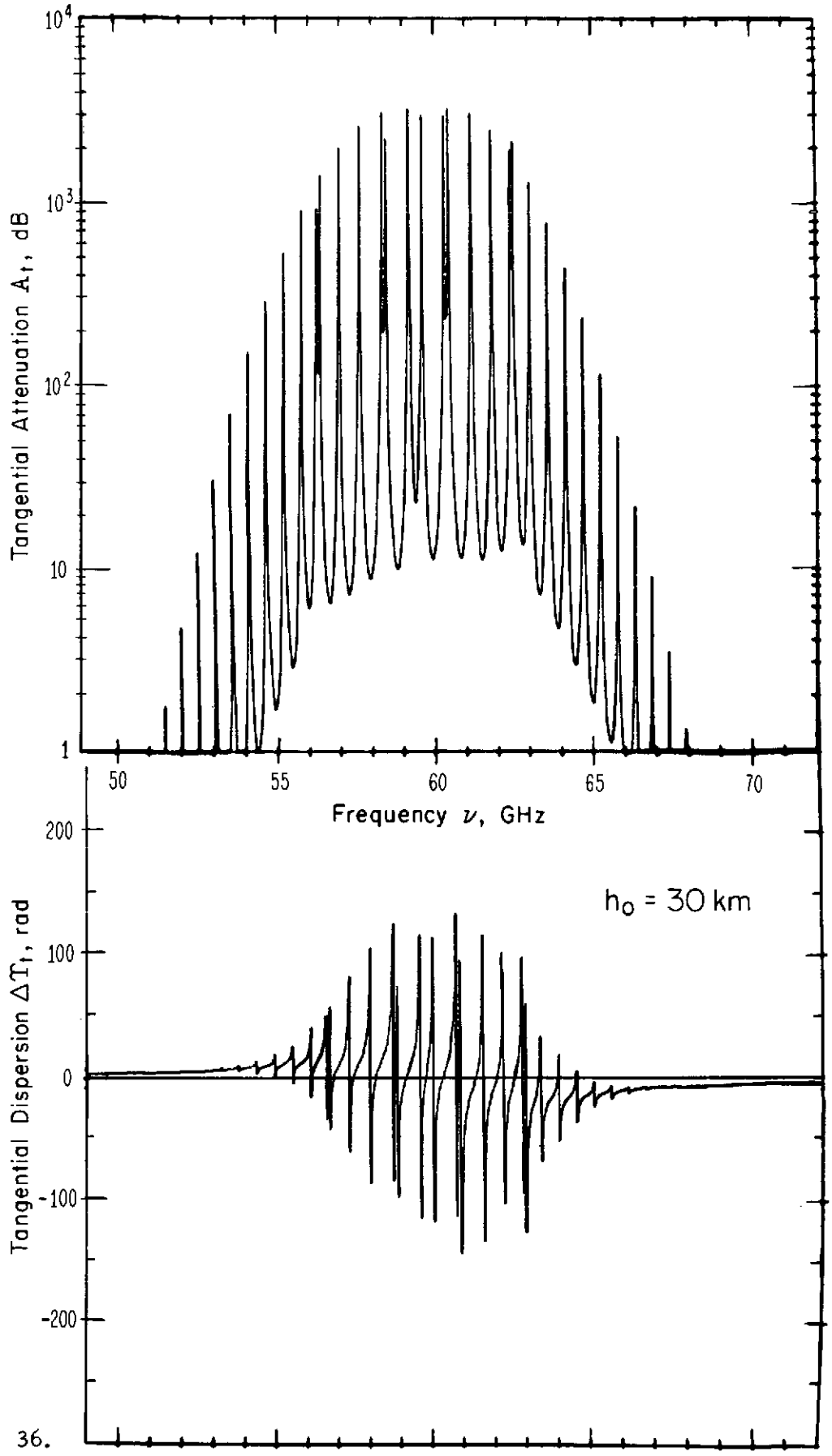
Tangential Attenuation A_t, dB
10^4
10^3
10^2
10
1
50
55
60
65
70
Frequency ν, GHz
Tangential Dispersion ΔT_t, rad
200
100
0
-100
-200
h_o = 30 km

Figure 36.

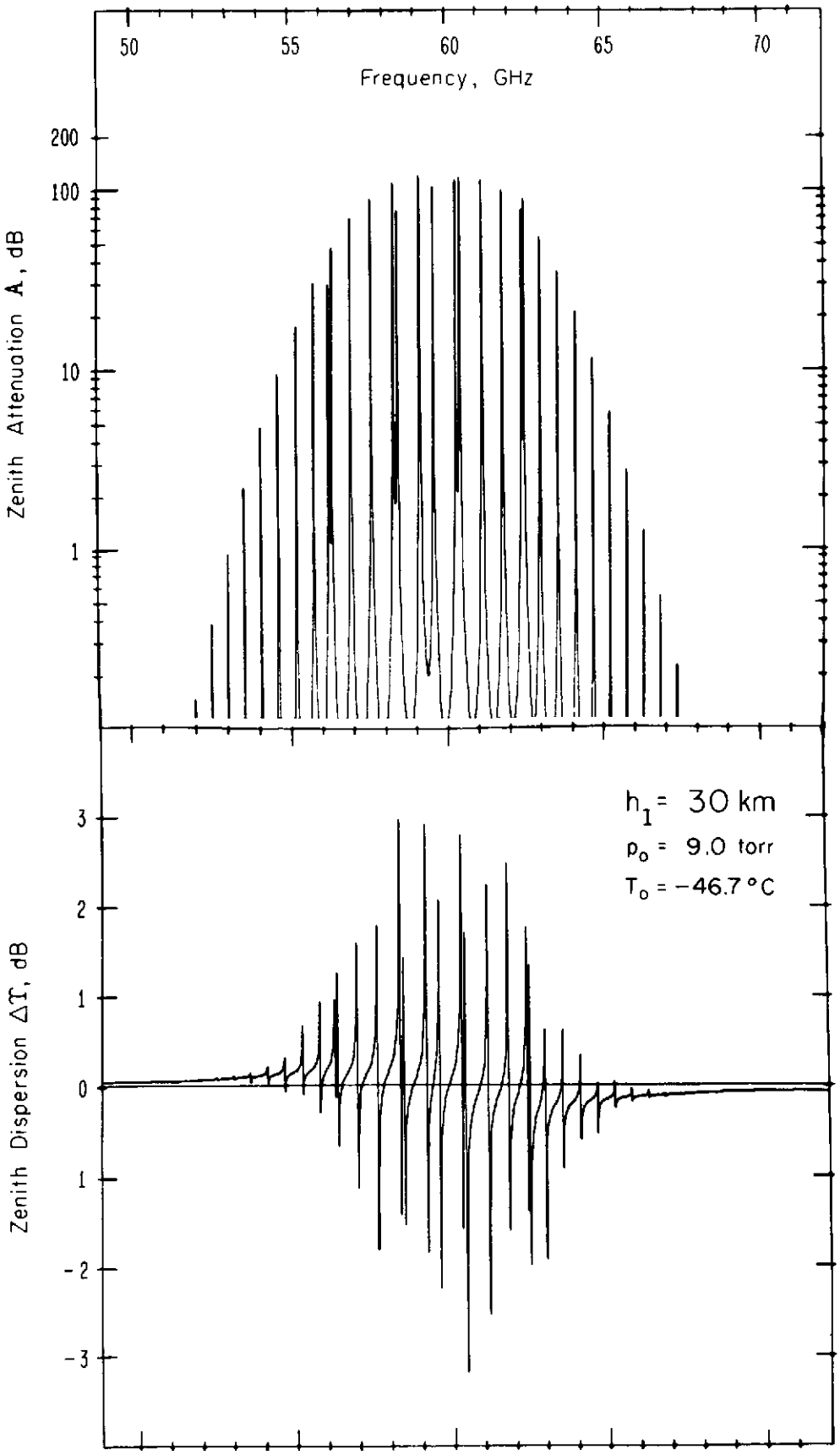
50
55
60
65
70
Frequency, GHz
200
100
10
1
Zenith Attenuation A, dB
h_1 = 30 km
p_o = 9.0 torr
T_o = −46.7 °C
3
2
1
0
1
-2
-3
Zenith Dispersion ΔT, dB

Figure 37.

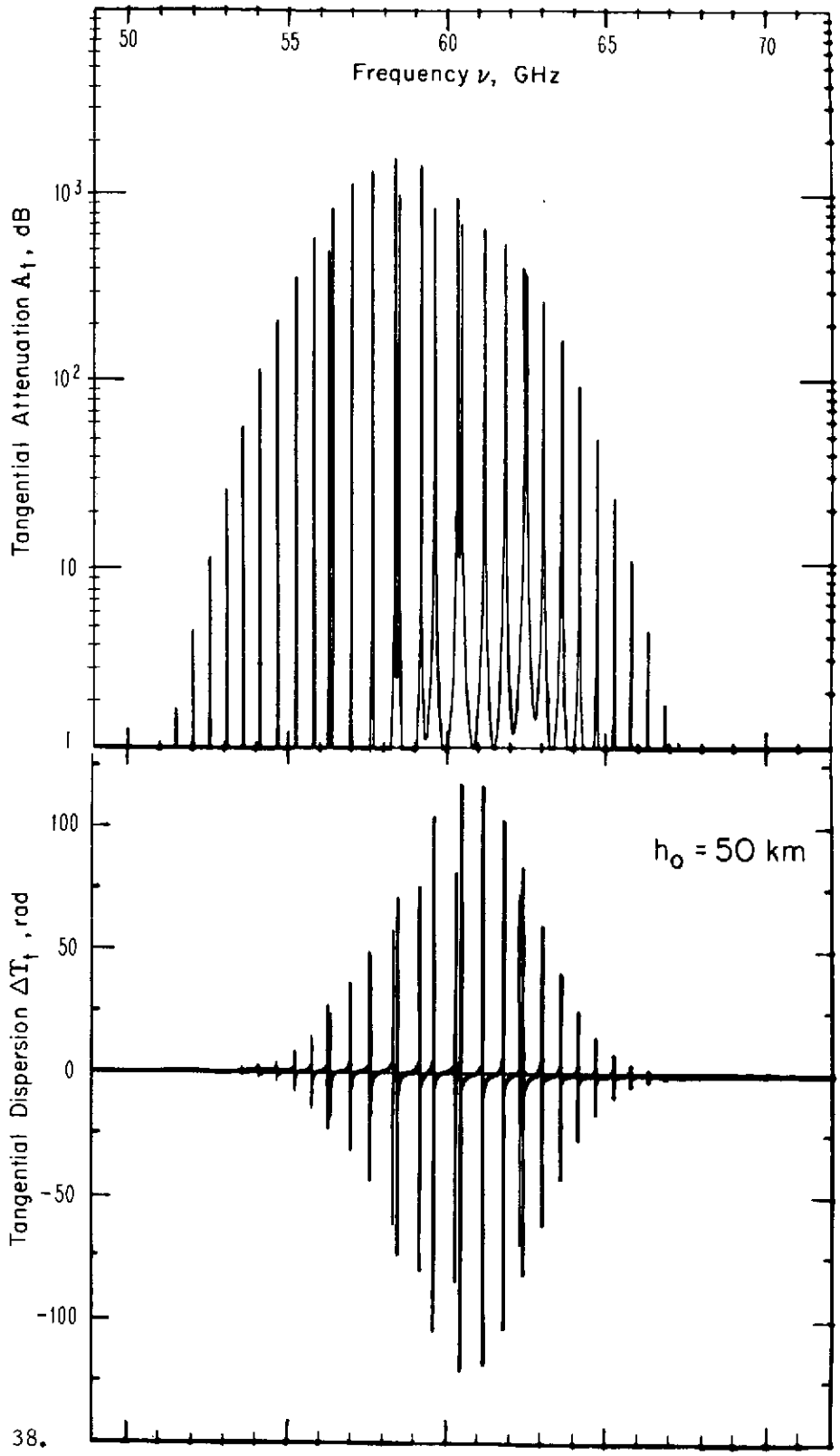
50
55
60
65
70
Frequency ν, GHz
Tangential Attenuation A_t, dB
10^3
10^2
10
1
100
50
0
-50
-100
Tangential Dispersion ΔT_t, rad
h_o = 50 km

Figure 38.

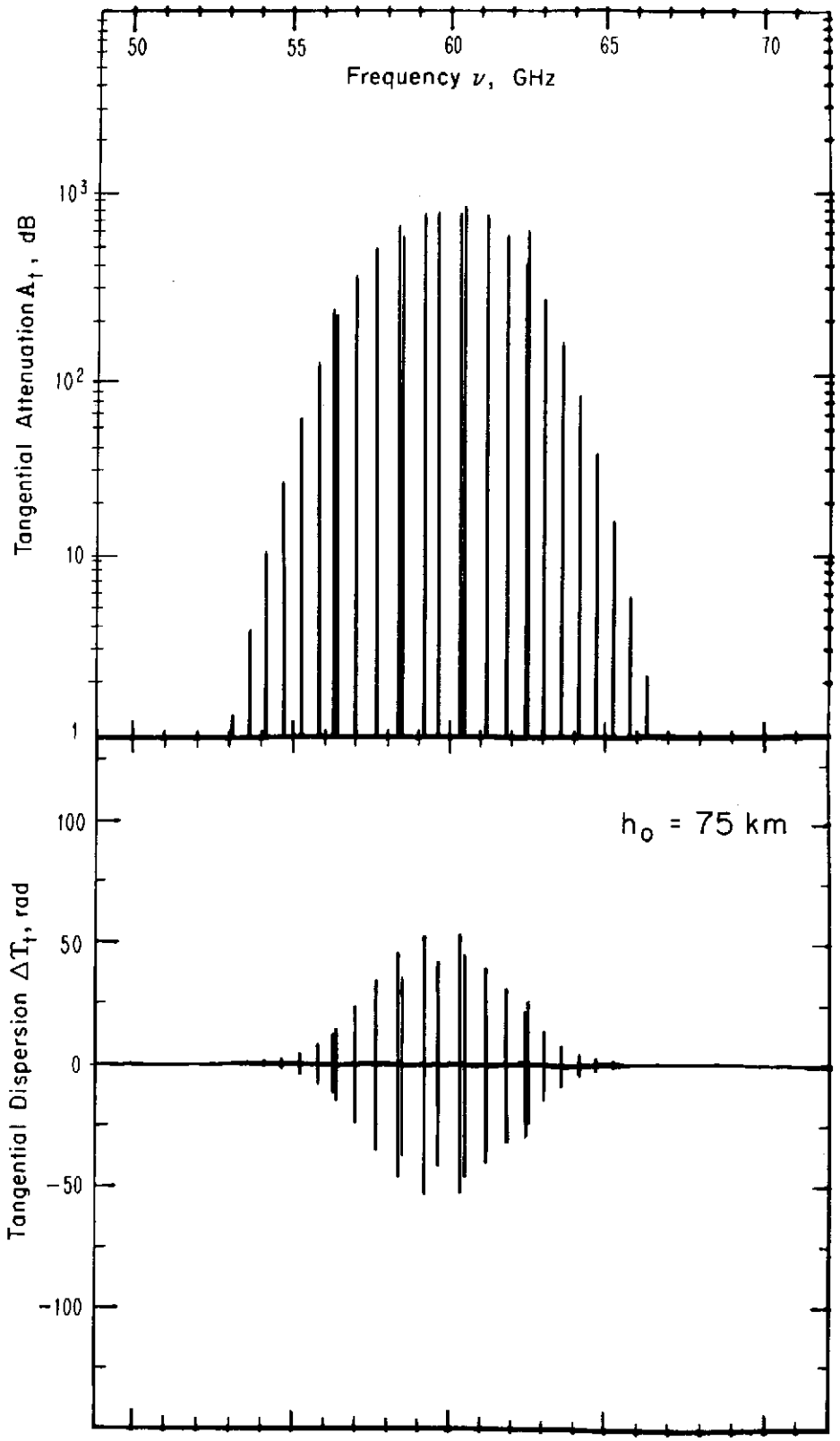
50
55
60
65
70
Frequency ν, GHz
10^3
10^2
10
1
Tangential Attenuation A_t, dB
100
50
0
−50
−100
Tangential Dispersion ΔT_t, rad
h_o = 75 km

Figure 39.

Table 12. Stronger Spectral Lines of Minor Atmospheric Gases in the 40 to 140 GHz Frequency Band

Molecule (type of rotor)	Center Freq. ν_0	Max. Absorpt. Pure Gas, 300°K α_0	Zenith Absorpt. (max.) A_0	Ground Level Concentration clean/polluted		Elec. Dipole Moment
	[GHz]	[dB/km]	[dB]	[ppm/vol]		[Debye or $3.336 \cdot 10^{-30}$ Asm]
O_3 (asymmetr.)	96.2288	426 a)	.16 *)	0 to 0.07	up to 3	0.53
	101.7368	803	.3			
	110.835	1230	.4			
	124.086	1750	.5			
	125.389	1030		3 to 6 at h = 20km		
	136.883	300				
	142.172	2330	.75			
N_2O (linear)	50.2460	20 a)		0.5	up to 10	0.167
	75.3696	65 a)				
	100.4917	152 a)				
	125.6137	282 b)				
	150.735	480 b)				
CO (linear)	115.2712	104 b)		0.01 to 0.2	up to 150	0.112
	230.5380	838 b)				
SO_2 (asymmetr.)	12 lines listed between 53.529 and 131.015 GHz c)			0 to 0.02	up to 20	1.615
NO_2 (asymmetr.)	10 lines listed between 40.358 and 41.278 GHz c)			0 to 0.01	up to 5	0.316
CH_2O (asymmetr.)	8 lines listed between 45.063 and 140.839 GHz c)			0 to 0.01	up to 5	2.34
O_2 (linear, fine structure)	1^+ (Table 7)	1.56	120 (Fig. 25)	209460		Magnetic Moment
	1^-	6.06	≈ 110			

*) Calculated by Waters (1970) for U. S. Standard Atmosphere (1962) and daytime ozone distribution (max. 5×10^{13} molecules/cm³ at h = 20km).

a) Waters (1970)
b) French (1968)
c) Cord et al. (1968)

Equation (46) was evaluated numerically for O_2 and H_2O attenuation, for elevation angles $\theta = 0°$ to $90°$ and $h = 0$ over the frequency band 0.1 to 100 GHz, by Blake (1972, Fig. 102). The sensitivity of millimeter wave receivers is not limited by atmospheric but by detection noise. Uncooled Schottky-diode mixers, for example, exhibit at 60 GHz presently single sideband noise temperatures on the order of 1200°K.

In radio communication, data are transmitted through the atmosphere in such a way that the system channel parameters are matched to the propagation characteristics of the medium to maximize received data; in passive remote sensing, the medium itself provides the data. Meeks and Lilley (1963) introduced the idea of using O_2-MS emission to remotely sense the temperature structure of the lower ($h > 30$ km) atmosphere from an orbiting satellite. Their work has been extended by Lenoir (1968) and Croom (1971) and was applied by Westwater (1970) and Waters (1970, 1973) to ground-based radiometric sensing. All these treatments take advantage of microwave spectroscopic properties of O_2 and other atmospheric gases and their dependences upon frequency and meteorological conditions, which has been the subject of this report.

Finding the temperature $T(\ell)$ in equation (46) as a function of an independent variable [e.g., $p(h)$] from observations of T_A at selected frequencies ν requires numerical inversion methods. The reliability of the inversion depends to a great extent on the accuracy to which $\alpha(\nu, p, T, H, r_k)$ due to the O_2-MS is known. A general description of the atmospheric O_2-MS can be accomplished only by theory. However, existing data are insufficient for a proper test of the available theory. More laboratory work on the intensity distribution of the atmospheric O_2-MS is required under careful control of conditions (Meeks and Lilley, 1963; Wilheit, 1969; Liebe, 1969b; Waters, 1970).

4. CONCLUSIONS

The review of molecular theory for millimeter wave properties of air, its translation into engineering terms (Section 2), the development of analytical schemes to predict propagation characteristics on the basis of meteorological phenomena, and the description of computer routines together with many examples of unique atmospheric transfer properties (Section 3) shall provide a sound basis for the development of future systems operating in the 40 to 140 GHz frequency range.

The main emphasis has been placed on the atmospheric O_2-MS which dominates transfer properties throughout the 40 to 140 GHz band and existing gaps in the knowledge of the spectrum have been identified. It was attempted not to seriously violate real atmospheric situations; however, over the full range of meteorological variables, it remains to be established how reliable the discussed analytical schemes really are. Presently, the correlation between atmospheric attenuation and phase dispersion rates on one hand and meteorological conditions (Eq. 3) on the other hand is not very accurate. The correspondence between both sets of data needs to be improved by inputs from controlled laboratory measurements on isolated line parameters and continuum spectra data. A manageable theory should be brought forward which predicts the continuum spectrum based on properties of the line spectrum, circumventing more or less arbitrary empirical models.

ACKNOWLEDGMENT

The authors would like to acknowledge the valuable support received from the Atmospheric Collision Processes Section of the NOAA Aeronomy Laboratory through the useage of most of the gases listed in Table 1.

5. REFERENCES

Anderson, R. S., W. V. Smith, and W. Gordy (1952), Line breadths of the microwave spectrum of oxygen, Phys. Rev. 87, 561-567.

Artman, J. O., and H. P. Gordon (1954), Absorption of microwaves by oxygen in mm wavelength region, Phys. Rev. 96, 1237-1241.

Blake, L. V. (1972), Radar/radio tropospheric absorption and noise temperature, NRL Report 7461, Naval Research Laboratory, Washington, D. C. 20390.

Boudouris, G. (1963), On the refractive index of air, and absorption and dispersion of centimeter waves by gases, J. Res. NBS 67D, 631-684.

Carter, C. J., R. L. Mitchell, and E. E. Reber (1968), Oxygen absorption measurements in the lower atmosphere, J. Geophys. Res. 73, 3113-3120.

Coates, R. J. (1958), Measurements of solar radiation and atmospheric attenuation at 4.3 mm, Proc. IRE 46, 122-126.

Cord, M. S., J. D. Petersen, M. S. Lojke, and R. H. Haas (1968), Microwave spectral tables, vol. IV, National Bureau of Standards Monograph No. 70.

Crane, R. K. (1971), Propagation phenomena affecting satellite communication systems operating in the centimeter and millimeter wavelength bands, Proc. IEEE 59, 173-188.

Croom, D. L. (1971), The 2.53-mm molecular rotation line of atmospheric oxygen, Planet. Space Sci. 19, 777-789.

Dillon, T. A. (1969), Theory of pressure broadening for isolated and overlapping spectral lines and calculations of the 60-GHz oxygen lines, Ph.D. Thesis, University of Colorado, Boulder, Dept. of Physics.

Dillon, T. A., and J. T. Godfrey (1972), Pressure broadening of the O_2 microwave spectrum, Phys. Rev. A5, 599-605.

Evenson, K. M., H. P. Broida, J. S. Wells, R. J. Mahler, and M. Mizushima (1968), Electron paramagnetic resonance absorption in oxygen with the HCN laser, Phys. Rev. Letters 21, 1038-1040.

Faddeyea, V. N., and N. M. Terent'ev (1961), Tables of values of the function w(z) = ... for complex argument, Pergamon Press, New York.

French, I. P. (1968), Microwave and far-infrared absorption as a diagnostic for the wake of hypersonic projectiles, J. Quant. Rad. Transfer 8, 1665-1673.

Grauling, C. H., Jr., (1972), 60 GHz radiometric local vertical sensor experiment, Final Report NAS1-10131, Westinghouse DESC, prepared for NASA Langley Research Center, 208 pp.

Guidice, D. A. (1971), Investigation of the 60-GHz atmospheric oxygen mantle for application to vertical sensing, Environmental Research Paper No. 38, AFCRL-71-0116, Air Force Systems Comd., USAF.

Haroules, G. G., and W. E. Brown (1969), A 60-GHz multi-frequency radiometric sensor for detecting clear air turbulence in the troposphere, IEEE Trans. Aerospace and Electr. Systems, AES-5, 712-723.

Hayes, R. D. (1964), Total atmospheric attenuation at mm wavelengths, Ph. D. Thesis, Georgia Institute of Technology, School of Electrical Engineering, Atlanta, Ga.

Hill, R. M. and W. Gordy (1954), Zeeman effect and line breadth studies of the microwave lines of oxygen, Phys. Rev. 93, 1019-1023.

Klass, P. J. (1971), Satellite radio spectrum expanded, Aviation Week & Space Technology, August, 14-15.

I. T. U. (1971), Final acts of the World Adm. Radio Conference for Space Telecommunication, WARC ST 71, International Telecommunication Union, Geneva.

LeFande, R. A. (1968), Attenuation of microwave radiation for paths through the atmosphere, NRL Rept. 6766, Naval Res. Lab., Washington, D. C. 20390.

Lenoir, W. B. (1968), Microwave spectrum of molecular oxygen in the mesosphere, J. Geophys. Res. 73, 361-376.

LeVine, H. (1970), Propagation delay in the atmosphere, NASA Rept. No. X-521-404, Goddard Space Flight Center, Greenbelt, Md.; also (1972) Radio Science 7, 625-629.

Liebe, H. J. (1969a), Calculated tropospheric dispersion and absorption due to the 22-GHz water vapor line, IEEE Trans. Ant. Prop. AP-17, 621-627.

Liebe, H. J. (1969b), Atmospheric propagation properties in the 10- to 75-GHz region: A survey and recommendations, ESSA Technical Rept. ERL 130-ITS 91, September (U. S. Government Printing Office, Washington, D. C.), 31 pp.

Liebe, H. J., and W. M. Welch (1972), Attenuation and phase dispersion in the atmosphere due to the microwave spectrum of oxygen, AGARD, 18th Meeting of E. M. Wave Propagation Panel, Gausdal, Norway, September (AGARD-CPP-107, 5/ 1-20).

Liebe, H. J., W. M. Welch, and R. Chandler (1973), Laboratory measurements of electromagnetic properties of atmospheric gases at millimeter wavelengths, IEE Conference Publication No. 98, Propagation of Radio Waves Above 10 GHz, London, April, 244-249.

Machta, L., and E. Hughes (1970), Atmospheric oxygen in 1967 to 1970, Science 168, 1582-1584.

Mardon, G. (1969), Application of millimeter waves, Chapter V in Mm and Sub-Mm Waves (F. S. Benson, editor), ILIFFE Books, Ltd., London.

McKnight, J. S., and W. Gordy (1968), Measurements of the sub-mm-wave rotational transition of oxygen at 424 GHz, Phys. Rev. Letters 21, 1787-1791.

Meeks, M. L., and A. E. Lilley (1963), The microwave spectrum of oxygen in the earth's atmosphere, J. Geophys. Res. 68, 1683-1703.

Miller, W. L., and A. R. Gordon (1931), Numerical evaluation of infinite series and integrals occurring in heat flow, J. Phys. Chem. 35, 2785-2884.

Mingelgrin, U., R. G. Gordon, L. Frenkel, and T. E. Sullivan (1972), Microwave Spectrum of compressed O_2-Foreign gas mixtures in the 48-81 GHz region, J. Chem. Phys. 57, 2923-1931.

Mingelgrin, U. (1972), Classical scattering calculations for diatomic molecules and application to the microwave spectrum of O_2, OT/ITS Tech. Res. and Engrg. Rept., TRER 32, July (U. S. Government Printing Office, Washington, D. C.), 58 pp.

MITRE (1965), Line integral refractometer, Final Rept. MTP-19 (AF 19-628-5165), (J. F. Sullivan and H. M. Richardson). Also in Proc. AGARD, 18th Meeting of E. M. Wave Propagation Panel, Gausdal, Norway, September 1972 (AGARD-CPP-107, 10/ 1-11).

Mizushima, M., and R. M. Hill (1954), Microwave spectrum of O_2, Phys. Rev. 93, 745-748.

Mizushima, M., J. S. Wells, K. M. Evenson, and W. M. Welch (1972), Laser magnetic resonance of the O_2 molecule using the 337 μm HCN laser, Phys. Rev. Letters 29, 831-833.

Morgan, L. A., and C. A. Ekdahl, Jr. (1966), Mm-wave propagation, Tech. Rept. No. RADC-TR-66-342, Res. and Tech. Div. Rome Air Development Center, Griffiss AFB, N. Y. 13440.

Murray, R. G. (1971), Secure communications at millimeter wavelengths, Rept. No. ECOM-5412, U. S. A. Electronics Comd., White Sands Missile Range, N. M.

Newell, A. C., and R. C. Baird (1965), Absolute determination of refractive indices of gases at 47.7 GHz, J. Appl. Phys. 36, 79-83.

Reber, E. E. (1972), Absorption of the 4- to 6-mm wavelength band in the atmosphere, J. Geophys. Res. 77, 3831-3845.

Reber, E. E., R. L. Mitchell, and C. J. Carter (1970), Attenuation of the 5 mm wavelength band in a variable atmosphere, IEEE Trans. AP-18, 472-479.

Sabatini, R. R. -editor (1972), The NIMBUS 5 user's guide, NASA Goddard Space Flight Center, ERTS/NIMBUS Project, 162 pp.

Schaper, L. W., D. H. Staelin, and J. W. Waters (1970), The estimation of tropospheric electrical path length by microwave radiometry, Proc. IEEE 58, 272-273.

Schulze, A. E., and C. W. Tolbert (1963), Shape, intensity and pressure broadening of the 2.53 mm wavelength oxygen absorption line, Nature 200 (4908), 747-750.

Snider, J. B., and E. R. Westwater (1969), Atmospheric attenuation at 15, 31, and 52 GHz, ESSA Tech. Rept. ERL 156-WPL 11 (U. S. Govt. Printing Office, Washington, D. C.).

Stafford, L. G., and C. W. Tolbert (1963), Shapes of oxygen absorption lines in the microwave frequency region, J. Geophys. Res. 68, 3431-3435.

Tinkham, M., and M. W. P. Strandberg (1954), Interaction of molecular oxygen with a magnetic field, Phys. Rev. 97, 951-966.

Thompson, M. C., Jr. (1968), Space averages of air and water vapor densities by dispersion for refractive correction of range measurements, J. Geophys. Res. 73, 3097-3102.

Thompson, M. C., Jr., and M. J. Vetter (1968), Refractometer that measures the difference in refractive indices of a gas at two frequencies, U. S. Patent No. 3, 400, 330, Sept. 3.

Thompson, M. C., Jr., L. E. Vogler, H. B. Janes, and L. E. Wood (1972), A review of propagation factors in telecommunications applications of the 10- to 100-GHz radio spectrum, OT/ITS Tech. Res. and Engrg. Rept. TRER 34, August (U. S. Govt. Printing Office, Washington, D. C.), 76 pp.

Thompson. W. I., III (1971), Atmospheric transmission handbook, Tech. Rept. No. DoT-TSC-NASA-71-6 (NASA, Washington, D.C. 20590).

Tolbert, C. W., and A. W. Straiton (1963), Synopsis of attenuation and emission investigation of 58- to 62-GHz frequencies in the earth's atmosphere, Proc. IEEE 51, 1754-1760.

U. S. Standard Atmosphere (1962), prepared under the sponsorship of NASA, USAF, and U. S. Weather Bureau (U. S. Govt. Printing Office, Washington, D. C.).

VanVleck, J. H. (1947), The absorption of microwaves by oxygen, Phys. Rev. 71, 413-424.

Waters, J. W. (1970), Ground-based microwave spectroscopic probing of the stratosphere and mesosphere, Ph. D. Thesis, M. I. T. Dept. of Electrical Engrg., Cambridge, Ma.

Waters, J. W. (1973), Ground-based measurement of millimeter wavelength emission by upper stratospheric O_2, Nature, in press.

Welch, W. M., and M Mizushima (1972), Molecular parameters of oxygen, Phys. Rev. A5, 2692-2695.

West, B. G., and M. Mizushima (1966), Absorption spectrum of oxygen molecule in the 55-65 GHz region, Phys. Rev. 143, 31-36.

Westwater, E. R. (1970), Ground-based determination of temperature profiles by microwaves, Ph. D. Thesis, University of Colorado, Boulder, Dept. of Physics and Astrophysics.

Whitehurst, R. N., J. Copeland, and F. H. Mitchell (1957), Solar radiation and atmospheric attenuation at 6 mm, J. Appl. Phys. 28, 295-298.

Wilheit, T. T., Jr. (1969), Studies of microwave emission and absorption by atmospheric oxygen, Ph. D. Thesis, M. I. T. Dept. of Physics, Cambridge, Ma.

Zhevakin, S. A., and A. P. Naumov (1967), Magnetic permeability of molecular oxygen, Radio Eng. Electronic Phys. (Engl. transl.) 12, 1249-1252.

Zimmerer, R. W., and M. Mizushima (1961), Precise measurement of the microwave absorption frequencies of the oxygen molecule and the velocity of light, Phys. Rev. 121, 152-159.